PRECIPITATING CLOUD SYSTEMS OF THE ASIAN MONSOON*

Richard H. Johnson [1]

and

Robert A. Houze, Jr.[2]

*Ch. 10 of *Monsoon Meteorology*, 1987,

C.-P. Chang and T.N. Krishnamurti, eds.

---

[1] Department of Atmospheric Science, Colorado State University, Fort Collins, Colorado

[2] Department of Atmospheric Sciences, University of Washington, Seattle, Washington

10. PRECIPITATING CLOUD SYSTEMS OF THE ASIAN MONSOON

RICHARD H. JOHNSON AND ROBERT A. HOUZE, JR.

1 INTRODUCTION

The earth's monsoon circulations are characterized by regions of large-scale ascent and heavy rains, which are essential to agricultural production throughout much of South Asia. Tragic consequences occur when this precipitation is inadequate or ill timed. The cloud systems from which the rain falls strongly influence large-scale monsoonal flow patterns, and the global atmospheric circulation through the enormous amount of latent heat released and the effects of the clouds on the transfer of solar and terrestrial radiation. Understanding of the structure and behavior of monsoon cloud systems is therefore prerequisite to accurate representation of diabatic processes in large-scale numerical simulation and prediction of monsoons and of the global circulation. Local forecasting of monsoon rains also requires detailed understanding of the precipitating cloud systems. Precipitation throughout the world is characterized by mesoscale organization (Houze and Hobbs 1982), and accurate prediction of rainfall on a day-to-day basis throughout a monsoonal wet season can therefore be expected to entail a clear perception of the mesoscale structure of the cloud systems producing the precipitation.

Given the importance of the mesoscale aspects of precipitating cloud systems to monsoon meteorology, it is somewhat surprising that relatively little attention has been given to their observation and description. The characteristics of precipitating clouds in monsoons prior to the Global Atmospheric Research Program's (GARP) Monsoon Experiment (MONEX) for 1978 to 1979 were reviewed comprehensively by Ramage (1971, his Chap. 4) and for the Indian monsoon in particular by Rao (1976, his Chap. 12). Ramage categorized monsoon precipitation into "showers" from towering cumulus and cumulonimbus and "rains" from deep nimbostratus with embedded convection. He then showed, using data from India, Africa, and Southeast Asia, that an inverse relation appears to exist between thunderstorm frequency and rains: "Beneath scattered convective cells showers may be heavy but average rainfall per unit area is only a fraction of that caused by the rains" (Ramage 1971, p. 106). Ramage further showed that while rains tend to occur within synoptic-scale systems, rainfall, radar, and satellite data reveal "considerable spatial variability on a scale larger than a cumulus cloud but smaller than synoptic" (Ramage 1971, p. 111). He added, "though this *mesoscale* is a feature of all synoptic disturbances, nowhere in the monsoon area are sounding data sufficient to describe it three-dimensionally" (Ramage 1971, p. 111). Thus, it was evident well before MONEX that precipitation in monsoons fell primarily from extensive nimbostratus with embedded convection and was organized on the mesoscale within large-scale flow patterns. But much remained to be learned about the details of the cloud systems.

Although MONEX was designed primarily to document large-scale aspects of monsoons, it nevertheless provided an opportunity to probe the internal structure of the mesoscale cloud systems that account for monsoon rainfall. Aircraft provided digital radar observations, cloud photogrammetry, cloud microphysical information, dropwindsondes, and other measurements. Quantitative ground-based radar measurements were obtained, and geosynchronous satellites were launched and positioned to provide data. Aircraft dropwindsonde missions were primarily aimed at documenting synoptic-scale circulations; however, during the course of the flights, a substantial number of cloud penetrations were made. Consequently, these flights, together with the satellites and ground-based digital radar, provided a unique set of data on the structure of monsoon cloud systems—both on their internal structure and their organization in relation to the environment.

MONEX was carried out in two phases: winter MONEX from December 1978 to March 1979, and summer MONEX from May to August 1979. These names reflect the seasons of the Northern Hemisphere, since that is where the special measurements were obtained. The locations of the experiments are shown in Fig. 10.1, which also indicates the names of the various geographical regions referred to throughout this chapter. Winter MONEX was concerned with the wintertime low-level outpouring of cold air from the Asian continent southwestward over the South China Sea and the attendant convergence, upward air motion, and clouds over the Indonesian-Malay-

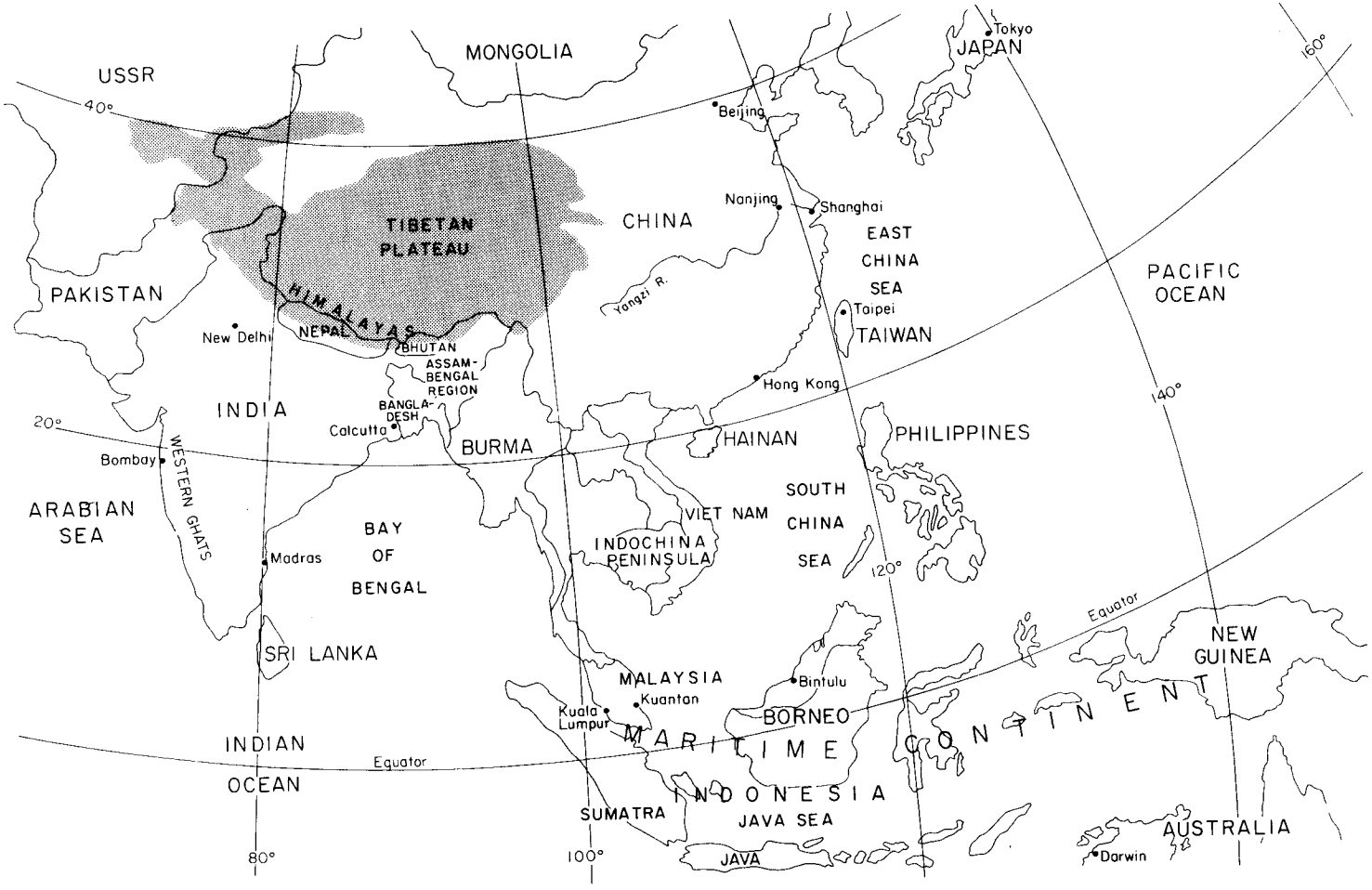

Fig. 10.1. Geography of the Asian monsoon region. The terrain above 3000 m is shaded.

sian maritime continent. Summer MONEX dealt with the southwesterly influx of warm, moist, low-level air over India and surrounding regions during the warm season and the extensive cloud systems and other phenomena associated with that influx. The purpose of this chapter is to describe results of winter and summer MONEX insofar as they have provided insight into the precipitating cloud systems of each monsoon. We will also attempt to indicate where further work is needed on this subject.

2 WINTER MONSOON

2.1 Climatological setting

2.1.1 Background and definitions. During the winter monsoon, cross-equatorial exchanges of mass, heat, and moisture are often pronounced, particularly in the longitude belt encompassing the maritime continent. Part of the enhanced interhemispheric coupling during the Northern Hemisphere winter can be attributed to cold surges that develop over China and propagate equatorward over the South China Sea and adjacent areas. The influence of these cold outbreaks, which occur at irregular intervals of several days to a week or more, can extend into the Southern Hemisphere and are part of a concurrent intensification of the East Asian Hadley cell (Ramage 1971; Murakami and Unninayer 1977; Murakami 1978; Chang et al. 1979; Chang and Lau 1980) and east-west Walker circulations (Murakami 1978; Chang and Lau 1980).

There are a number of dramatic effects of the winter monsoon circulation and attendant cold surges on synoptic and planetary scale convective patterns of the monsoon region. These effects include (1) a general increase in the amount of deep convection over the maritime continent during the winter monsoon, with periods of marked enhancement at times of strong cold surges (including localized episodes of heavy rainfall and flooding); (2) a modulation of the timing of the onset of the Southern Hemisphere (Australian) summer monsoon with influences on associated convective patterns and circulation features; (3) the generation of near-equatorial cloud systems over the maritime continent; and (4) the possible influence of cold surges on the development of Southern Hemisphere tropical cyclones. These interactions, as well as others not mentioned, are varied and complex, and our understanding of the convective phenomena, even in a descriptive sense, is far from complete. For example, the mesoscale organization of convection within most of the synoptic systems described above has yet to be studied. For a review of the limited knowledge of winter monsoon convection that does exist, a framework providing the general characteristics of the mean monsoon circulation and its interannual variability must be established first.

We define the winter monsoon period as the months of December, January, and February, while recognizing that this terminology reflects a Northern Hemisphere perspective since this same period coincides with the Australian summer monsoon. Harris et al. (1969) have shown that winter monsoon circulation normally exhibits important changes from early to late winter. The low-level, northeast monsoon flow over the South China Sea is strongest and deepest in early winter; by the latter part of the season it becomes shallower and weaker. Conversely, the Australian summer monsoon, which typically has its onset in early Northern Hemisphere winter (Troup 1961; Davidson et al. 1983), is most intense during late winter (late January to February) when the near-equatorial trough lies between 10 and 15°S. These variations in the monsoon flow over the course of the season are also reflected in changes in cloudiness and deep convective activity over the winter monsoon area (Murakami 1980; Murakami 1983; McBride 1983). Thus, while we discuss in this section the nature of winter monsoon convection as revealed from winter MONEX observations, we realize that there is a broad range of conditions, with both spatial and temporal variations, within which monsoon convection exists.

2.1.2 General characteristics of the mean flow. A schematic diagram illustrating the typical geographical distribution of winter monsoon circulation systems and convection is presented in Fig. 10.2. Deep convection and heavy rainfall can occur throughout the entire tropical monsoon region; however, these phenomena are normally concentrated in areas where local or regional forcing is a maximum. The most extensive, vigorous cloud regime of the winter monsoon region, coincident with the zone of heaviest area-averaged rainfall, extends along and to the north of the Southern Hemisphere monsoon trough from Sumatra across Indonesia to the southwest Pacific (Atkinson and Sadler 1970; Ramage 1971; Sadler 1977). Within this region, over Malaysia, Indonesia, northern Australia, and New Guinea, there exist both significant diurnal variations in this intense convective activity due to land and sea breeze effects (Holland and Keenan 1980; Short and Wallace 1980; Murakami 1983) and synoptic variability in the form of eastward- and westward-propagating cloud systems (Williams 1981; McBride 1983).

We will briefly examine in this section characteristics of the mean circulation for the winter MONEX period during 1978 and 1979. The large-scale mean flow fields at 850 and 200 mb over the winter MONEX region are depicted in Fig. 10.3 (from Sumi and Murakami 1981). In their analyses (Fig. 10.3 and several to follow) Sumi and Murakami have used First GARP Global Experiment (FGGE) levels IIa and IIb sounding data. From Fig. 10.3 it is evident that at low levels northeast

trades prevail over the western Pacific and Southeast Asia from about 20°N to the equator. Transient increases of this northeast flow occur during the winter cold-surge events. A near-equatorial trough extends along 5°N from 170°E across Borneo and Malaysia to the Bay of Bengal (80°E). Proceeding southward across the equator, the low-level flow turns to westerly with an increase toward the Southern Hemisphere monsoon trough, which extends between 10° and 20°S across northern Australia and the southwest Pacific. Analyses of the 850-mb flow for the months of December 1978 and January and February 1979 by Murakami and Sumi (1982) reveal month-to-month changes in the flow pattern within the Southern Hemisphere monsoon trough, with a peak intensity of the monsoon low-level westerlies occurring during January.

At 200 mb (Fig. 10.3a) two extensive east-west ridges exist over the entire winter monsoon region with one axis along 10°N and the other along 15°S. The 200-mb ridge in the Southern Hemisphere, as Sumi and Murakami point out, is centered above the Australian monsoon low-level trough.

An analysis of the divergent component of the wind of these two levels is illustrated in Fig. 10.4 (Sumi and Murakami 1981). Centers of low-level convergence and upper-level divergence are found to be colocated just east of New Guinea over the southwest Pacific. These features reflect the existence of a maximum in deep convective

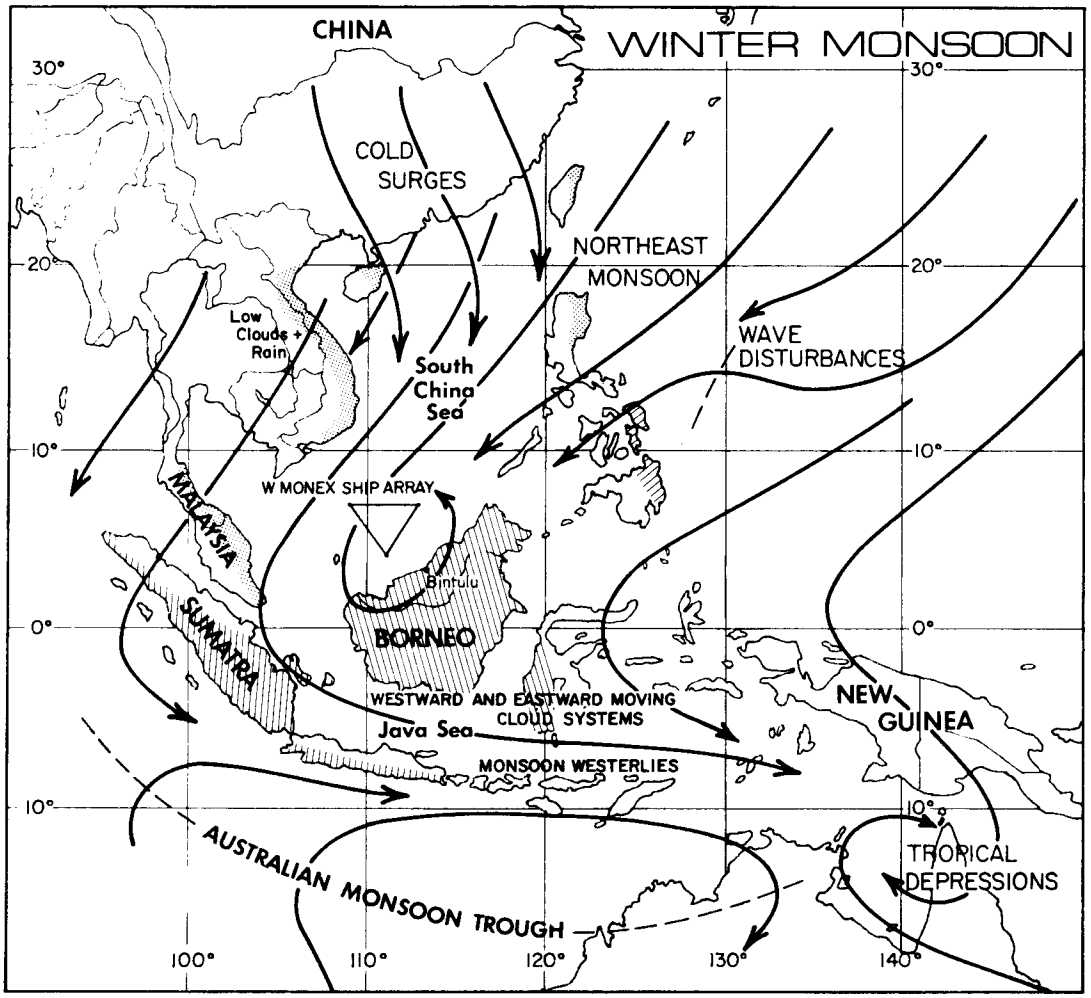

Fig. 10.2. Primary synoptic-scale circulation features that affect cloudiness and precipitation in the region of the winter monsoon. Convection associated with land and sea breeze circulations exists throughout the maritime continent. Preferred coastal locations of enhanced low-level cloudiness and rainfall associated with the northeast monsoon and cold surges are indicated (stipples); cloudiness maxima over water are omitted. Hatching denotes November 1 to April 30 precipitation west of 130°E exceeding 150 cm (from Cobb and Coleby 1966). The winter MONEX ship array (December 6 to 28, 1978; southernmost ship moved 1° south of indicated position after December 17) is shown.

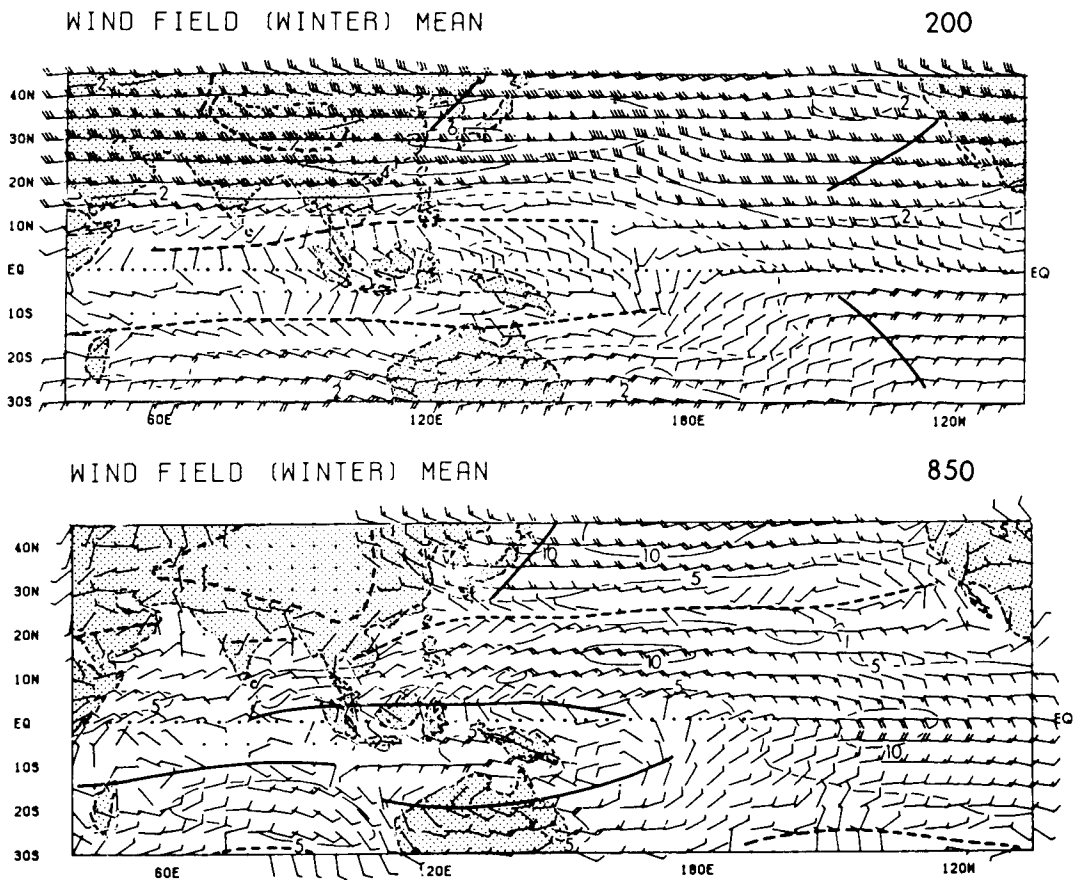

Fig. 10.3. The 1978–79 winter (December-January-February) mean winds (barbs) and isotachs (solid lines; units of m s^{-1}). (*a*) At 200 mb. (*b*) At 850 mb. Also shown are the major trough (heavy solid lines) and ridge (heavy dashed lines) axes. (From Sumi and Murakami 1981.)

activity over this region, at least on an average basis for the winter of 1978 to 1979. A secondary center of upper-level divergence can be seen over the eastern Indian Ocean. The prevalence of deep convection along the broad east-west-oriented centers in Fig. 10.4 is supported by the analysis of Sumi and Murakami (1981) of satellite-observed outgoing longwave radiation (Fig. 10.5). An east-west zone of maximum cloudiness is inferred from Fig. 10.5 to exist centered near 10°S extending from just west of Sumatra to near 180°E, with a primary center over and just east of New Guinea.

The broad-scale pattern of monsoon convection deduced by Sumi and Murakami (1981) and Murakami and Sumi (1982) from general circulation characteristics and outgoing longwave radiation is consistent with that determined recently by other investigators. For example, Wei et al. (1983), using FGGE level IIIa analyses generated by the U.S. National Meteorological Center, have determined global distributions of vertically integrated diabatic-heating rates, which, for the winter mean conditions just presented, show good agreement with Fig. 10.4 in terms of inferred geographical distributions of monsoon convection. In particular, both studies show a winter mean maximum in deep convective activity east of New Guinea centered near 10°S and 160 to 170°E. This time-mean picture is further substantiated by direct satellite measurements of the cloud systems themselves (to be discussed in the next section).

2.1.3 Satellite climatology. The placement of the Japanese geostationary meteorological satellite (GMS-1) in orbit in 1978 was an important milestone for the study of convection over the winter monsoon region. Already, several studies have used GMS-1 data to develop cloud climatologies on both large and regional scales. Of course, prior to GMS-1, polar-orbiting satellites provided significant information on the distribution of cloud systems over this area. From both

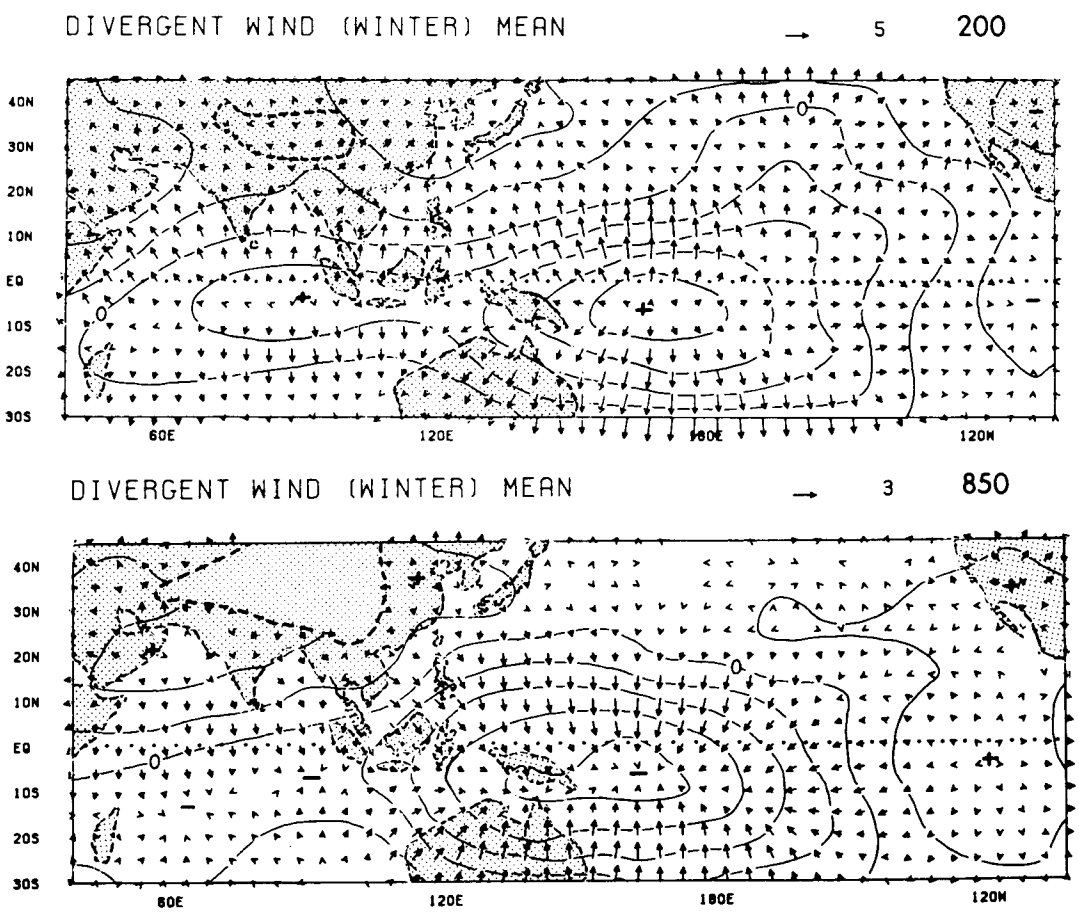

Fig. 10.4. The 1978–79 winter mean divergent winds (arrows) and velocity potential (solid lines; units of 10^6 m^2 s^{-1}) fields. (*a*) At 200 mb. The unit vector is 5 m s^{-1}. Velocity potential intervals are 2 units. (*b*) At 850 mb. The unit vector is 3 m s^{-1}. Velocity potential intervals are 1 unit. (From Sumi and Murakami 1981.)

data sources it has become evident that characteristic cloud patterns exist during the monsoon. Some of these patterns are illustrated in GMS–1 images from the winter MONEX period on December 10 and 11, 1978, at GMT (Fig. 10.6). A moderate cold surge began late on the tenth, and one can see a marked increase in cloudiness over the entire region by the eleventh. Patterns of low clouds (stratus and cloud streets), evident over the East China Sea, northwest Pacific, and South China Sea, are commonly observed with monsoon cold surges and are capped by a strong inversion. Such cloud systems mark a zone of significant air mass transformation at low levels from cold, dry continental air over China to moist, tropical air toward the equator. Cloudiness and precipitation are enhanced within and to the south of this zone along the windward shores of landmasses throughout the region (e.g., over Taiwan, the Philippine Islands, Hainan, Vietnam, Malaysia, and Borneo). In addition to cold surges, other convective features, such as near-equatorial disturbances, are commonly identified by forecasters of the region and researchers as being important components of the total winter monsoon convective pattern (Fig. 10.2).

While the winter mean statistics of inferred cloud cover show a broad cloudiness maximum to the north of the Australian monsoon trough (Fig. 10.5), closer examination of GMS–1 data reveals several important transitional features during this period. Some of these temporal variations in satellite-derived cloudiness have been examined by Murakami (1983). Murakami has defined an intensity index I_c for deep convective activity that uses satellite infrared (IR) irradiance data from GMS–1. This index is designed to measure, to a reasonable approximation, the fraction of cumulonimbus in a region that penetrates and extends above 400 mb. The horizontal distribution of deep convection obtained by his technique for December 1978 and January 1979 is shown in Fig. 10.7. During December, several convective maxima are observed: (1) near the north coast of

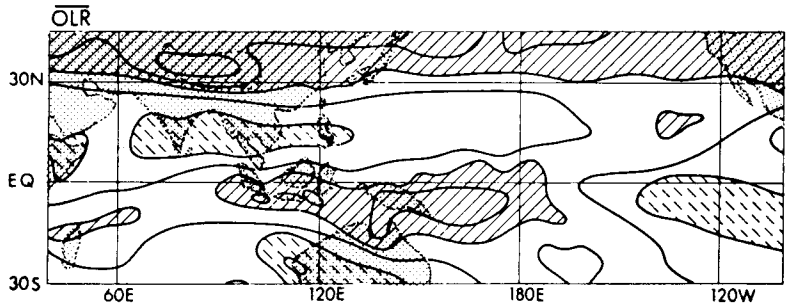

Fig. 10.5. The 1978–79 winter mean outgoing longwave radiation (10 W m^{-2}). Intervals are 2 units. Solid (dashed) hatching denotes regions of less (greater) than 24 (28) units. (From Sumi and Murakami 1981.)

Borneo, (2) over Java, (3) over New Guinea, and (4) near 5°S and 170°E. Following the onset of the Australian monsoon in the latter part of December (Davidson et al. 1983), the east-west zones of deep convective activity shift 5 to 10° to the south (see also Webster and Stephens 1980). The most notable changes during the two-month period are a sharp reduction in deep convection over northern Borneo and a significant increase over northern Australia. While these synoptic-scale changes in the distribution of convective activity are readily discernible from satellite data, little to no information is available concerning the nature of the organization of convection within the cloud systems throughout the period of transition.

In addition to latitudinal shifts in cloudiness through the winter monsoon, McBride (1983), using satellite data, has identified temporal changes in the synoptic-scale organizational character of the convection. Employing the technique of time-longitude display of strips of infrared satellite imagery (Chang 1970), McBride has found that, following the Australian monsoon onset on December 26, a marked increase in the spatial organization of convection occurred. Well-organized bands of convection having dimensions of 35° longitude by 15° latitude were observed to propagate in both eastward and westward directions in the latitude belt between 5° and 15°S throughout the months of January, February, and March 1979. These features are readily detectable from satellite depictions and may be of significance for large-scale dynamical theories of monsoon circulations (Lim and Chang 1981).

On regional scales only a few satellite climatological studies have been undertaken. The most distinctive feature of regional satellite imagery is the very pronounced, topographically controlled diurnal cycle of convection over the winter monsoon area (Holland and Keenan 1980; Short and Wallace 1980; Murakami 1983). Using 3-hourly GMS–1 data, Murakami (1983) has found, during December and January 1979, a peak in convective activity over land (northern Australia and the Indonesian islands) at 1800 LST and over the water adjacent to these land areas at 0900 LST. A slightly earlier time of occurrence, 0600 LST, of the over-water maximum was found over the equatorial South Pacific. It is well known that this diurnal cycle of convection over tropical island regions is caused by diurnally oscillating boundary layer convergence patterns established by land and sea breeze circulations. Over the open ocean various other mechanisms, such as differential radiative heating within and in the environment of cloud systems (Gray and Jacobson 1977; Cox and Griffith 1979; Webster and Stephens 1980), have been proposed to account for the observed diurnal cloudiness variations.

An excellent illustration of the dominance of diurnal controls on deep convection is found over and in the vicinity of Borneo during the winter monsoon period (in the region of the I_c maximum seen along the north Borneo coast in Fig. 10.7a). Several authors (Houze et al. 1981; Johnson and Priegnitz 1981) have used GMS–1 data and radar observations to examine the diurnal variation of cloudiness along the north coast of Borneo during winter MONEX. In this region, offshore convection is generated at night in response to low-level convergence along the north coast as the land breeze meets the northeast monsoon flow over the South China Sea (Fig. 10.2). During the daytime, the flow at the coast reverses direction as the sea breeze becomes established, and convection over land then predominates. This diurnal cycle is depicted in a satellite climatology of upper-level cloudiness along the north coast of Borneo for December 1978 (Fig. 10.8). From near sunrise (0800 LST, Fig. 10.8a) to shortly after noon (1400 LST, Fig. 10.8b), a maximum in the fractional area covered by upper-level clouds exists over water. By evening and into the early nighttime hours (Figs. 10.8c and d), the upper-level cloud maximum shifts to land. The striking regularity of this pattern is apparent from the relatively large fractional-area coverages and sharp features that are retained following the 31-day averaging of the

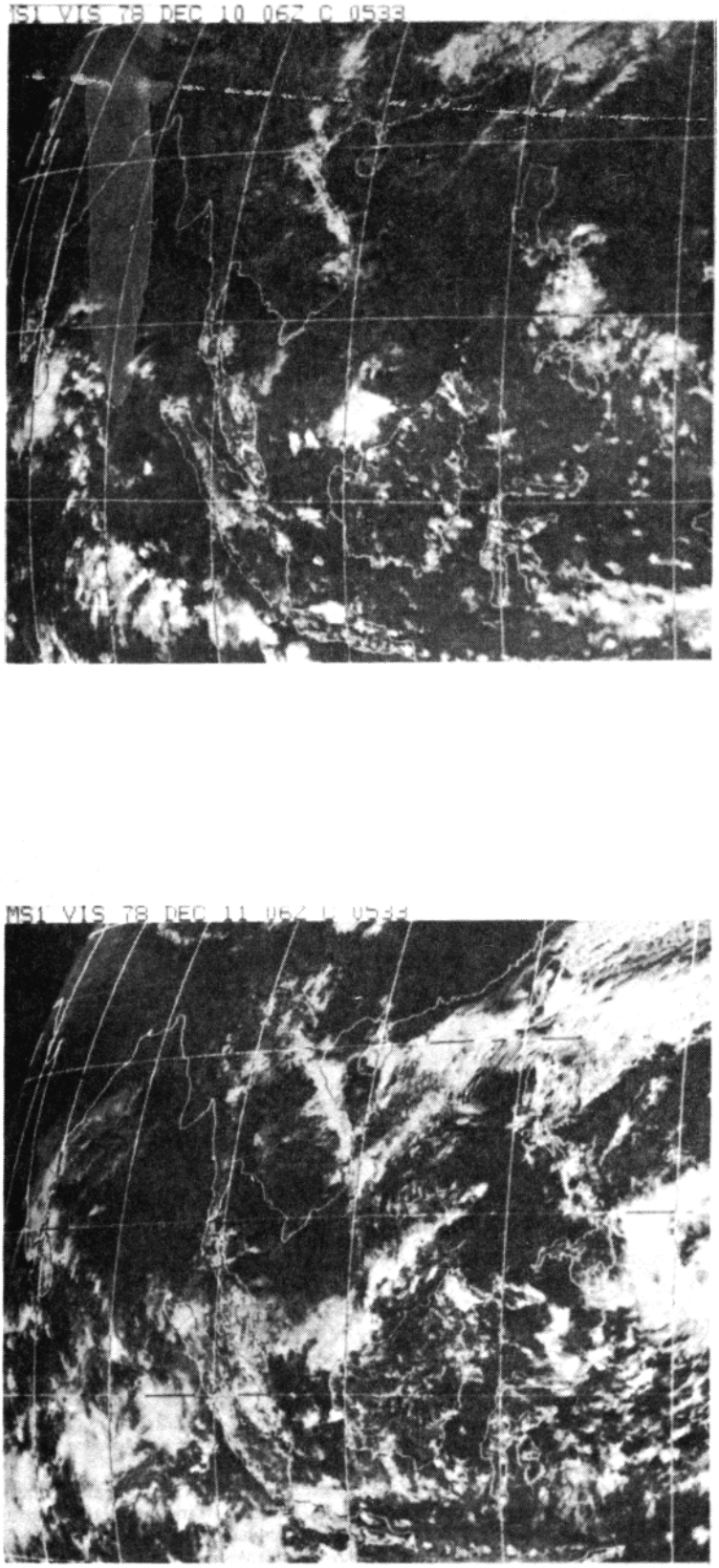

Fig. 10.6. Visible GMS satellite imagery at 0600 GMT (1400 LST at center of photograph). (*a*) For December 10, 1978. (*b*) For December 11, 1978. (From Sadler 1979.)

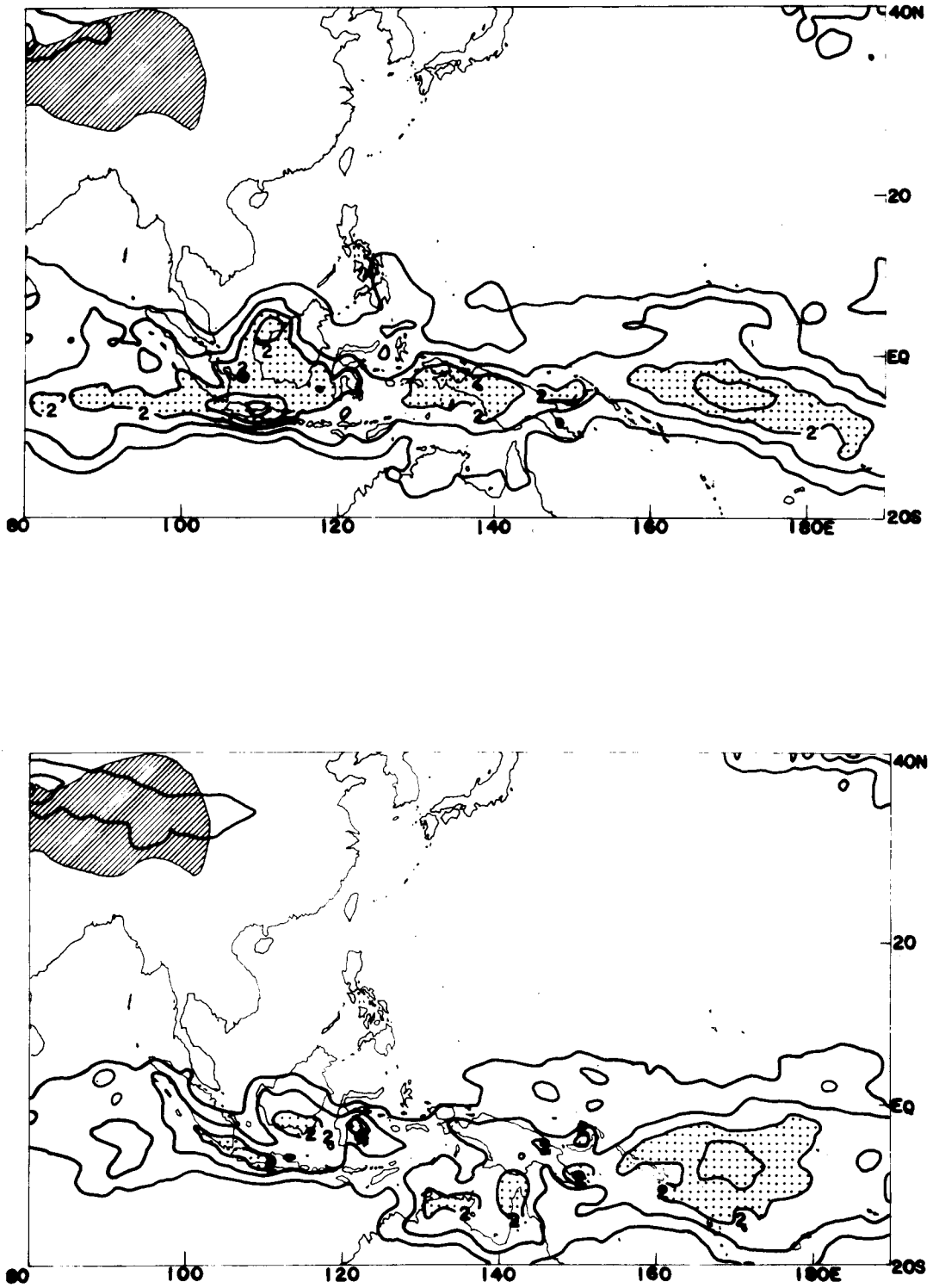

Fig. 10.7. Horizontal distribution of monthly mean values of I_c. (*a*) For December 1978. (*b*) For January 1979. The I_c can range between 0 and 10: 0 means that no cumulus tops extend above 400 mb; 10 means that all cumulus tops extend to the tropopause. The contour interval is 0.5 unit starting at 1.0. Values larger than 2.0 are shaded. The hatched area denotes elevations above 3000 m on Tibetan Plateau. (From Murakami 1983.)

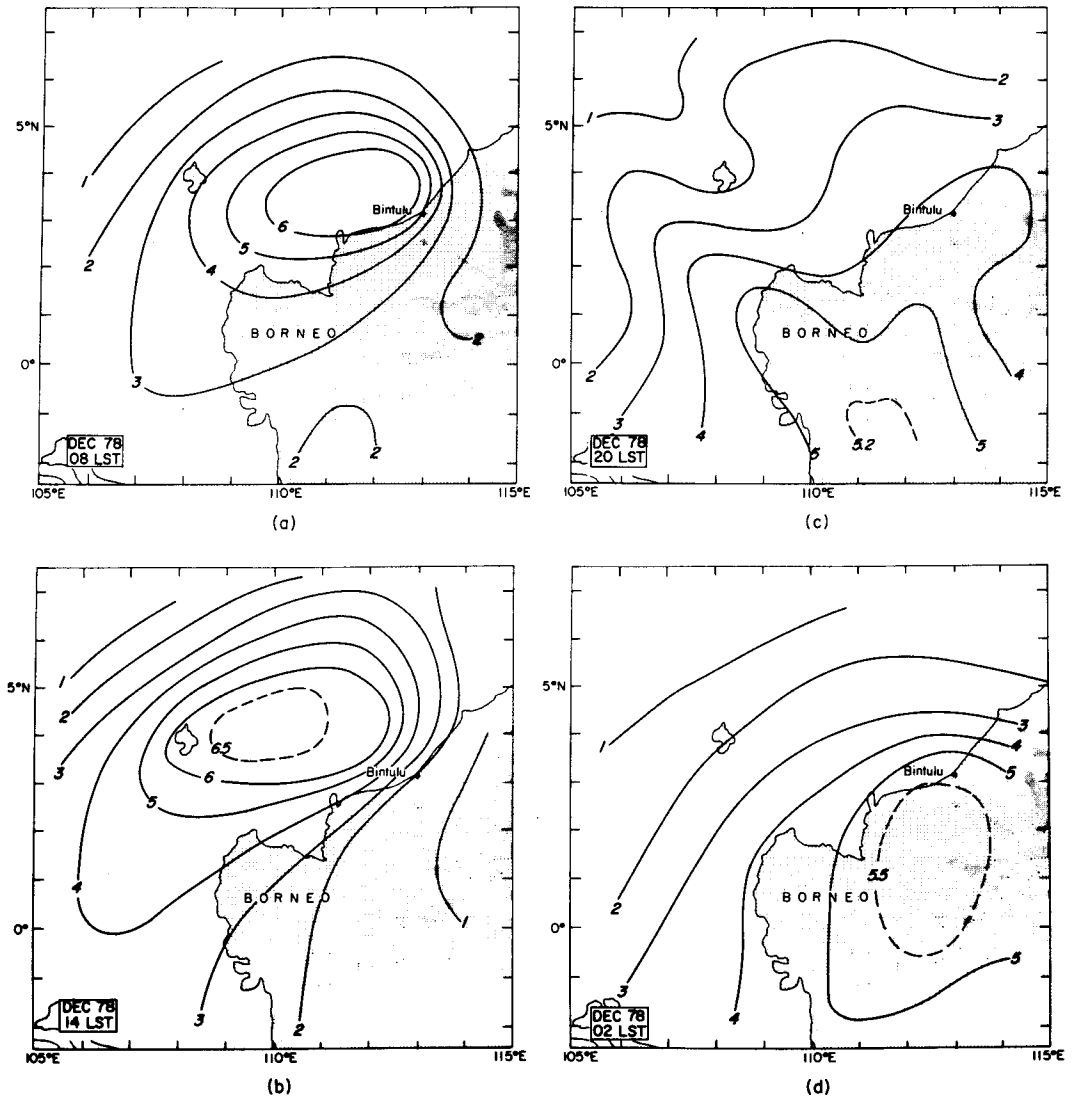

Fig. 10.8. Mean patterns of the fractional area covered by upper-level cloud for (*a*) 0800 LST, (*b*) 1400 LST, (*c*) 2000 LST, and (*d*) 0200 LST, determined from infrared satellite data for December 1978. Contours are labeled in tenths and were drawn for data in 275-km × 275-km grid squares. Dark shading within Borneo shows land areas above 3000 ft (914 m) altitude. (From Houze et al. 1981.)

data both in 1978 and other years studied by Houze et al. (1981).

The times of maximum satellite-derived cloudiness reported by Houze et al. (1981) over water (1200 LST) and land (0000 LST) are 3 and 6 h, respectively, later than those determined by Murakami (1983) for deep convective activity over the entire Indonesian Island region. This time lag can be attributed to the life cycle behavior of convective systems. In particular, it is observed that the expansion of upper-level cirrus cloud tops in these systems to their greatest areal extent typically follows the period of most intense deep convective activity by several hours. This explanation was given by Houze et al. (1981) to account for the similar lags observed between times of maximum fractional-area coverages of radar-determined precipitation and satellite upper-level clouds over land and water areas along north Borneo. The fact that there is generally good agreement between the times of the extrema in radar-determined precipitation coverage (Houze et al. 1981) and the I_c values of Murakami (1983) suggests that the technique proposed by Murakami to infer deep convective activity from satellite data is probably reliable.

2.1.4 Representatives of the FGGE year. In any limited experiment whose objective is to investigate a slowly varying meteorological phenomenon, such as the monsoon, the question of the long-term variability of that phenomenon becomes important. Indeed, can one generalize results obtained from data from the limited field phase periods of winter and summer MONEX if those periods had abnormal meteorological conditions? Presumably, for monsoon convective systems, whoe lifetimes are $\approx$1 day or less, information on the structure and properties of the convection gained from MONEX will have general applicability to other years. However, as was pointed out many years prior to MONEX (Ramage 1968), the geographical distribution of convection and precipitation in the near-equatorial winter monsoon region may have pronounced interannual variability, and inferences drawn on this aspect of monsoon convection based on any one year of data may not apply well at all to the next. As discussed recently by Lau and Li (1984), the interannual variability of the winter monsoon is not well known. There is some evidence to indicate that it may have important linkages with the El Niño and Southern Oscillation circulation phenomena, but further study of this problem is needed.

Although a precise index of its intensity is not available, the winter monsoon of 1978 to 1979 was weaker than normal as measured by precipitation amounts and cold-surge intensity (Greenfield and Krishnamurti 1979). Sumi and Murakami (1981) have compared winter MONEX mean circulation conditions with those of three previous winters from 1970 to 1973. They found that in most years the updraft portion of the large-scale, winter monsoon circulation is centered over Indonesia, with Hadley overturnings along 130°E and east-west upper-level outflows converging into the equatorial Pacific ($\approx$150°W) and Indian ($\approx$50°E) oceans (also consistent with the analyses of Krishnamurti et al. 1973; Webster et al. 1977; Chang and Lau 1980). However, the 1978 to 1979 winter monsoon circulation was considerably different (Fig. 10.4), with the updraft split into two parts, one over the equatorial western South Pacific ($\approx$170°E) and one over the eastern Indian Ocean ($\approx$95°E). The abnormal circulation features found by Sumi and Murakami (1981) are consistent with the observations of relatively weak winter monsoon convection and cold-surge activity in the longitudes of the maritime continent.

While the large-scale circulation and geographic distribution of convection during winter MONEX exhibited important departures from normal, the tropospheric flow in the region of the field experiment, that is, over the South China Sea, closely resembled climatological conditions for that region. Over the southern South China Sea, where monsoon convection was reasonably well sampled by aircraft, radar, and soundings, low-level northeasterlies were overlain by upper-level southeasterlies, a situation that is normal during the winter monsoon (Atkinson and Sadler 1970). It is tempting to conclude that the convection in this region during winter MONEX likely occurred in an environment similar to that existing in other winters and that the character of the cloud systems determined during December 1978 may well be considered representative of most winter monsoon periods. However, such a conclusion is not necessarily justified, and further measurements will probably be required to establish the representativeness of the winter MONEX results.

2.2 Synoptic-scale variability of convection

2.2.1 Cold surges and their associated cloud systems.

2.2.1.1 South China Sea and Borneo region. Throughout the winter monsoon, with only brief exceptions, cold, dry air flows equatorward off mainland China out over the South China Sea. Significant surface sensible and latent heat exchanges occur in the first several hundred kilometers offshore during the entire northeast monsoon, and there is a marked enhancement of these surface fluxes at times of cold surges. The nature of the air mass transformation and the associated cloud fields that develop over the ocean under these circumstances has been studied extensively over the East China Sea with data from the 1974 and 1975 Air Mass Transformation Experiments (AMTEX) (Ninomiya and Akiyama 1976; Agee and Lomax 1978; Nitta and So 1980).

During the period from December 10 to 12, 1978, one of the three moderate cold surges of the winter MONEX field phase occurred over the South China Sea. It began on the tenth, with passage at Hong Kong occurring at 900 GMT on this day, reached peak intensity on the eleventh and subsequently weakened on the twelfth. Visible satellite imagery at 600 GMT on the eleventh (Fig. 10.6b) depicts the cloud regimes associated with this cold surge during the period of maximum surge intensity. Overall cloud coverage associated with strong cold surges can be significantly greater than that observed with moderate surges, such as shown for the eleventh (Ramage 1971; Riehl 1979); however, the cloud *patterns* in the winter MONEX moderate-surge events are typical of those occurring in the stronger cases.

Aircraft missions over the South China Sea were flown on December 10, 11, and 12 to investigate the temporal and spatial characteristics of the atmosphere during a cold surge. Data from the flights on the tenth and eleventh have been synthesized by Warner (1982b) in an effort to describe the north-south variations of the convec-

tive fields and their changes with time as the surge progressed. His results, in the form of a north-south cross section from Hong Kong to near Borneo (4°N, 111°E) for December 10 and 11, are shown in Fig. 10.9. Aircraft photogrammetry, dropwindsonde, and surface station rawinsonde data were used in his analysis.

On the tenth, when the surge first began, a distinct variation in sky condition was observed from north to south across the South China Sea. As illustrated in Fig. 10.9(a), clear skies within ≈ 100 km of the China coast were followed by 100 to 200 km of stratocumulus overcast, then ≈800 km of gradually deepening cumulus humilis (in streets), and, finally, within 500 to 700 km of the coast of Borneo, towering cumulus and cumulonimbus. As Riehl (1979) has noted, such a transition in cloud types resembles that observed along trade wind trajectories (Malkus and Riehl 1964), except that in the trade wind case the transition occurs over much greater distances. A further analogy to the trade winds is the strong subsidence inversion that exists atop the cloud layer over the northern South China Sea (Warner 1982b). Cross sections of temperature and dew point (presented as departures from a mean dropwindsonde sounding) show a gradual transition in the lower troposphere from cold, dry air at 22°N to warm, moist tropical air at 12°N, with relatively uniform conditions prevailing to the south.

Significant changes in the cloud fields occurred as the surge intensified on the eleventh. First, there was an increase in the areal coverage of convection over the entire winter monsoon region

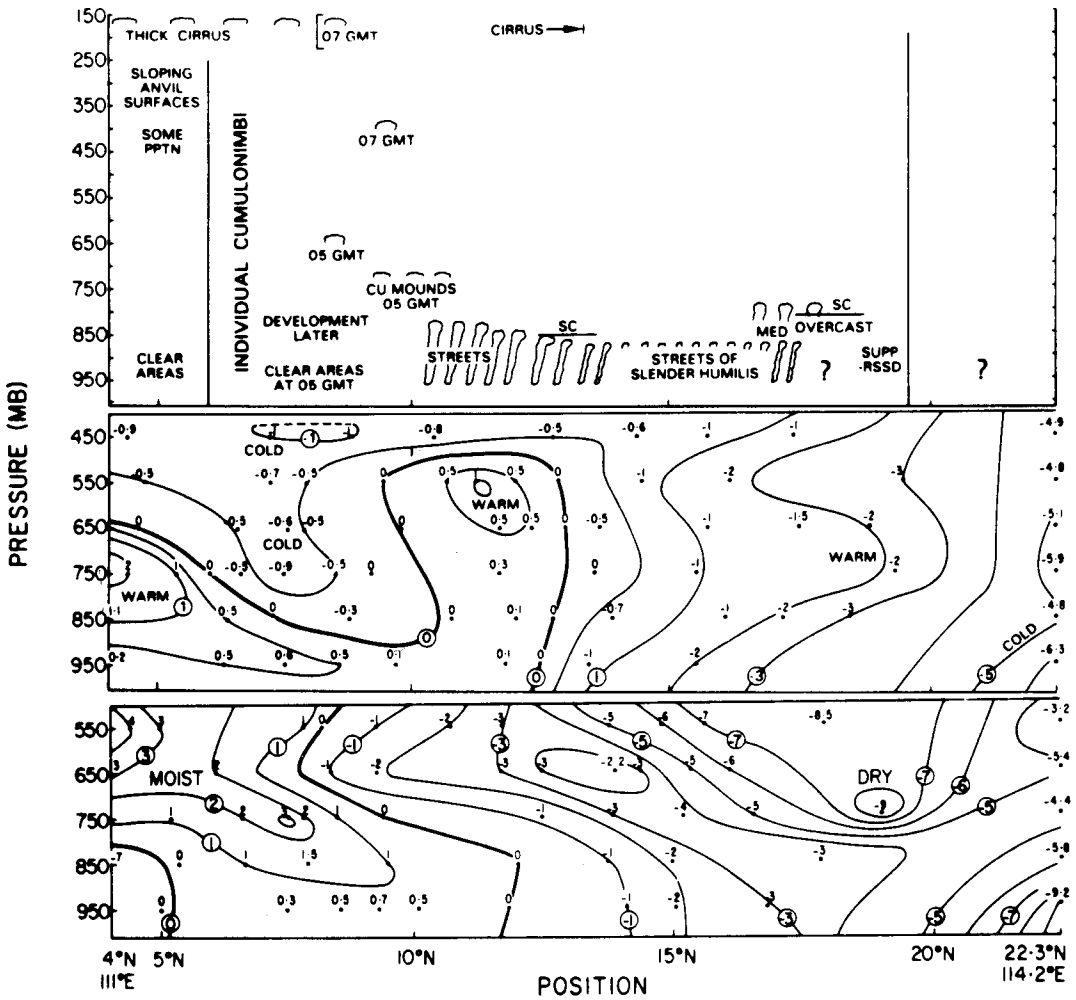

Fig. 10.9. (*a*) Vertical sections for December 10, 1978, ≈6 GMT, from Hong Kong to 4°N, 111°E of clouds *(top)* and variations of temperature (T, °C) and of dew point (T_D, °C) *(bottom)*. Terms T and T_D are variations from the sounding: 950 mb, 22.9, 21.2°C; 850, 17.8, 14.8; 750, 13.5, 6.9; 650, 7.2, 0.4; 550, −0.5, −7.8; 450, −9.3, −17.5. (From Warner 1982b.)

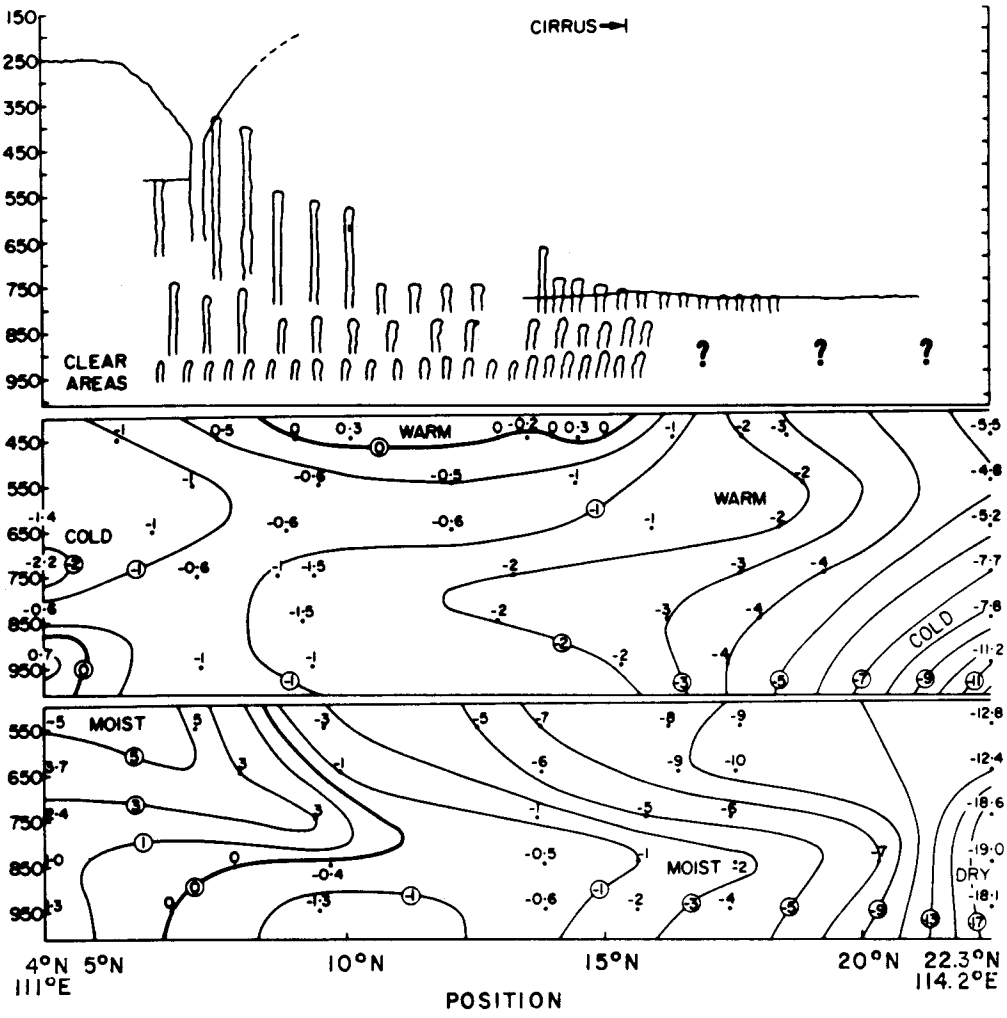

Fig. 10.9. (*b*) As in Fig. 10.9(*a*), except for December 11, ≈6 GMT. (From Warner 1982b.)

(Fig. 10.6). Second, there was a 1- to 2-km deepening of the lower-tropospheric cumulus field over much of the South China Sea (Fig. 10.9b). This deepening of the cumulus layer very likely occurs in response to increased low-level winds and surface sensible and latent heat fluxes on the eleventh. In addition, there was an increase and expansion of the cumulonimbus activity to the north of Borneo. Enhanced deep convective activity in the near-Borneo region accompanying cold surges has been studied by using data from prior years by Chang et al. (1979), who attribute the increased convection to stronger low-level convergence during the surges. Zhu (1983) has recently confirmed this finding by using winter MONEX data and showing, from computations with FGGE IIIb data, that the low-level convergence in a band over the South China Sea along the north coast of Borneo is approximately twice as large during surge periods as it is during lull periods. Chang et al. (1979) note that in some cases of strong cold surges, a vortex disturbance to the north of Borneo can intensify to the level of a weak tropical cyclone. There is some evidence to indicate that a weak vortex to the north of Borneo developed in association with the December 10 to 12 cold surge (J. Simpson, personal communication); however, it remained weak and did not reach tropical cyclone intensity. A final feature dramatically evident from Fig. 10.9(b) is the marked increase in the south-north temperature and dew point gradients in the lowest 2 km. There is a doubling of these gradients over the northern part of the South China Sea from the tenth to the eleventh.

Other studies have also reported an increase in deep convection to the north of Borneo during winter MONEX cold-surge events (Houze et al. 1981; Johnson and Priegnitz 1981; Zhu 1983). A time series of satellite-derived, upper-level cloud

area coverage from Houze et al. (Fig. 10.10) shows that over the sea there is a definite increase in high clouds (associated with deep convection) during surge periods. On the other hand, over the northern Borneo land mass little correlation of upper-level cloud cover with synoptic forcing by cold surges was found. An analysis of precipitation echo area coverage by Houze et al. (1981) using the Massachussetts Institute of Technology radar stationed at Bintulu (Fig. 10.2) reveals very weak correlations between precipitation area and cold surges, both over land and sea. While these findings for limited areas of the Borneo region ($\approx 10^5$ km^2 for the satellite analysis and $\approx 10^4$ km^2 for the radar analysis) do give a quantitative measure of the effects of surges on monsoon convection, the extent to which they can be generalized to sea and land convective behavior over the entire monsoon region, or to other years, is not yet known.

It is well known that flooding conditions along the east coast of peninsular Malaysia and the north Borneo coast can occur during strong cold-surge events (Gan 1970; Ramage 1971; Cheang 1977). Winter MONEX provided little, if any, detailed information on the convective systems that produce such floods; however, some advances in our understanding can probably be gained from studies using existing conventional network and satellite data.

2.2.1.2 Southern Hemisphere. The effects of cold surges on monsoon convection in the Southern Hemisphere are complicated and not well understood. Increases in the strength of the low-level, cross-equatorial flow at times of cold surges have been documented, particularly in the straits between Borneo and West Malaysia/Sumatra (Chiyu 1979). The maximum amplitude of fluctuations of the low-level flow in this region due to cold surges appears to occur near the 600-m level, just above the top of the mixed layer. During winter MONEX, there were several occasions in December and January when corresponding increases of the low-level westerlies over the Java Sea (Fig. 10.2) accompanied these cross-equatorial exchanges (WMO 1980; Williams 1981; Wirjohamidjojo 1982). One such event, between January 13 and 22, has been studied in some detail by Williams (1981). Williams found that accompanying the cold surge at the beginning of this period, a large convective area located in the Java Sea region began moving eastward at about 10 m s^{-1}, expanding as it passed over Indonesia and northern Australia. Such propagating cloud patterns have been observed in this region at other times (Love 1982; McBride 1983), although their linkages with cold surges have not been fully explored. The mesoscale organization of precipitation in these eastward-propagating monsoon systems was not documented by the winter MONEX data network.

In addition to the features described above, there is some evidence to suggest that cold surges from the Northern Hemisphere also interact with circulations in the Southern Hemisphere monsoon trough in a manner that assists in the formation and development of tropical cyclones (Love 1982). The mechanisms that enhance the monsoon convection in these situations are not well known.

2.2.2 Easterly waves. During December 1978, four lower-tropospheric easterly waves were

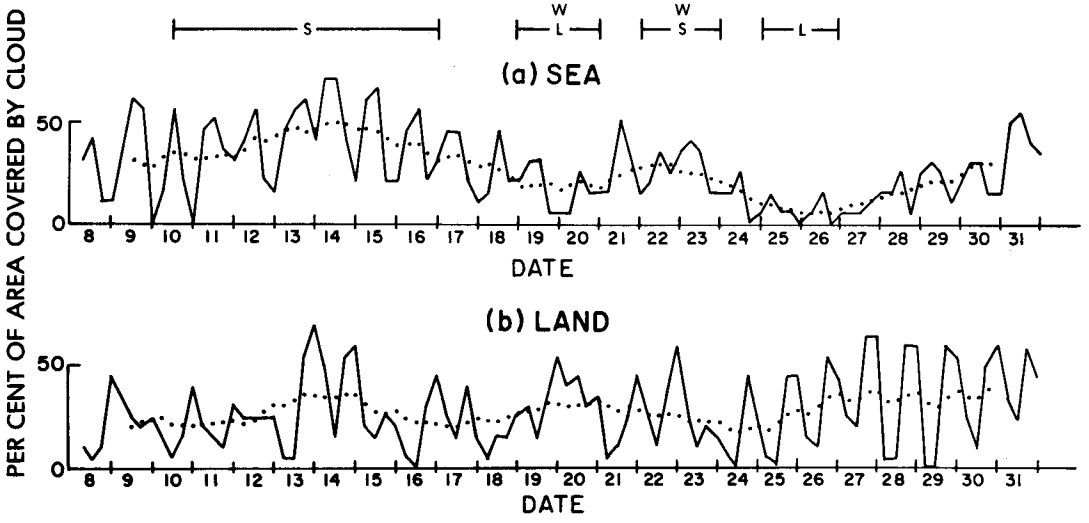

Fig. 10.10. Time series of percent of area covered by upper-level cloud, seen in infrared satellite imagery. (*a*) Over sea. (*b*) Over land areas along the north coast of Borneo. Solid curves show unfiltered observations at 6-h intervals. Dotted curves show overlapping 60-h means. Terms S, W, and L denote periods of surges, waves, and lulls in the synoptic-scale winds. Tick marks are at 0000 LST (1600 GMT). (From Houze et al. 1981.)

tracked, from satellite data and synoptic-chart analyses, across the western Pacific to the South China Sea along 5 to 10°N (Johnson and Priegnitz 1981). These waves appeared to interact with preexisting convection in the region in a variety of ways to produce heavy rain on the east coast of peninsular Malaysia on the fifth (32.9 cm in 24 h at Kuantan), a tropical depression east of the Philippine Islands on the fourteenth (Johnson and Priegnitz 1981), and a complex South China Sea disturbance north of Borneo on the sixteenth and seventeenth (Greenfield and Krishnamurti 1979; Simpson et al. 1981). The most significant effects of easterly waves on convection during winter MONEX appeared to occur north of ≈7°N, with much weaker effects to the south. For example, the time series of cloud cover (Fig. 10.10) prepared by Houze et al. (1981) indicates that there is little, if any, discernible impact of the waves on the magnitude of convective activity along the North Borneo coast. Forecasters in the region have found in other years, however, that the waves can affect convection farther to the south (B. K. Cheang, personal communications).

2.2.3 Near-equatorial disturbances. Frequently during the winter monsoon, near-equatorial disturbances of uncertain origin develop and produce marked modulations in convective activity. Over the South China Sea to the north of Borneo, vortex disturbances are known to form during the northeast monsoon and organize and intensify deep convection in the region (Cheang 1978; Chang et al. 1979). Chang et al. (1982) have found from studying weak Borneo vortex disturbances associated with five cold surges during the period December 1 to January 4 that deep convective activity is most commonly concentrated in the northwest portion of the circulation system. They conclude that on occasions when the vortex disturbances intensify, the organized deep cumulus convection plays an important role in the intensification process (also see Chang et al. 1979).

Other circulations with associated organized convective patterns occur in the region that are not well understood: local Hadley cell intensification accompanying significant, regional, heavy-rainfall events (Chiyu 1984), vortex circulations along the west coast of Sumatra, eastward- and westward-propagating cloud systems over Indonesia, and others.

2.2.4 Interplay of synoptic and diurnal variability. We have seen that synoptic-scale forcing of deep convection in the winter monsoon area can be quite pronounced in some regions. It was earlier noted that, in addition, diurnal forcing mechanisms (e.g., land/ sea breeze circulations, differential radiative cooling, etc.) can also exert a profound control on convection. An important question is whether or not the diurnal modulation of convection is modified in any way during periods of strong synoptic forcing, such as cold surges. This question was addressed by Houze et al. (1981) and Johnson and Priegnitz (1981).

It is clearly evident from Fig. 10.10 that during winter MONEX the diurnal variation in convective activity continues despite periods of longer-term modulations in the magnitude of deep convection. In a sense, then, the atmosphere in the equatorial monsoon region may be considered as responding to the superposition of forcing on various time scales, with the diurnal and three-to-seven-day (cold-surge and wave disturbance time periods) controls both apparent in time series depictions of the total cloud field in the region.

While it is evident that the areal coverage of convection varies on the two time scales described above, it is not obvious that internal properties of the cloud systems themselves, such as vertical motion and precipitation rate, should also exhibit similar variations. Some quantitative information concerning vertical motions within convective systems during winter MONEX has been obtainable from several data sources. First, the favorable placement of three Soviet research vessels in a nearly equilateral triangular array off the north coast of Borneo (Fig. 10.2) has permitted direct computations of vertical motion in the region of the convection (Johnson and Priegnitz 1981; Johnson 1982). Second, winter MONEX radar and aircraft observations have been used by Churchill and Houze (1984b) to deduce vertical motion in mesoscale cloud systems.

Johnson (1982) has used sounding data from the Soviet ships on 11 days in December to compute vertical motion within the mesoscale anvil clouds characterizing the convective systems. The days were segregated according to whether or not synoptic-scale forcing was weak or strong. A period of weak synoptic forcing (December 7 to 10) was referred to as an *undisturbed period,* and a period of strong synoptic forcing (wave disturbances and cold surges; December 11 to 17) was referred to as a *disturbed period.* Vertical motion determined for the entire triangular area was partitioned into cloud and clear-air environment components by assuming subsidence in the clear air at a rate just sufficient to offset radiational cooling to space. The results (Figs. 10.11 and 10.12) at 1400 L, a time when the triangle area had a maximum in area covered by cloud (refer to the position of cloud area maximum in Fig. 10.8), show similar cloud area vertical velocities for both undisturbed and disturbed periods. The characteristic pattern is upward motion in the upper troposphere from about 500 mb to the tropopause, with a peak of 10 to 20 cm s^{-1} near 250 mb, and downward motion below (-3 cm s^{-1} average peak near 650 mb). The upward-motion peak is within the upper-tropospheric mesoscale anvil clouds and reflects the effects of condensation in the anvil

(Brown, 1979). The downward motion in the lower troposphere is associated with hydrometeor melting and precipitation evaporation (Brown 1979; Leary and Houze 1979b).

The important point to be stressed from results in Figs. 10.11 and 10.12 is that while the areal extent of convection is greater during the period disturbed by synoptic-scale forcing (Figs. 10.6 and 10.10), the magnitude of the in-cloud mesoscale vertical velocity does not change significantly. This finding suggests that the magnitude of the vertical velocity in mesoscale anvil cloud systems depends primarily on cloud processes (e.g., condensation, evaporation, and freezing within the clouds), not large-scale forcing. Thus, while the amount and timing of monsoon convection (and its associated diabatic-heating properties) are controlled by diurnal and synoptic variations, the internal characteristics of the convection are apparently not particularly sensitive to these large-scale modulations. This finding may be important for large-scale models of the tropical atmosphere, particularly those that prescribe vertical distributions of diabatic heating and calculate the associated global circulation (Hartmann et al. 1984).

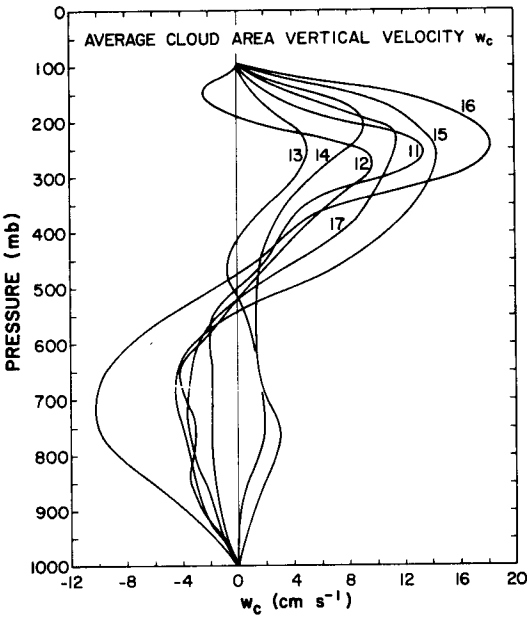

Fig. 10.12. As in Fig. 10.11, except that the data is for a disturbed period (December 11 to 17). (From Johnson 1982.)

2.3 Characteristics of clouds over the South China Sea

The foregoing discussion of the winter monsoon has been concerned mainly with the location of convection in relation to features of the environmental flow pattern. Planetary scale overturning, synoptic-scale disturbances, and diurnally varying local land-sea circulations control when and where convection occurs. Once present, however, the convection influences the structure and continued evolution of the parent circulations. The importance of latent heat released in convection to the development of monsoonal circulations has been indicated by global-modeling studies (Manabe et al. 1970; Webster 1972). For an understanding of the mechanisms by which the monsoon convection feeds back to the large-scale flow in which it is embedded, it has been necessary to determine characteristics of the ensemble of clouds present and to observe and study the structures of examples of the individual clouds, ranging from the smallest cumulus to large cumulonimbus cloud clusters. In this section, we review winter MONEX studies aimed at understanding the wintertime cloud population over the South China Sea and the internal structures of the individual clouds.

Cloud patterns over tropical oceans typically contain a wide spectrum of convective clouds. The number of clouds decreases with increasing cloud size; small nonprecipitating cumulus clouds are numerous, while large complexes of cumulonimbus are comparatively rare. Yet the latter account for most of the rain. This type of cloud population was seen over the tropical Atlantic during the GARP Atlantic Tropical Experiment (GATE) (Houze and Betts 1981), and the data from winter MONEX, discussed here, indicate that the ensem-

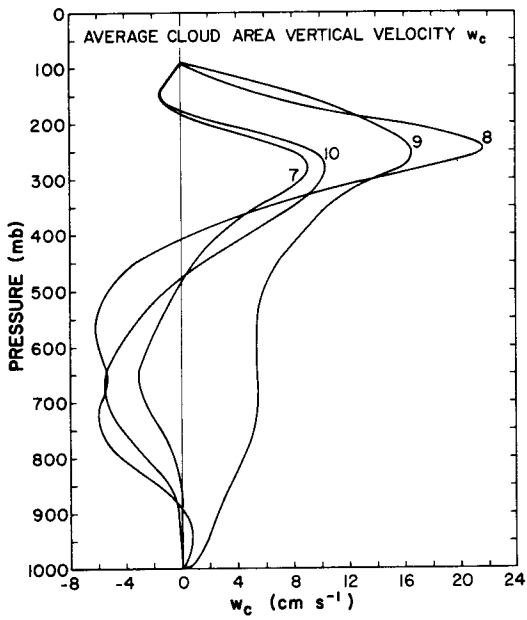

Fig. 10.11. Average cloud area vertical velocity w_c at 1400 LST (16 GMT) for an undisturbed period (December 7 to 10). Days are indicated along the curves. (From Johnson 1982.)

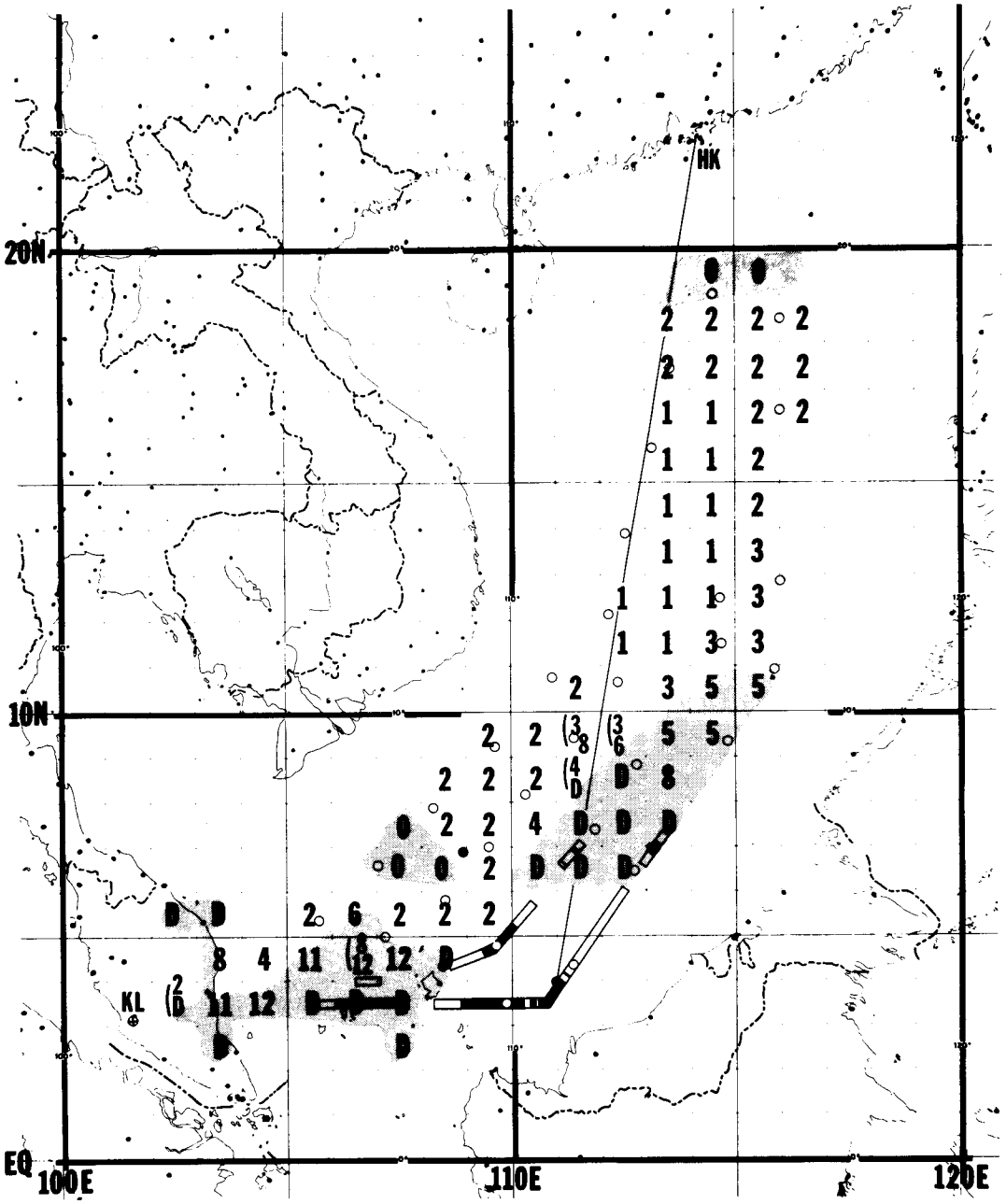

Fig. 10.13. Peak heights (km) of cumulus towers originating near the surface, in 1° × 1° squares, as seen from aircraft on December 10, 1978, 2:30 to 12 GMT. Shading emphasizes deep clouds and suppressed areas. Term D means deep cumulonimbus. Bracketed pairs of values refer to earlier and later measurements, at ≈5 GMT *(top)* and 7 GMT *(bottom)* for those near 9°N. Open boxing shows the track of the aircraft when flying below dense, high overcast. Solid boxing shows flight in clouds at 6.8 km (*top;* Electra) and 7.8 km (*bottom;* P3). Small open circles show dropwindsonde locations. Small solid circles represent the Soviet ship triangle. A line is drawn from Hong Kong to 4°N, 111°E. (From Warner 1982b.)

ble of clouds over the South China Sea in December has similar characteristics.

Cloud population characteristics are tedious to extract from the types of data taken in winter MONEX. Consequently, much of the documentation has concentrated on only a few days of the experiment, with particular emphasis on December 10, 1978. On this day a weak cold surge was developing over the South China Sea, and the cloudiness appeared to be rather typical for this type of situation. The cloud pattern has been mapped by Warner (1981, 1982b), who used photogrammetric techniques on pictures taken aboard research aircraft. His results for December 10, 1978, shown in vertical cross section in Fig. 10.9(a), are summarized in plan view in Figs. 10.13 and 10.14. At low levels, a northeasterly flow of 10 to 15 m s^{-1} predominated, and cloud heights were generally low over the South China Sea between 10 and 20°N where they were evidently suppressed by subsidence. South of 10°N, cloud heights increased dramatically. Warner identified five categories of convective clouds in this population: fractus, humilis, mediocris, con-

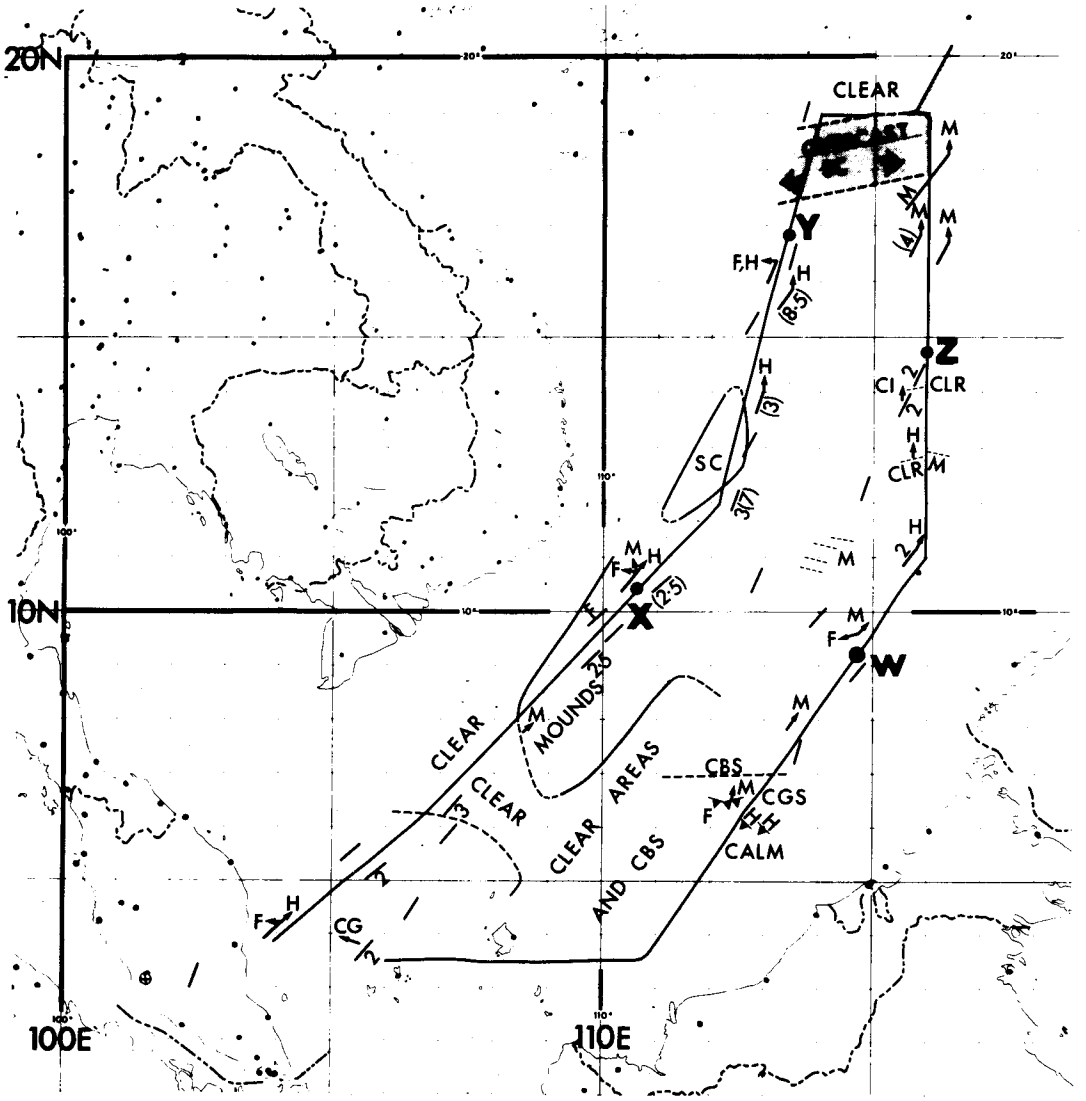

Fig. 10.14. Map of cloud organization. A continuous line shows the track of the WP-3D aircraft. Short solid lines show the direction of streets of cumulus fractus and usually humilis clouds. Numbers alongside are street spacings (km). Where this type of parallel organization was weak, the spacing is enclosed in parentheses. Short arrows occasionally show directions of tilt of cumulus fractus (F), humilis (H), and mediocris (M). Organization other than parallel, for example, at an angle to the winds, is indicated by dashed lines. Terms W, X, Y, and Z indicate positions of photographs shown in Figs. 10.18, 10.17, 10.15, and 10.16, respectively. (From Warner 1982b.)

gestus, and cumulonimbus. In addition, stratocumulus and cirrus layers were noted. Comparison of Figs. 10.13 and 10.14 shows the expected relation between cloud types and heights; the fractus, humilis, and mediocris had low tops, while the congestus and cumulonimbus exhibited high tops.

Warner's photogrammetry showed the fractus to have typical depths of 0.2 km and widths of 0.25 km, while for humilis the dimensions were 0.7 and 0.4 km, respectively. The number densities of these small clouds were as great as 1.5 km^{-2}. Photographs showing fractus and humilis are shown in Figs. 10.15 and 10.16 (positions of photographs are shown in Fig. 10.14). In the example in Fig. 10.15, the clouds were smaller and aligned in cloud streets, while in Fig. 10.16 the clouds were somewhat larger, more densely packed, and not aligned. The number densities and spatial arrangement of fractus and humilis (e.g., random distributions versus cloud streets) varied considerably over distances of 100 km.

Mediocris had typical depths of 2 km. Their number densities were quite variable, occasionally reaching one per 25 km^2. A photograph showing mediocris as the largest clouds in a field also containing fractus and humilis is provided in Fig. 10.17.

Congestus were $\approx$3 km in depth. They are much rarer than mediocris, occurring primarily in the vicinity of the deep cumulonimbus clouds found over the southern part of the South China Sea. Figure 10.18 shows congestus in the foreground of a large cumulonimbus complex.

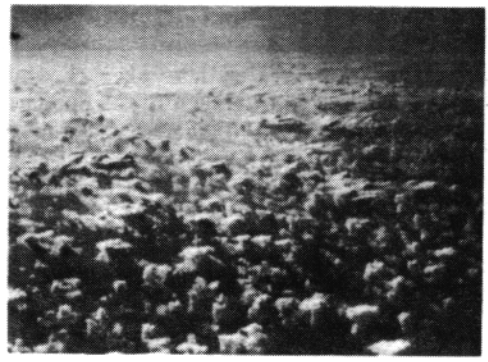

Fig. 10.16. Fractus and humilis with great number density over the South China Sea, December 10, 1978, 736 GMT. Photograph by C. Warner looking westward from the WP-3D aircraft flying at an altitude of 7.8 km at 14.7°N, 116°E. (From Warner 1981.)

The deep cumulonimbus near the North Borneo coast produced the widespread upper-level cloud seen at the time of its maximum area in Fig. 10.6(a) and flown under and through by the research aircraft (Fig. 10.13). This giant cloud system is an example of a cloud cluster of the type seen in GATE (Houze and Betts 1981), and it has been studied extensively by several investigators

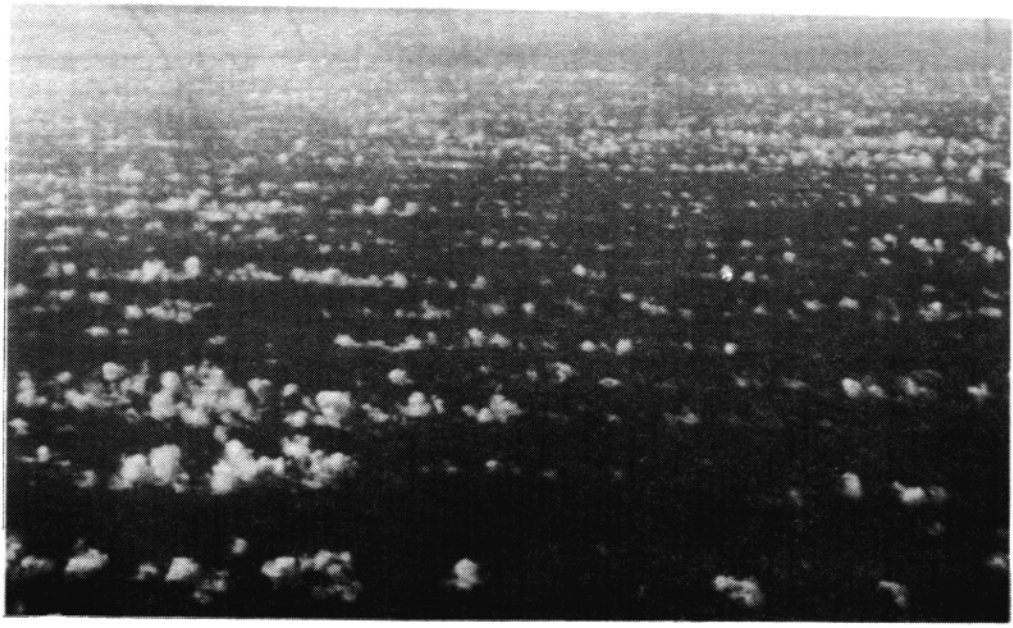

Fig. 10.15. Cloud streets of fractus and humilis over the South China Sea. December 10, 1978, 608 GMT. Photograph by R. A. Houze looking west from the WP-3D aircraft flying at an altitude of 6.8 km at 16.9°N, 113.4°E.

Fig. 10.17. Fractus, humilis, and mediocris over the South China Sea, December 10, 1982, 451 GMT. Photograph by J. Simpson looking northwest from the WP-3D aircraft flying at an altitude of 6.1 km (483 mb) at 10.4°N, 110.6°E. (From Warner 1982b.)

Fig. 10.18. Congestus clouds over the South China Sea to the north of a dark mass of cumulonimbus 300 km distant, which was later penetrated by the WP-3D aircraft, December 10, 1978, 838 GMT. Photograph by R. H. Simpson looking toward 220° from the WP-3D flying at an altitude of 7.8 km at 9.2°N, 114.7°E. (From Warner 1981.)

(Holland and Keenan 1980; Houze et al. 1981; Johnson and Priegnitz 1981; Warner 1981, 1982b; Johnson 1982; Johnson and Kriete 1982; Churchill and Houze 1984a, 1984b). Its life cycle followed the conceptual model illustrated in Fig. 10.19. This model, put forth by Leary and Houze (1979a) and subsequently discussed and refined by Houze et al. (1981), Houze and Betts (1981), Houze (1982), and Houze and Hobbs (1982), appears to apply to mesoscale convective systems rather generally, although the mechanism initiating the original convective cells varies. In this case, the deep convection was triggered by the nocturnal land breeze's convergence with the prevailing monsoon current just off the coast. Just before local midnight (1600 GMT), convective cells appeared in a line parallel to and within 20 to 30 km of the coastline. In this early stage, the cells increased in both number (Fig. 10.20a) and intensity (indicated by a decreasing minimum cloud top temperature in Fig. 10.21). The maximum number and intensity of cells were reached at about 000 GMT, when the total area covered by precipitation (indicated by the radar echo curve in Fig. 10.21) was greatest. However, the number density of cells (i.e., the number of cells

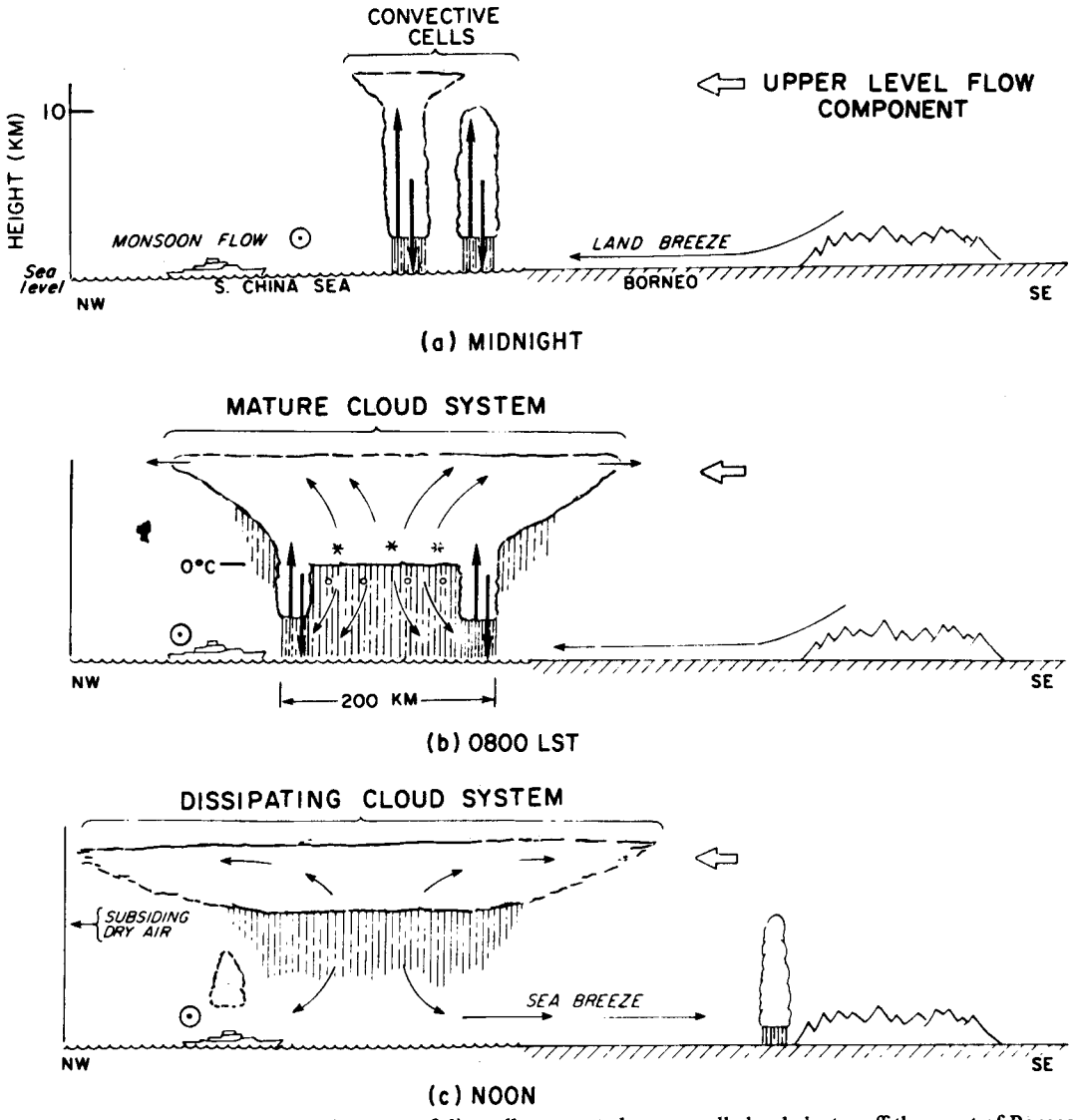

Fig. 10.19. Schematic of the development of diurnally generated, nonsquall cloud cluster off the coast of Borneo. Three periods of development are illustrated: (*a*) midnight, (*b*) 08 LST and (*c*) noon. Various arrows indicate airflow. A circumscribed dot indicates a northeasterly monsoon flow out of the page. A wide-open arrow indicates the component of the typical east-southeasterly upper-level flow in the plane of the cross section. Heavy vertical arrows in (*a*) and (*b*) indicate cumulus-scale updrafts and downdrafts. Thin arrows in (*b*) and (*c*) show a mesoscale updraft developing in a mid- to upper-level stratiform cloud with a mesoscale downdraft in the rain below the middle-level base of the stratiform cloud. Asterisks and small circles indicate ice above the 0°C level melting to form raindrops just below this level. (From Houze et al. 1981.)

per unit area of echo), shown in Fig. 10.20(b), was maximum at the beginning of the cluster (about 1600 GMT, December 9). During the later stage, an increasing proportion of the total rain area detected by radar was stratiform (Fig. 10.20c). After 2330 GMT, the area-integrated precipitation in the form of stratiform rain exceeded that of the convective cells. Altogether, about 46% of the total amount of rain observed in this cloud system was stratiform (Fig. 10.20d).

This ratio of stratiform to total rain is similar to that found in other tropical cloud clusters (Table 10.1). The mesoscale updraft and downdraft associated with the stratiform region of tropical cloud clusters have been discussed by Houze and Betts (1981), Houze (1982), and Houze and Hobbs (1982). These drafts are in the range of 10 to 50 cm s^{-1}. The mesoscale updraft occurs in a cloud layer extending from about 650 mb ($\approx$0°C) to the top of the troposphere, while an unsatu-

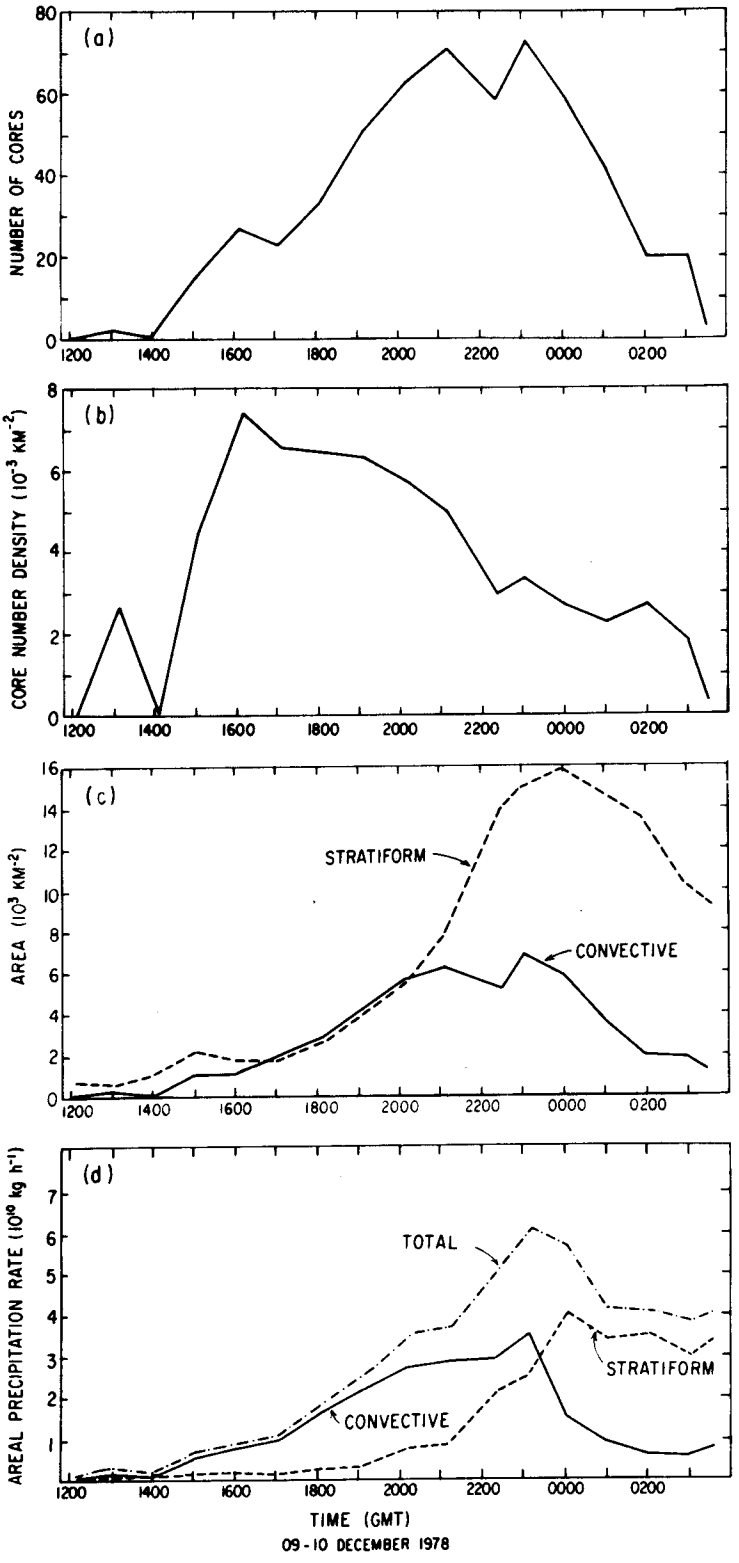

Fig. 10.20. (*a*) Number of convective cores. Radar echo and precipitation characteristics of the large cloud cluster north of Borneo on December 9 to 10, 1978. (*b*) Number density of convective cores in the cluster, computed by dividing the values shown in (*a*) by the total area covered by precipitation at 3 km shown in (*c*). (*c*) Area covered by objectively determined stratiform (dashed curve) and convective precipitation (solid curve) at 3 km defined by a 1-dBZ threshold. (*d*) Area-integrated precipitation rate for the cluster at 3 km. The top (dot-dashed line) represents the sum of the convective (solid line) and stratiform (dashed line) components of precipitation. (From Churchill and Houze 1984a.)

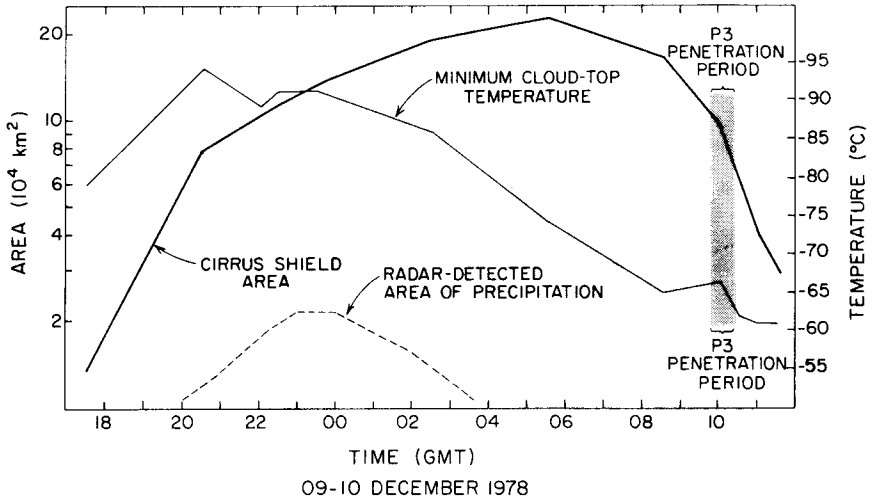

Fig. 10.21. Cirrus shield area, precipitation area, and minimum cloud top temperature for the large cloud cluster north of Borneo on December 9 to 10, 1978. The area covered by the cirrus shield (thick curve) and the minimum cloud top temperature (thin curve) were determined from infrared satellite imagery. The area covered by precipitation from 20 GMT, December 9, to 333 GMT, December 10, is shown by the radar echo area (dashed curve) determined from the land-based radar. The shaded column indicates the period during which the WP-3D aircraft was in the cluster. (From Churchill and Houze 1984a.)

rated mesoscale downdraft (of the type described by Zipser 1969, 1977) exists below this level. Thermodynamic data from winter MONEX ship and aircraft soundings indicate that the December 10 cloud cluster near the North Borneo coast indeed had an unsaturated mesoscale downdraft in the low to mid troposphere (Johnson and Priegnitz 1981; Johnson and Kriete 1982; Warner 1982b; Churchill and Houze 1984a). Vertical motions deduced kinematically from wind data obtained on December 10 confirm the mesoscale downdraft and in addition, show that mesoscale updraft was present in the stratiform cloud layer aloft (Johnson 1982). Vertical motions deduced from the ice budget of the stratiform cloud layer provide an additional confirmation of the mesoscale updraft (Churchill and Houze 1984b).

TABLE 10.1 *Stratiform rain amounts in squall and nonsquall tropical cloud clusters*

Investigators	Type of cluster	Stratiform rain amount
Houze (1977)	Squall	40%
Gamache and Houze (1983)	Squall	49%
Chong (1983)	Squall	31%
Houze and Rappaport (1984)	Squall	42%
Leary (1984)	Nonsquall	30%
Churchill and Houze (1984a)	Nonsquall	46%

Note: Amount is expressed as a percentage of the total rain produced by the cluster.

Moreover, ice particle images obtained on research flights through the stratiform cloud layer were consistent with the presence of the mesoscale updraft (Churchill and Houze 1984a; Houze and Churchill 1984). In stratiform regions, the winter MONEX cloud clusters, sampled on December 10 and on other days, exhibited apparent ice particle growth by deposition and aggregation. Upward motions in the higher cloud layers of stratiform regions appeared to be strong enough to produce water saturation (inferred from the observation of branched crystals) yet weak enough to allow ice particles with terminal fall speeds of 1 to 2 m s^{-1} to drift downward.

The vertical air motions and ice particles in the stratiform areas contrasted sharply with those seen in convective regions. Warner and McNamara (1984) found peak drafts in winter MONEX convective cells to by typically 1 to 6 m s^{-1} (Fig. 10.22, dark shading). These values are similar to the updraft speeds they found in summer MONEX convective cells (lightly shaded and nonshaded bars in Fig. 10.22), as well as to vertical velocities observed in GATE convection (LeMone and Zipser 1980; Zipser and LeMone 1980) and convection in hurricanes (Jorgensen 1984). As pointed out by Zipser and LeMone (1980), these updraft speeds in tropical oceanic convection are smaller (by about a factor of two) than those observed in midlatitude continental thunderstorms. Nonetheless, they are large compared with the mesoscale updraft in the stratiform regions of cloud clusters, and correspondingly the ice particle growth in winter MONEX convective cells was seen to be dominated by riming rather

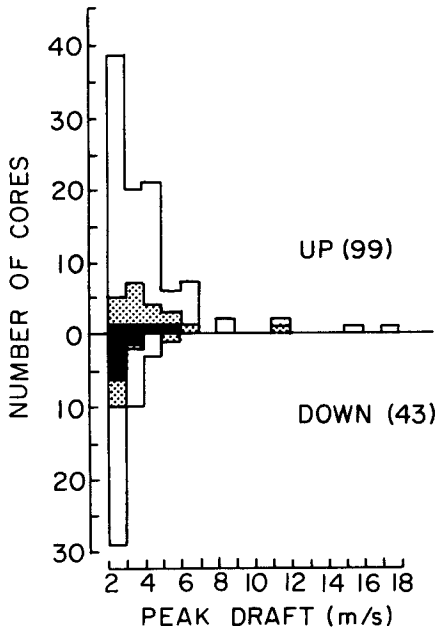

Fig. 10.22. Histograms of peak drafts with updrafts extending above and downdrafts below the centerline. Solid shading indicates draft cores in WMONEX, light shading those over the Arabian Sea, and the remainder those over the Bay of Bengal. (From Warner and McNamara 1984.)

than by aggregation of crystals (Churchill and Houze 1984a; Houze and Churchill 1984).

2.4 Effects of mesoscale convective systems on larger scales of motion

2.4.1 Regional circulation feedbacks. In the previous section it was noted that the winter MONEX mesoscale convective systems to the north of Borneo exhibit many similarities to those observed in other tropical regions (e.g., in GATE). Because of the similarities in convective structure, it is not surprising that similar feedbacks to larger scales of motion have been found. These feedbacks extend throughout the troposphere from the boundary layer to the tropopause.

Observations from GATE have permitted a number of detailed analyses of the boundary layer modification by both squall and nonsquall cloud clusters to be completed (Houze and Betts 1981). Studies of squall clusters have shown that extensive areas (≈500 km on a side) of the boundary layer can be significantly modified by downdraft outflows from the precipitating cloud systems (Houze 1977; Zipser 1977; Fitzjarrald and Garstang 1981; Johnson and Nicholls 1983). The resultant wakes, which are of variable depth and horizontal dimension, often persist for extended periods of time (≈12 h or longer). They can modify the convective field in their vicinity by (1) suppressing future convection throughout much of their interior and (2) generating new convection on their boundaries by providing a mechanism to produce low-level convergence.

The slow recovery of wakes, which frequently reach synoptic-scale dimension, is assisted by the lower-tropospheric subsidence driven by precipitation evaporation beneath the stratiform portions of the mesoscale convective systems. The subsidence contributes to the maintenance of a strong inversion atop the mixed layer, which suppresses its growth. Evidence of the warm, dry subsiding air in the lower troposphere is found upon examination of sounding data from the Soviet research vessel *Akademician Korolov* at 4°N, 111°E as well as from aircraft dropwindsonde data in the path of the convection to the north of Borneo (Webster and Stephens 1980; Warner 1982b; Johnson and Kriete 1982). Tephigram plots from Warner (1982b) in Fig. 10.23 illustrate the char-

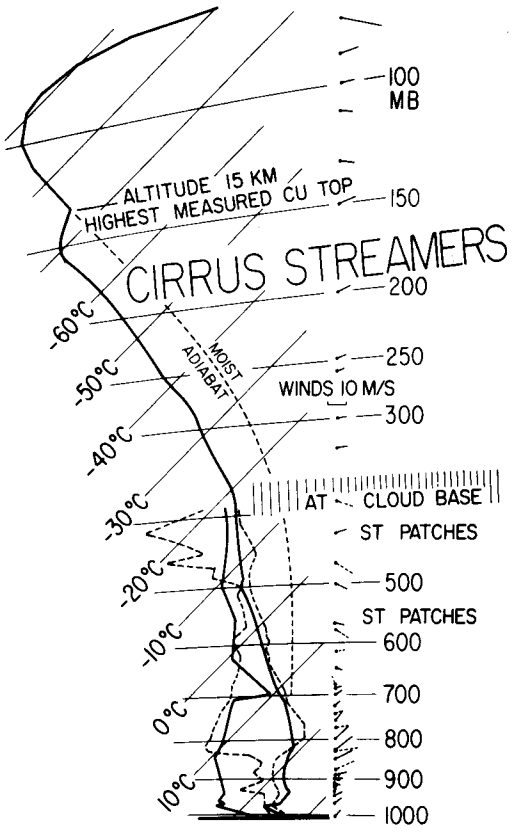

Fig. 10.23. Tephigrams from the Soviet ship *Akademician Korolov* at 4°N, 111°E at 900 GMT (solid lines) and from aircraft dropwindsonde at 4.3°N, 111.3°E at 941 GMT (dashed lines). The aircraft was flying near the base of dense, high overcast in the area. Patches of stratus were seen near 435 and 560 mb. Cirrus streamers were present in the interval from 150 to 230 mb. The highest measured cumulus top on December 10 reached 15 km (130 mb). (From Warner 1982b.)

acterisitc onion-shaped structure of the soundings in the lower troposphere beneath the upper-tropospheric stratiform cloud shield (Zipser 1977; Leary 1980), with warm, dry air capping a shallow mixed layer. The modified air mass in this region was advected to the southwest by the northeast monsoon flow and eventually incorporated into the channeled, low-level, cross-equatorial flow between Borneo and Sumatra.

The generation of the new convection by expanding wakes, whose boundaries are frequently defined by cloud arc lines, occurs in the winter MONEX region (Warner 1982b; Churchill and Houze 1984a) as it does elsewhere in the tropics (e.g., in the GATE region; Houze and Betts 1981). Churchill and Houze describe the development of the very large mesoscale convective system on December 10. Downdraft outflows, as evidenced by cloud arc lines viewed from research aircraft, were prevalent during the expansion of the cloud system. Clearly, boundary layer processes are important in this upscale development of convection; however, winter MONEX boundary layer data are too sparse to use to examine the processes in detail.

Mesoscale convective effects on the large-scale circulation also occur in the middle and upper troposphere. Midlevel cyclonic circulations as observed in GATE cloud clusters (Leary 1979; Gamache and Houze 1982; Houze and Rappaport 1984) are more difficult to identify with winter MONEX data due to the sparsity of observations. Nevertheless, significant large-scale convergence has been observed near the 0°C level in winter MONEX mesoscale convective systems (Johnson and Priegnitz 1981; Warner 1982b; Johnson and Kriete 1982). Figure 10.24, taken from Johnson and Kriete, illustrates the relative flow field in a NW–SE cross section through the mesoscale anvil of December 10 at 600 GMT. In this figure streamlines depict the mesoscale circulation deduced from sounding data, and shading indicates relative humidity values greater than 80% (defining the approximate location of the upper-level cloud system). From these results and those reported in the studies cited above, it is clear that the mesoscale cloud system feeds back to the large scale to alter the mid- to upper-tropospheric flow in two ways: by creating (1) midlevel (≈500 mb) inflow (and convergence; Johnson and Priegnitz 1981) and (2) upper-level outflow (centered near 175 mb) and divergence on a 500-to-1000-km scale. It is important to note that these circulation features closely resemble those observed in similar mesoscale convective systems elsewhere in the tropics (the eastern Pacific: Zipser 1969; the east-

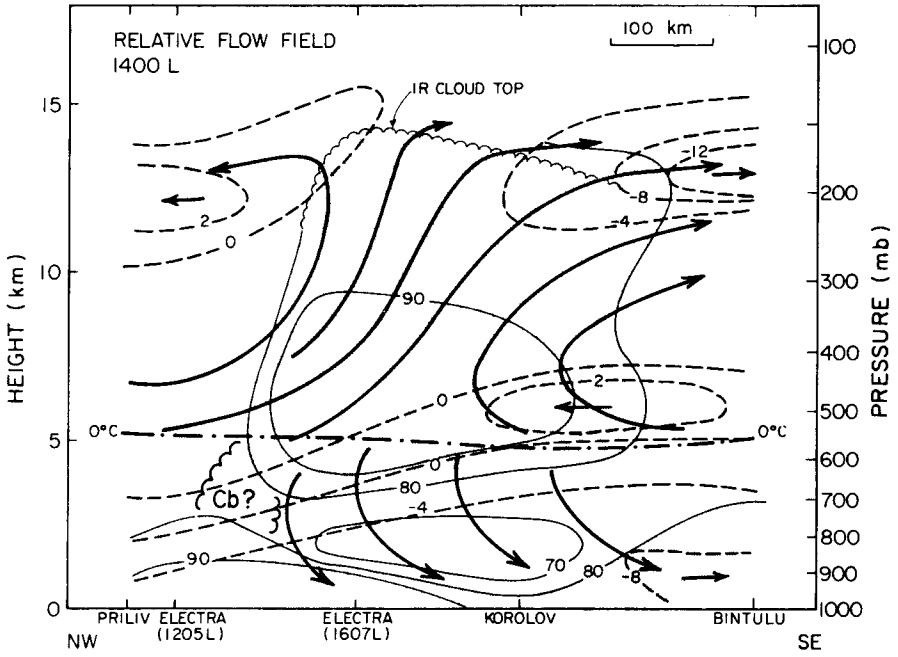

Fig. 10.24. NW–SE cross section of mesoscale anvil system at 600 GMT (14 LST). Streamlines, which indicate the mesoscale flow relative to the anvil cloud, have been determined by assuming 6-m s^{-1} movement of the anvil from right to left and using the vertical velocity for the anvil system at this time computed in Johnson (1982). Solid contours indicate relative humidity, with shading for values greater than 80%. The horizontal component of the wind (units of m s^{-1}) in the plane of the section is shown by dashed lines. Data from *Electra* dropwindsondes extend from ≈450 mb to the surface. Term Cb denotes possible cumulonimbus at the leading edge of an anvil cloud system, though data do not exist to confirm its existence. (From Johnson and Kriete 1982.)

ern Atlantic: Houze 1977; Zipser 1977; Gamache and Houze 1982; Houze and Rappaport 1984) and at midlatitudes (Ogura and Liou 1980; Fritsch and Maddox 1981; Leary and Rappaport 1983; Maddox 1983; Smull and Houze 1984).

2.4.2 Vertical heating profiles and planetary scale circulation feedbacks. The mesoscale convective systems observed during winter MONEX exhibited cloud and precipitation structures more elaborate than simple hot towers. Convective-scale towers with nearly undilute ascent from the boundary layer to the tropopause indeed exist in the tropics, and their important role in the general circulation was elucidated by Riehl and Malkus (1958). However, it appears from Line Islands, GATE, MONEX, and other field experiments carried out in the past 25 years that there is, in addition, a significant mesoscale component to oceanic tropical convective systems. The finding by Cheng and Houze (1979), for example, that approximately 40% of the precipitation in GATE was associated with the mesoscale stratiform portion of tropical cloud clusters suggests that a determination of the diabatic heating within these clusters will require careful consideration of both convective-scale and mesoscale components.

Houze (1982) has examined this issue by investigating the vertical distribution of heating in an idealized tropical oceanic cloud cluster. A four-stage schematic of the life cycle of an idealized cluster proposed by Houze based on GATE and MONEX results is shown in Fig. 10.25. It consists of an early stage (Fig. 10.25a), when only convective cells exist; a mature stage (Fig. 10.25b) when both convective cells and a mesoscale stratiform precipitation region coexist; a weakening stage (Fig. 10.25c), characterized by primarily stratiform precipitation; and a dissipating stage (Fig. 10.25d), when precipitation ends and the upper-level cloud breaks up. Houze in his analysis considers the diabatic processes of condensation, evaporation, freezing, melting, and radiation.

Using observed properties of the cloud clusters studied by Leary and Houze (1980), Houze (1982) computed the total heating by the idealized cluster during its mature stage over the area A in Fig 10.25(b). The results are shown in Fig. 10.26 (solid curve) along with the separate contribution by the convective-scale component (dashed curve). The total heating, which in Houze's analysis is the sum of the contributions of convective cells, mesoscale stratiform cloud and precipitation processes, and radiative heating, has a pronounced peak in the upper troposphere between 8 and 10 km and reduces to near zero below about 4 km. The concentration of heating in the upper troposphere is a consequence of two primary factors: (1) a midtropospheric peak in the convective-scale heating and (2) an upper-tropospheric-heating maximum and lower-tropospheric-cooling maximum associated with the stratiform precipitation region of the idealized cluster (Fig. 10.27, thin curve). Houze shows that the primary contributor to the convective-scale heating is condensation in the convective updrafts. The mesoscale heating profile is primarily determined by condensational heating in the stratiform cloud region above the 0°C level and melting and evaporative cooling below.

The conclusions reached by Houze (1982) regarding the vertical distribution of the heating in tropical cloud clusters are supported, as he points out, by a number of GATE studies of the variation of rawinsonde network–determined vertical motion within clusters over their life cycles. Typically, the maximum upward vertical motion is in the low to mid troposphere in the early stage of the cluster development (convective cells predominate, yielding a heating profile like the dashed curve in Fig. 10.26) and, subsequently, there is a shift in the peak upward motion to the upper troposphere during the mature and dissipating stages (stratiform precipitation predominates and the heating profile is as illustrated in Fig. 10.27). Houze (1982) shows that diabatic heating computed from large-scale rawinsonde data (e.g., the apparent heat source of Yanai et al. 1973) frequently exhibits a similar variation over the cluster life cycle because the vertical advection term is the dominant one in the expression for total heating. Thus, the heating profiles computed by Houze (1982) based on estimates of actual physical processes in an idealized cloud cluster are confirmed to some degree by independent large-scale rawinsonde measurements.

Further quantitative confirmation of the idealized cluster model of Houze (1982) has been recently provided by Johnson and Young (1983). They used sounding data from the winter MONEX Soviet ship triangle (Fig. 10.2) to compute the apparent heat source for the North Borneo cluster at times during which it was determined that primarily stratiform rainfall existed over the triangle. The composite profile for seven separate days in December 1978 (Fig. 10.27, heavy curve) is in good agreement in both shape and amplitude with that of Houze (1982). As well as can be determined, the area-averaged precipitation rates in the two studies are approximately the same. The good agreement between these two independent estimates of mesoscale anvil heating is mutually supportive of both studies' findings, and furthermore, it can be concluded that the hypotheses advanced by Houze (summarized in Fig. 10.25) to account for the net heating in mesoscale anvils are probably quite realistic.

The significance of these findings for planetary scale circulation studies and global circulation models is at least twofold. First, it has been shown by a number of authors through application of linear and nonlinear models that the response of the

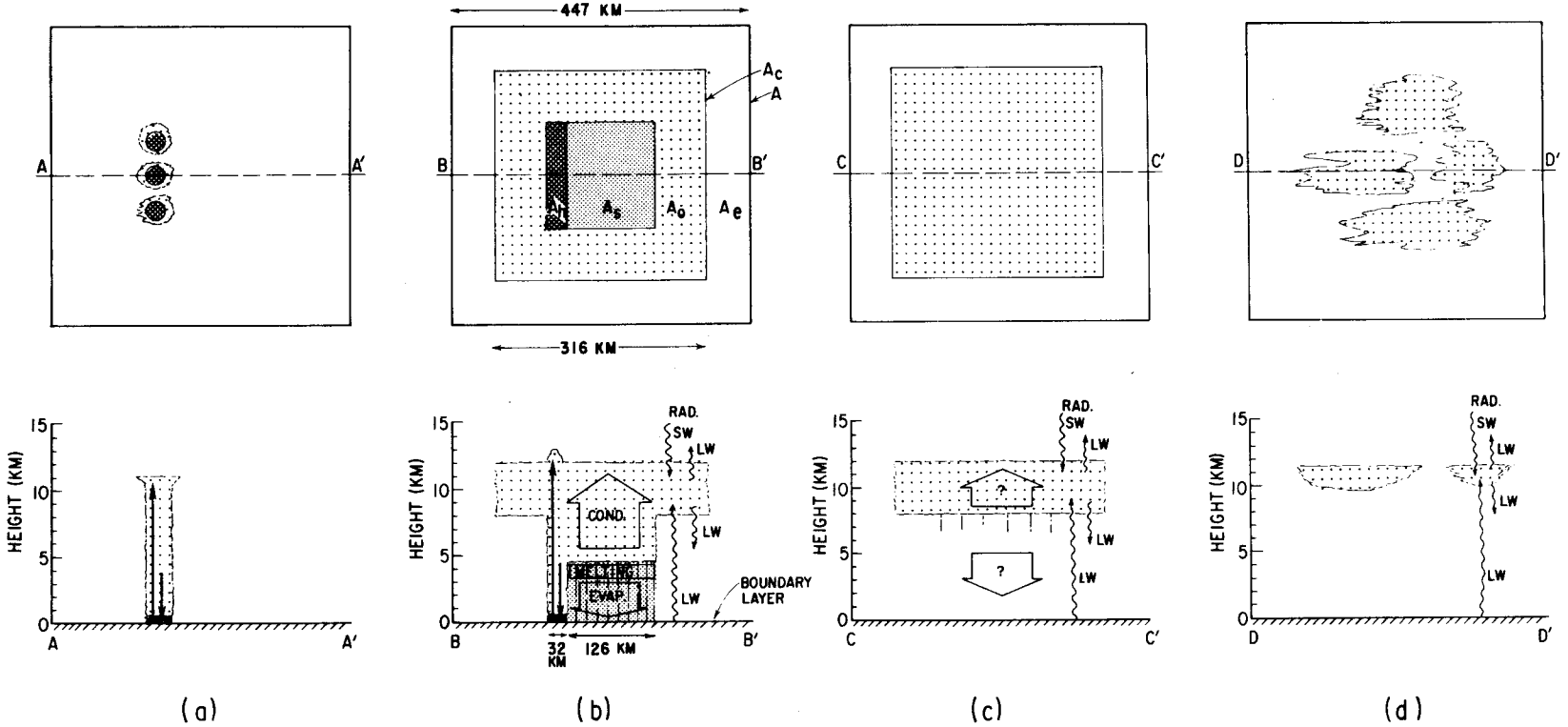

Fig. 10.25. Schematic of a tropical cloud cluster in four successive stages of development. (*a*) Early stage in which cluster consists of isolated precipitating convective towers. (*b*) Mature stage in which a cloud shield has developed and covers area A_c, convective cells (hot towers) are located in area A_h, stratiform precipitation is falling from a middle-level cloud base within area A_s, and an area A_o is covered by upper-level cloud overhang. (*c*) Weakening stage in which convective cells have disappeared, stratiform precipitation remains, and upper cloud is becoming thin and breaking up. (*d*) Dissipating stage in which no precipitation remains and upper cloud is becoming thin and breaking up. In (*a*) and (*b*), cumulus-scale updrafts and downdrafts are denoted by straight solid arrows. In (*b*) and (*c*), mesoscale updraft and downdraft are shown by wide, open arrows; condensation (COND.) in the mesoscale updraft, evaporation (EVAP.) in the mesoscale downdraft, and the melting layer in the stratiform precipitation region are indicated. Question marks indicate that the existence of the mesoscale drafts in stage (*c*) is uncertain. Shortwave (SW) and longwave (LW) radiation (RAD.) are denoted by wavy arrows. The upper panels of (*a*) to (*d*) are plan views. The lower panels are vertical sections along the indicated horizontal line segments. Area A is a large-scale region containing the cloud cluster, and A_e is a cloud-free environmental area surrounding the cluster. (From Houze 1982.)

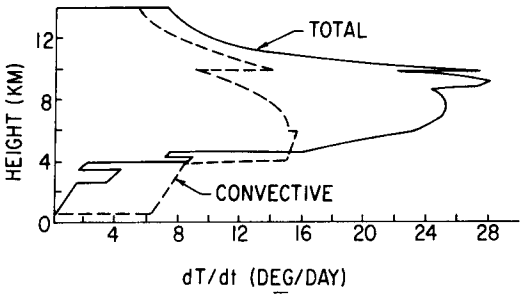

Fig. 10.26. Total heating of large-scale area A (seen in Fig. 10.25[*b*]) by the idealized mature cloud cluster (solid curve). The total heating by the convective towers alone (dashed curve) is shown for comparison. (From Houze 1982.)

atmospheric models to convective heating is critically dependent on the vertical distribution of the heating. Hartmann et al. (1984), for example, have recently demonstrated that simulations of the tropical east-west or Walker circulation are quite sensitive to the assumed shape of the heating profile. They find that the most realistic Walker circulation is obtained when the assumed profile is such that it has a sharp maximum in the upper troposphere near 400 mb with no heating below 600 mb, like the mature-cluster heating profile or solid curve in Fig. 10.26. Unrealistic results are obtained when a profile of heating is used that resembles the convective-scale heating (dashed curve in Fig. 10.26).

Second, the presence of mesoscale stratiform precipitation regions in tropical cloud clusters has an impact on parameterization of cumulus convection in large-scale prediction models (Anthes 1983; Frank 1983; Pielke 1984). Diagnostic studies have shown that mesoscale transports of mass, heat, and moisture can be comparable to convective-scale transports (Johnson 1980; Leary and Houze 1980). Johnson (1984) has used the winter MONEX mesoscale anvil vertical heating profiles of Johnson and Young (1983) to partition the total heating profile of Yanai et al. (1973) for the tropical western Pacific into cumulus and mesoscale components. The findings, which are in accord with Houze (1982), suggest that certain types of cumulus parameterization schemes—that is, those that assign a vertical distribution of heating—may incur serious errors if the proportion of cumulus versus mesoscale-produced rainfall in the region of model application is different from that in the region where the assigned distribution was derived. Schemes that permit vertical heating distributions to evolve during the course of model integrations (e.g., Arakawa and Schubert 1974) are preferred, at least on a physical basis, over those that prescribe the distributions. However, the cloud models invoked to simulate the evolving heating distribution should take into account the mesoscale stratiform contributions to the diabatic processes. A closed scheme including these mesoscale aspects has not yet been developed.

2.4.3 Radiative effects. An important feature of mesoscale convection and its feedback to the large-scale circulation is the field of radiative

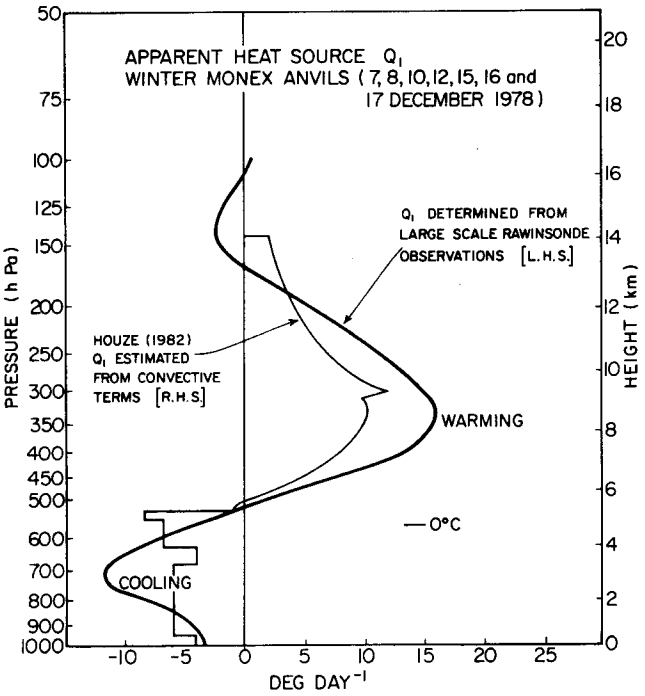

Fig. 10.27. Comparison of apparent heat source Q_1 obtained by Johnson and Young (1983) using rawinsonde data (heavy curve) with that obtained by Houze (1982) using radar cloud structure and precipitation data (light curve). L.H.S. (R.H.S.) refers to the left-hand side (right-hand side) of the heat budget equation written in a form with all diabatic terms on the R.H.S. The curve from Houze (1982) represents the total heating by nonradiative mesoscale processes. (From Johnson and Young 1983.)

heating within and in the environment of the precipitating cloud systems. The North Borneo mesoscale convective systems and others within the monsoon region produce extensive upper-tropospheric cloud shields that persist for extended periods of time. Differential radiative heating, both in the horizontal and in the vertical, in the region of these clouds can significantly affect the evolution of clusters. Gray and Jacobson (1977) and Cox and Griffith (1979) have proposed that changes in the horizontal variation of radiative divergence in the vicinity of cloud clusters form day to night can lead to a mass circulation that enhances cloud development at night.

With reference to winter MONEX convection, Webster and Stephens (1980) have examined the vertical variation of radiative heating in upper-level cloud shields. Their results, depicted in Fig. 10.28, show that for deep mesoscale anvil clouds like those observed in winter MONEX, the combination of shortwave heating near cloud top (during the day) and longwave cooling above longwave warming in the cloud layer is destabilizing (see also Albrecht and Cox 1975; Cox and Griffith 1979). Webster and Stephens find that for deep, moderately precipitating anvils, the radiative effects are secondary to condensation effects; whereas for shallow cirrus, radiative destabilization can be of primary importance in the maintenance of the cloud systems. If we extend these findings to the synoptic- to planetary scale dimension of the monsoon convective system, it is evident that cloud-induced radiative perturbations may be an important mechanism by which the deep convection feeds back to alter the large-scale flow.

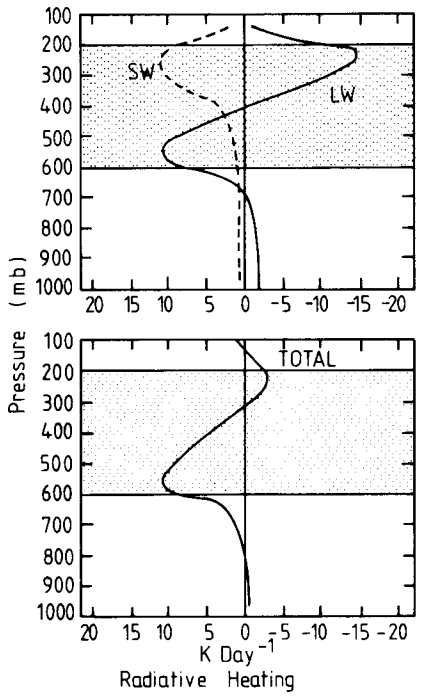

Fig. 10.28. Vertical distribution of radiative heating in the visible (dashed) and infrared (solid) relative to a cloud slab between 200 and 500 mb. (From Webster and Stephens 1980.)

2.4.4 Effects in the lower stratosphere. In addition to the effects of monsoon convection on the troposphere that we have just discussed, winter MONEX data have also provided some information on the impact of the mesoscale convective systems on properties of the lower stratosphere. Various authors have recently explored the roles of deep convection in the monsoon area as a source of energy for stratospheric motions (Holton 1972) and a global source of stratospheric water vapor (Newell and Gould-Stewart 1981; Danielsen 1982; Kley et al. 1982; Atticks and Robinson 1983). For a test of the ideas that are proposed on these subjects, it is important to know the effects of the individual cloud systems on the lower stratosphere.

Johnson and Kriete (1982) examined the passage of three mesoscale convective systems across the southern portion of the winter MONEX ship array during December. A time section containing sounding data from *Akademician Korolov* from the December 8 to 10 (Fig. 10.29a) depicts the three cloud systems, using an analysis of relative humidity (shaded areas indicate relative humidity greater than 80%). Heavy rain and a wind shift at the surface accompanied the passage of each system at the ship. An analysis of the temperature departures from the December mean reveals several significant anomalies. First, in the lower troposphere, warming is observed trailing each convective system (average movement of the storms is at 6 m s^{-1} from right to left in the plane of the section). This warming was discussed earlier in connection with the mesoscale downdrafts that existed beneath the stratiform precipitation portions of the clusters. A second significant anomaly pattern is seen near the tropopause and in the lower stratosphere atop each of the mesoscale anvil clouds. Here cooling is observed having an amplitude of about 6°C. The preponderance of negative temperature anomalies near the tropopause throughout this three-day period is a reflection of warmer conditions there later in the month.

These cool anomalies in the lower stratosphere above mesoscale convective systems have also been observed in midlatitudes (Fritsch and Maddox 1981); Ninomiya et al. 1981. As discussed in Johnson and Kriete (1982), they may result from at least three possible processes, singly or in combination: overshooting cumulonimbus tops (Frank 1977), mesoscale ascent above the top of

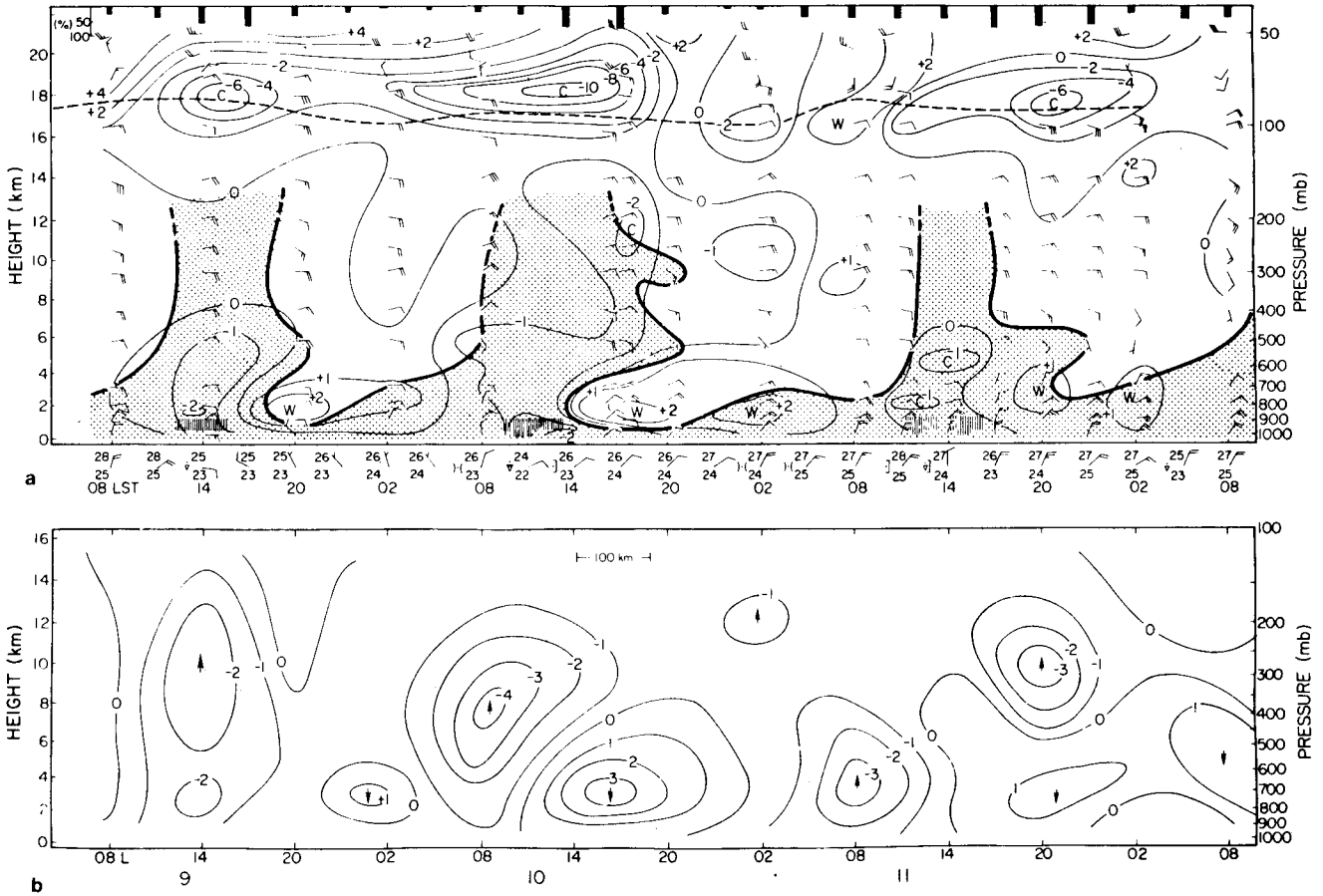

Fig. 10.29. Vertical cross-sections through three mesoscale convective systems for the period December 9 to 11, 1978. (*a*) Rawinsonde time series at *Akademician Korolov*. Stippling denotes regions of greater-than-80% relative humidity. Closely spaced vertical lines near the surface indicate periods of rain at the ship, with longer lines representing heavy rain. Solid contours are temperature deviations (K) from the December 6 to 28 mean. Wind speeds are in units of m s^{-1} (a half barb = 2.5 m s^{-1} and a full barb 5 m s^{-1}). Horizontal dashed line near the top marks the tropopause. Bars at the top indicate a fraction of the ship triangle (Fig. 10.2) area covered by bright IR satellite cloudiness. (*b*) Vertical *p* velocity [100 mb per day ($\approx$1 cm s^{-1} at 950 mb and 2 cm s^{-1} at 400 mb)] for the ship triangle. The distance scale indicated represents the advective length scale based on $\approx$6-m s^{-1} movement of the mesoscale anvil cloud. (From Johnson and Kriete 1982.)

the anvil clouds (Fritsch and Brown, 1982), or radiative cooling near the cloud top (Cox and Griffith 1979; Griffith et al. 1980). The presence of mesoscale ascent in the upper-level anvil portion of the cloud system is indicated from kinematically computed vertical motion based on the triangular array of MONEX research ships (Fig. 10.29b). Further work is needed to understand the causes of these features and their impact on the stratospheric circulation in the monsoon region.

3 THE SUMMER MONSOON

3.1 Climatological setting

3.1.1 Background and definitions. The outstanding feature of the summer monsoon is the abundant rainfall that occurs over the Indian subcontinent and China. Precipitation patterns over the summer monsoon region have been studied for many years by Indian, Chinese, and other scientists, and phases of the monsoon in this area of the world have been established based on long records of rainfall observations. It is the purpose of this section to review new knowledge gained from summer MONEX of the rain-producing cloud systems of this region. These systems are highly varied and complex, and owing to the formidable task of measuring their structure and properties over the immense domain of the summer monsoon, only limited new findings have been possible from summer MONEX data.

The period of the summer monsoon cannot be precisely defined, but there are several commonly referenced starting and ending dates. For the purposes of our discussion, the period from May to September will be considered as the time framework within which summer monsoon cloud systems will be examined. It will be kept in mind that times of onset, withdrawal, and active and break periods vary considerably across the region from India to China (Lau and Li 1984) and that the convective phenomena that exist in this region have a significant degree of spatial and temporal variability.

The low-level circulation and significant convective features in the summer monsoon region are illustrated in Fig. 10.30. As is the case with its winter counterpart, there are a number of dramatic convective features associated with the summer monsoon: (1) deep convection and heavy rainfall along the foot of the Tibetan Plateau, (2) onset vortex disturbances over the Arabian Sea, (3) orographic convection associated with the Western Ghats, (4) Bay of Bengal monsoon depressions, (5) midtropospheric cyclones over the northeastern Arabian Sea and northern Bay of Bengal, (6) Mei-Yu precipitation systems in China (or Baiu in Japan), and (7) large-scale modulations of convection during active and break monsoon periods. Our understanding of the mesoscale aspects of these and other summer monsoon convective systems is far from complete, and in this review we treat only the limited new results from summer MONEX, namely, those for convection over the Bay of Bengal region, the Arabian Sea, and the Tibetan Plateau and surrounding areas.

3.1.2 General characteristics of the mean flow. Following the onset of the monsoon, there is a strong low-level, cross-equatorial flow from the southern Indian Ocean to Asia with an intense low-level jet along the east coast of Africa and over the Arabian Sea (the Somali jet). Significant fluxes of moisture from the ocean surface to the atmosphere occur over this region, which fuel the deep convective rains over India and neighboring countries. Over the ocean, shallow cumulus, which are frequently aligned with the low-level flow, are visible evidence of the vigorous exchanges occurring in the boundary layer and have been used by Krishnamurti et al. (1979) and Young et al. (1980) as tracers of the air motion over vast oceanic regions where no other data exist.

Throughout the monsoon period a variety of cyclonic disturbances develop in the southwesterly low-level flow: the onset vortex, midtropospheric cyclones, monsoon depressions, and tropical cyclones. While many of these disturbances may originate from barotropic and/or baroclinic instabilities of the mean flow, deep convection evidently plays an important, though not well understood, role in their evolution. Additional deep convection is prevalent along the windward shores of the continent, central India, and the Himalayas. Heavy precipitation also occurs over southern and central China; however, its moisture source appears to be primarily from the equatorial regions of Indonesia and Borneo (Wang and Li 1982; Lau and Li 1984).

The deep convection over the foot of the Tibetan Plateau, along with strong sensible heat flux at the surface of this elevated landmass, provides the primary heat source that drives the summer monsoon. This heating leads to the development of an intense anticyclone in the upper troposphere over Tibet (e.g., see Fig. 10.36 presented later) with strong east-northeasterly flow at 200 mb over nearly the entire domain pictured in Fig. 10.30 (Atkinson and Sadler 1970). Consequently, deep convection that develops in the region exists in an environment of strong vertical wind shear. Since vertical wind shear is important in determining the structure and mesoscale organization of convection (Houze and Hobbs 1982), one might expect some differences in the characteristics of convective systems in the summer monsoon region from those over portions of the winter monsoon region where the vertical shear is less (Fig. 10.3).

In addition to convective disturbances over the

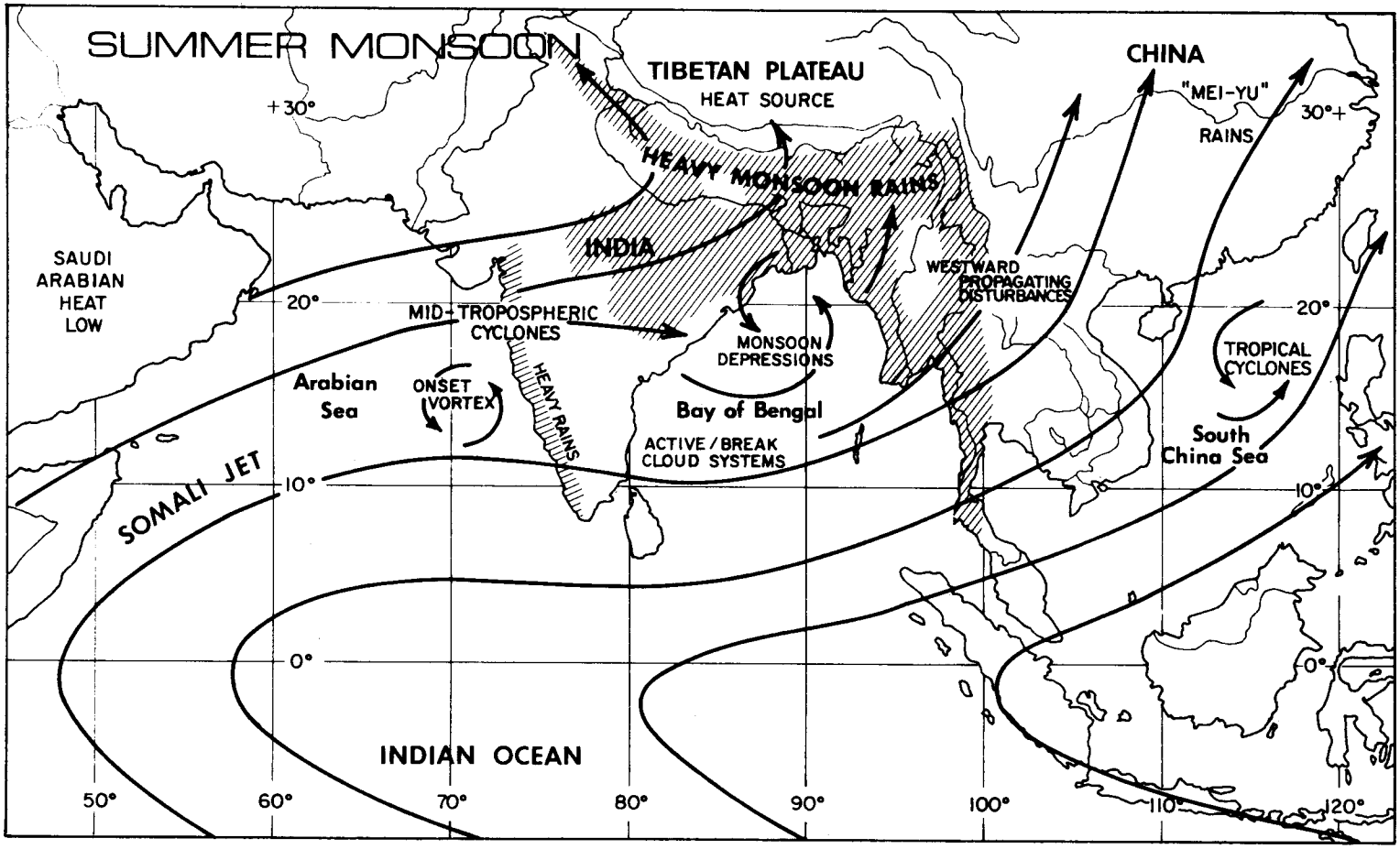

Fig. 10.30. Primary synoptic- and smaller-scale circulation features that affect cloudiness and precipitation in the region of the summer monsoon. Locations of June to September rainfall exceeding 100 cm over the land west of 100°E associated with the southwest monsoon are indicated (from Rao 1981). Those over water areas and east of 100°E are omitted.

ocean areas, many are observed over land throughout the monsoon period. Saha et al. (1981) have traced monsoon depressions forming in the Bay of Bengal back to disturbances that have traversed the northern South China Sea and then northern Indochina. Convective monsoon disturbances are also found inland over India; These appear as depressions (Koteswaram and George 1958; Krishnamurti et al. 1975) and as northward-migrating rainbands (Yasunari 1979; Sikka and Gadgil 1980; Krishnamurti and Subrahmanyam 1982). They are found also over China (Tao and Ding 1981; Lau and Li 1984).

3.1.3 Satellite climatology. In order to obtain geostationary satellite coverage during summer MONEX, the United States repositioned Geostationary Operational Satellite (GOES)-1 from the Atlantic Ocean to near 60°E for the duration of the experiment. Data from GOES-1 have been vitally important for the determination of low-level wind fields over the Indian Ocean and the Arabian Sea by using cloud-tracking techniques (Young et al. 1980). Analyses of cloud fields over the entire summer monsoon region are presently underway (Ackerman and Cox 1984, personal communication). Some analyses over a portion of the summer monsoon domain have been obtained by using the Japanese GMS-1 data (Murakami 1983) and will be reported to Section 3.4 in connection with discussions of the Tibetan Plateau heat source and its diurnal variations.

As examples of the horizontal distribution and temporal and spatial variability of monsoon convection, two mosaics of polar-orbiting satellite infrared images are presented in Fig. 10.31 (from Krishnamurti et al. 1979; a similar pair of mosaics can be seen in Figs. 5.43 and 5.45 of Ramage 1971). The first (Fig. 10.31a) is for June 18, 1979, during the convectively active onset period of the monsoon. Considerable deep convection is evident over both land and ocean areas of the region, with the onset vortex over the northern Arabian Sea and a tropical cyclone over the South China Sea. The second (Fig. 10.31b, on July 17) illustrates conditions during a break monsoon period (Sikka and Grossman 1981) when there is a dramatic decrease in convection over most of the summer monsoon region, particularly over the Arabian Sea and South China Sea areas.

3.1.4 Representativeness of the FGGE year. The summer monsoon of 1979 was extremely dry. The onset was about two weeks late, and after a period of near-normal development, the monsoon weakened again in August. Nonetheless, as Fein and Kuettner (1980) note, the 1979 monsoon contained the essential features (premonsoon period, onset, active phase, and break monsoon) that are normally observed in a typical summer monsoon. As is the case for winter MONEX, the mean flow conditions in the region of the field phase experiments were close to climatological conditions, so inferences drawn on convective and mesoscale structures and organization of the cloud systems from summer MONEX data should be generally valid for other systems in other years.

3.1.5 Components of summer MONEX. As described by Fein and Kuettner (1980), summer MONEX was divided into three consecutive components: the Saudi Arabia Experiment, the Arabian Sea Experiment, and the Bay of Bengal Experiment. The Saudi Arabia Experiment did not involve studies of clouds and will therefore not be considered here. The Arabian Sea Experiment, conducted from mid May to late June 1979, and the Bay of Bengal Experiment, carried out in July and August 1979, were concerned with regional phenomena over the oceanic regions surrounding the subcontinent at times during which several of the types of convective systems indicated in Fig. 10.30 occurred, and a considerable amount of data on convection in these regions was thus obtained. Although a formal subexperiment was not designated to study the Tibetan Plateau, several studies of FGGE and MONEX data have concentrated on that region, and important new results about convection in relation to the plateau, in its role as the primary heat source for the monsoon, have emerged. In Sections 3.2 to 3.4, we shall review in turn the results of the Arabian Sea Experiment, the Bay of Bengal Experiment, and the Tibetan Plateau research insofar as each has led to new insights into the structure and dynamics of summer monsoon convection.

3.2 Arabian sea experiment

As indicated in Fig. 10.30, the west coast of India is one of the areas of heavy rainfall during the summer monsoon. Observations from the Arabian Sea experiment have provided new insight into these cloud systems.

In a brief study conducted at the time of the experiment, Mukherjee (1980) documented the structure of a mesoscale low-level vortex located just off the coast. These small cyclones are noted for being associated with enhanced rainfall as they move northward up the coast. The horizontal (150 km) and vertical (1 km) scales of these vortices had not been determined prior to MONEX.

More detailed studies, also concerned with the clouds and precipitation along the west coast of India, have been carried out by Warner (1982a), Smith and Lin (1983), Grossman and Durran (1984), and Grossman and Garcia (1985). In addition, Krishnamurti et al. (1983) have prepared an atlas of summer MONEX rainfall patterns based on rain gauge data and satellite infrared brightness values. Both these infrared data and

a

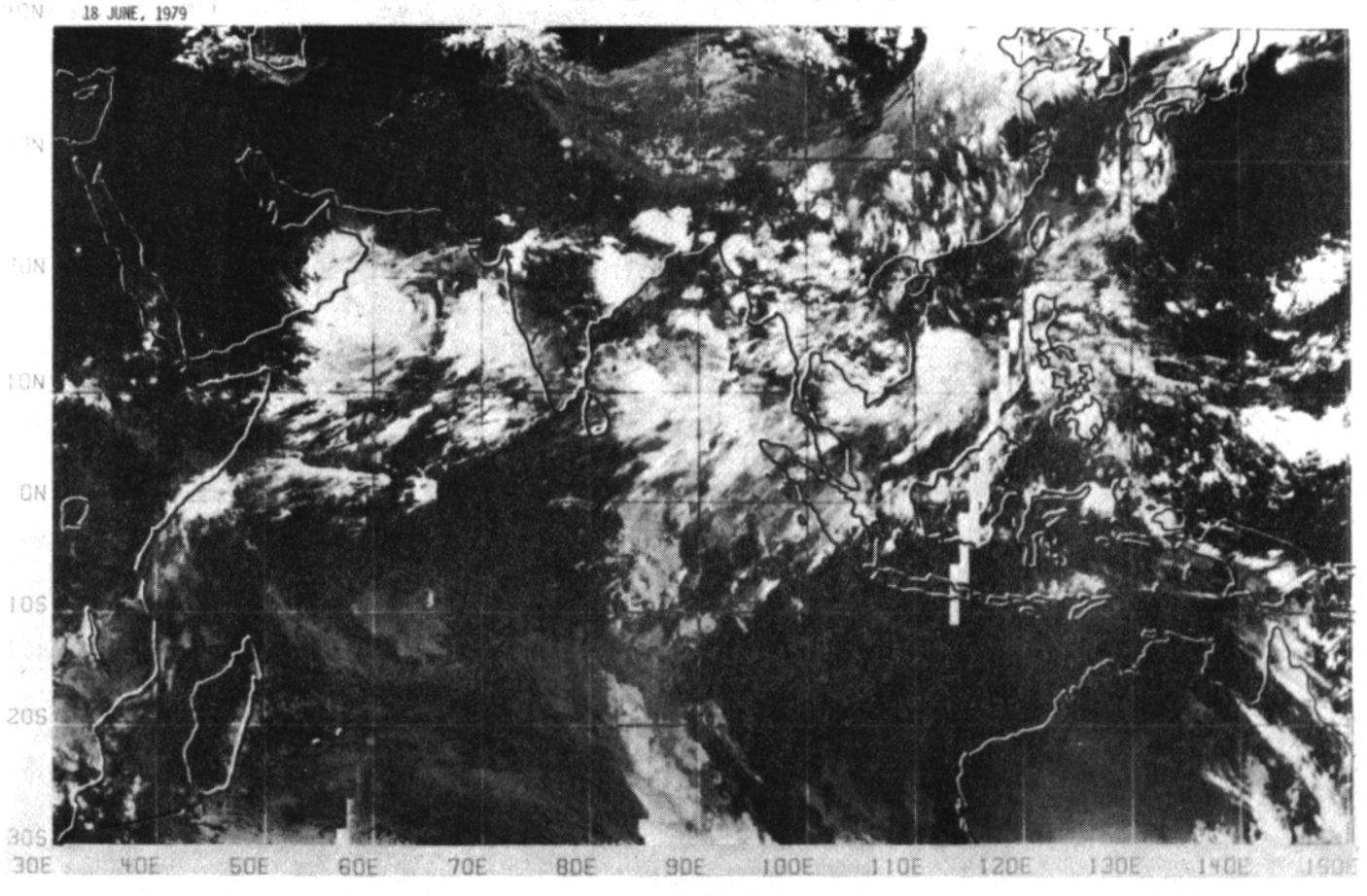

Fig. 10.31. Defense Meteorological Satellite Program (DMSP) infrared satellite mosaics. (*a*) For June 18, 1979, an active monsoon period. (*b*) For July 17, 1979, a break monsoon period. (From Krishnamurti et al. 1979.)

b

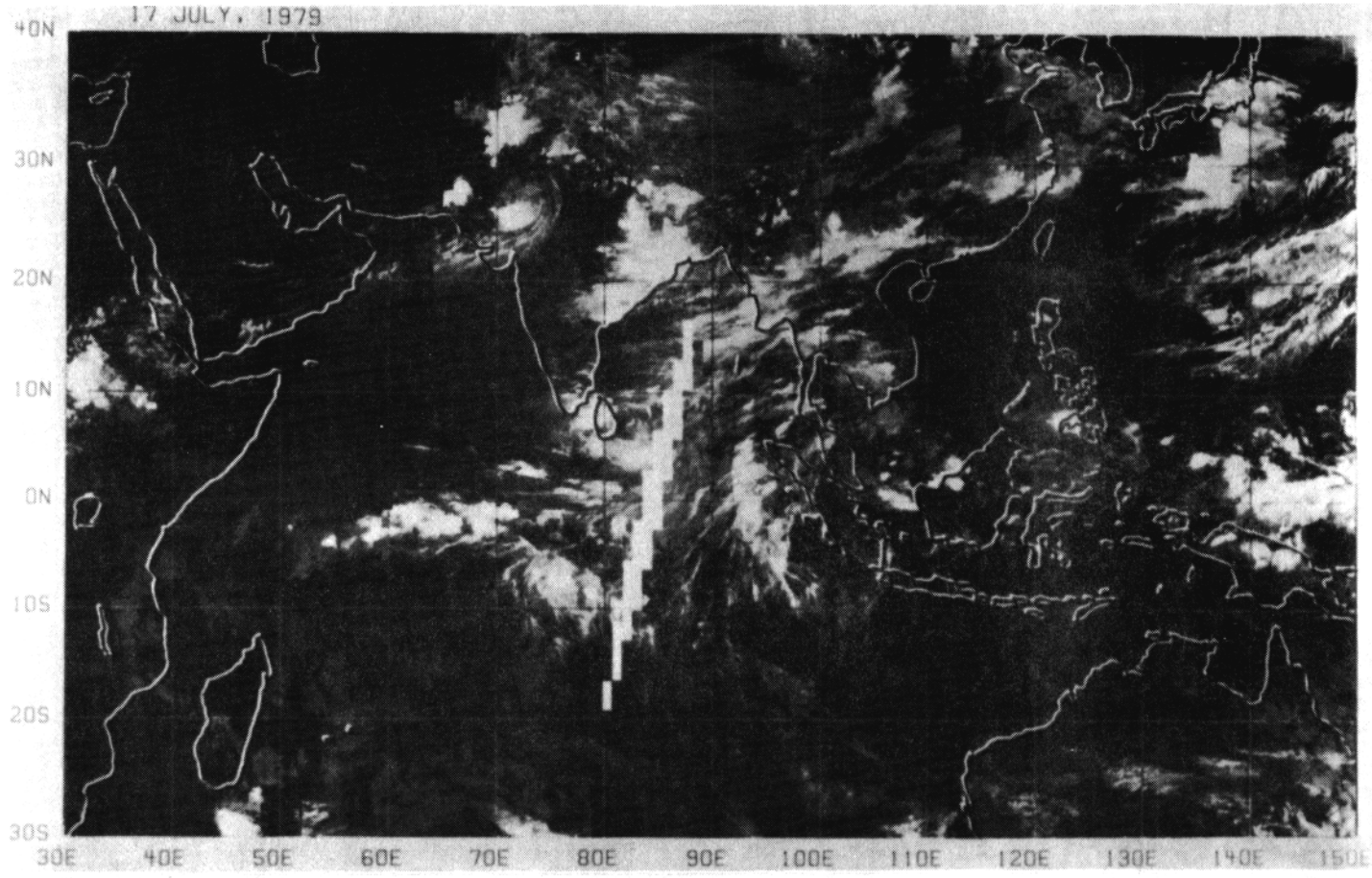

Fig. 10.31. (*continued*)

the visible satellite imagery analyzed by Grossman and Garcia (1985) indicate that the highest brightness values typically occur some 100 to 300 km off the west coast of India (e.g., Fig. 10.32). Whether the strong monsoon easterlies at high levels displace the highest cloud tops westward of a maximum rain region along the coast and western slopes of the moutains or whether the rainfall maximum is actually located offshore [as Krishnamurti et al. (Fig. 10.32) and Grossman and Garcia suggest] remains somewhat speculative.

Smith and Lin (1983) note that limited radar observations show that cumulus development typically extends offshore at least 30 km, but how much farther offshore the western Ghats rainfall enhancement occurs is uncertain. They develop an analytical model for flow over a mountain barrier that includes the effects of cumulus heating. With a heating maximum centered along the coastline approximately 100 km upwind of the crest of the western Ghats, a heat-induced offshore surface pressure trough is predicted by the model. This feature is consistent with observations and might suggest that the precipitation maximum does not extend too far offshore, although the results are not conclusive.

Grossman and Durran (1984) suggest how a maximum of rain farther offshore might be explained. They point out that the low-level coastward monsoonal flow has a high, moist static energy, and in an idealized monsoon, without complex orography, this air would be expected to rise over the landmass. However, using aircraft data from the day illustrated in Figs. 10.32 and 10.33 (flight path indicated in Fig. 10.33), they argue that the flow up to a depth of 300 m decelerated as it approached the western Ghats and began to rise at a rate of 2 to 3 cm s^{-1} some 200 km from land. They indicate that this rise rate was enough to release the conditional instability of the inflow air. Hence, deep convection could result before the low-level flow reached land. That the deceleration and convergence of the low-level flow approaching the coast could have been associated with flow of the air over the barrier formed by the western Ghats was indicated by a two-dimensional model simulation in which gentle ascent occurred through a deep layer 200 km upwind of the coastline (Fig. 10.34). While much stronger model ascent occurred over the windward slope of the mountain range, it was overlain by descent and strong horizontal wind shear, which would have discouraged convection directly over the range.

Warner (1982a) also studied winter MONEX aircraft data obtained on the day illustrated in Figs. 10.32 and 10.33. He mapped the cloud field photographed with automatic side cameras and referred to horizontal winds, vertical velocity, and radiation measurements obtained along the flight path. His cloud map for the eastbound (return) portion of the flight is shown in Fig. 10.33. The

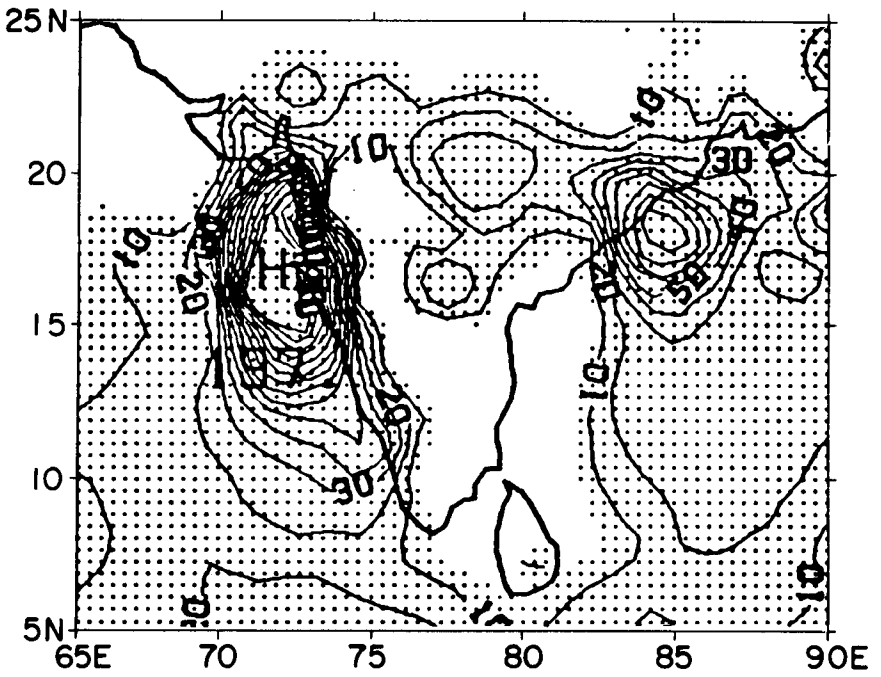

Fig. 10.32. Twenty-four-hour accumulated rainfall (mm per day) ending 000 GMT, June 24, 1979, determined from rain gauge and infrared satellite data. Shaded area indicates rainfall exceeding 5 mm per day. (From Krishnamurti et al. 1983.)

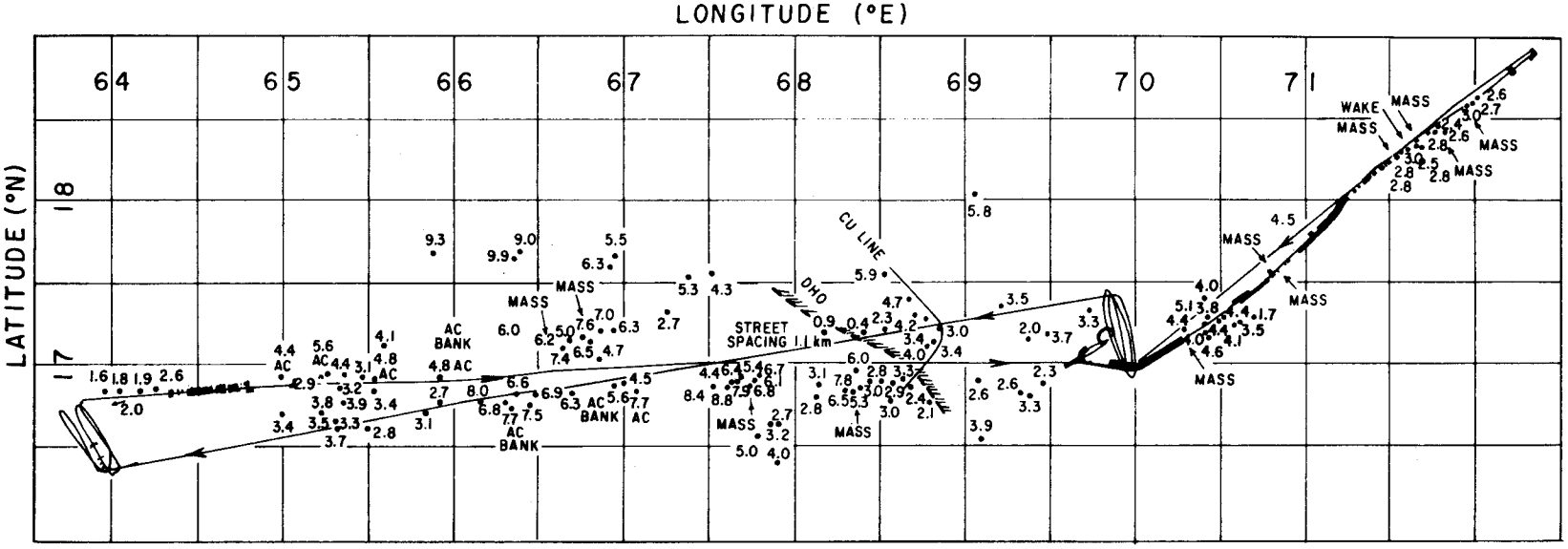

Fig. 10.33. Cloud map derived from side cameras aboard the National Center for Atmospheric Research *Electra* aircraft on a flight over the Arabian Sea on June 24, 1979, during summer MONEX. Arrowheads indicate the direction of flight. The map applies to the period 800 to 1030 GMT (12:30 to 15:00 LST). Dots indicate positions of clouds; adjacent numbers indicate the heights (km) of their tops. The DHO and hatching indicate boundaries of dense high overcast. AC BANK or MASS indicates a concentration of cumuliform clouds at high levels. WAKE indicates evidence of downdraft spreading over the ocean surface. Shading along the track shows a passage in the cloud. (From Warner 1982a.)

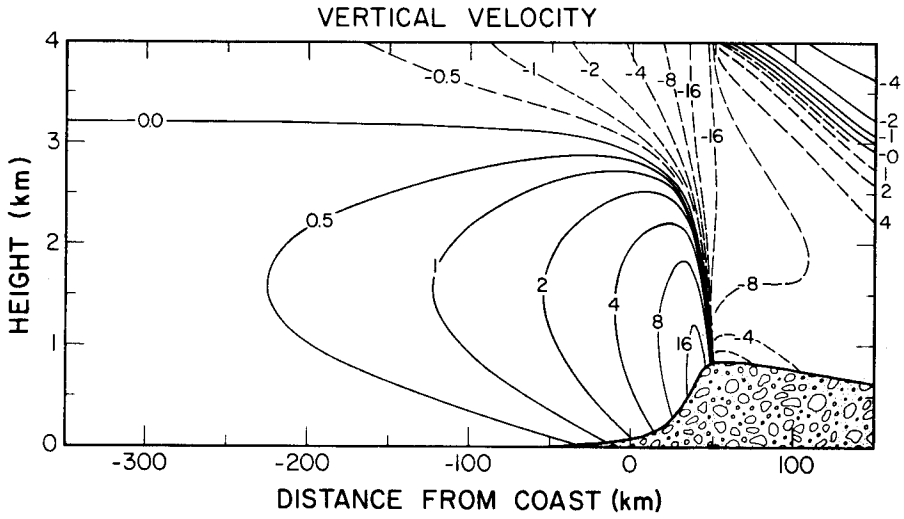

Fig. 10.34. Cross section perpendicular to the mountains of model-derived vertical velocity (cm s^{-1}). The contour interval doubles from 0.5 cm s^{-1}. (From Grossman and Durran 1984.)

boundary of dense, high overcast (DHO) coincides with the satellite-inferred rainfall contour of 30 mm per day, which lies at the edge of the strong gradient of rainfall in Fig. 10.32. The flight data show that for at least 100 km east of the DHO boundary no rain was seen from the aircraft. From 69.7 to 71.5°E the aircraft was mostly in cloud. Precipitation must have been confined to this zone of cloud penetration and not to quite as broad a region as implied by the contours in Fig. 10.32. Warner's cloud mapping for the westward (outbound) portion of the flight (not shown in Fig. 10.33) indicated much less time in cloud in this same region. Apparently, the penetrated cloud expanded considerably during the period between the outbound (≈ 900 to 1230 LST) and return (≈ 1230 to 1500 LST) flight legs. Work presently being carried out with radar and cloud microphysical data obtained on other summer MONEX research flights may determine more precisely the location and intensity of precipitation within these clouds, as well as in similar clouds on other days of the Arabian Sea Experiment. Such further research could help resolve the uncertainty regarding whether the maximum of western Indian rainfall is located offshore, as has been inferred from satellite data, or inland.

Warner's cloud map in Fig. 10.33 shows positions and cloud top heights of cumulus and altocumulus located below the DHO and farther west, out to 64°E. He notes descriptive and statistical similarity to the clouds seen over the South China Sea during winter MONEX (Section 2.3). However, there appeared to be no systematic variation of cloud top height along the low-level wind direction (parallel to the flight track), as was noted in winter MONEX.

Further work on observations of clouds and precipitation off the west coast of India are important since, as Grossman and Durran (1984) point out, the existence of major amounts of rain offshore would imply a largely unrecognized major source of latent heat for the summer monsoon. In addition to further work with summer MONEX data over the Arabian Sea, numerical models should be employed. In particular, models that include moisture and cloud microphysics are needed to test the hypothesized mechanism of offshore convective cloud formation.

3.3 Bay of Bengal Experiment

One of the major goals of summer MONEX was an improved understanding of the monsoon depressions that typically form over the Bay of Bengal during July and August. Among the important questions stated in *The Monsoon Experiment* (WMO 1976) were "What is the cloud-size spectrum associated with the monsoon disturbances?" and "Is the monsoon rain (in the depressions) associated with large scale dynamically forced ascent or small scale convection which is organized over larger areas?" So that these questions could be answered, an unprecedented effort was made to document the clouds and precipitation within an active depression. Furthermore, it was deemed essential to observe the depression over the bay, before it moved inland. Most past studies had by necessity been confined to data taken over land. Yet the important organizational and maturing stages of these storms occur while they are still over the northern bay. Consequently, long-range aircraft, which could reach the developing depressions while they were still over the sea, became the primary observing platforms for this experiment. Research flights of the National

Oceanic and Atmospheric Administration (NOAA) WP-3D and National Center for Atmospheric Research (NCAR) *Electra* aircraft documented a depression that occurred between July 3 and 8, 1979. On these flights, dropwindsondes were launched, clouds were photographed, the precipitation field was observed by airborne radar, and the clouds were penetrated to obtain microphysical measurements of the hydrometeors.

The dropwindsonde data have been used by Nitta and Masuda (1981) and Sanders (1984) to map the airflow in the July 1979 depression. The aircraft data were combined with rawinsonde observations from land stations to construct analyses over the Bay of Bengal and surrounding areas. The stream function fields obtained by Sanders for lower-(1000–700 mb) and middle-(700–400 mb) tropospheric layers at 1200 GMT, July 7, 1979, are shown in Fig. 10.35. Warner (1984a) has analyzed the flight-level winds for this day, and they are consistent with Sanders's analysis. Krishnamurti et al. (1980) incorporated the dropwindsonde data into an atlas of horizontal wind analyses for the period of the depression. They used all available data, including satellite cloud motion vectors, which allowed the upper-level flow to be mapped. Their 200-mb analysis for 1200 GMT, July 7, is shown in Fig. 10.36.

From Figs. 10.35 and 10.36, it can be seen that the flow associated with the depression formed a closed vortex at low and middle levels. Between middle and upper levels, the strong easterly shear, associated with the warmth of the Tibetan Plateau to the north, resulted in strong easterly flow at high levels, which gave the cirrus cloud tops associated with the depression the appearance of a complex of east-west extended streamers (Fig. 10.37).

Several attempts have been made to determine the vertical air motion pattern in the July 1979 Bay of Bengal depression. Nitta and Masuda (1981) calculated the vertical p velocity (ω) kinematically from their horizontal wind fields. Surgi (1983; also personal communication) has computed kinematic ω's from the wind analyses of Krishnamurti et al. (1980). Sanders (1984), however, warns against using the divergence field (i.e.,

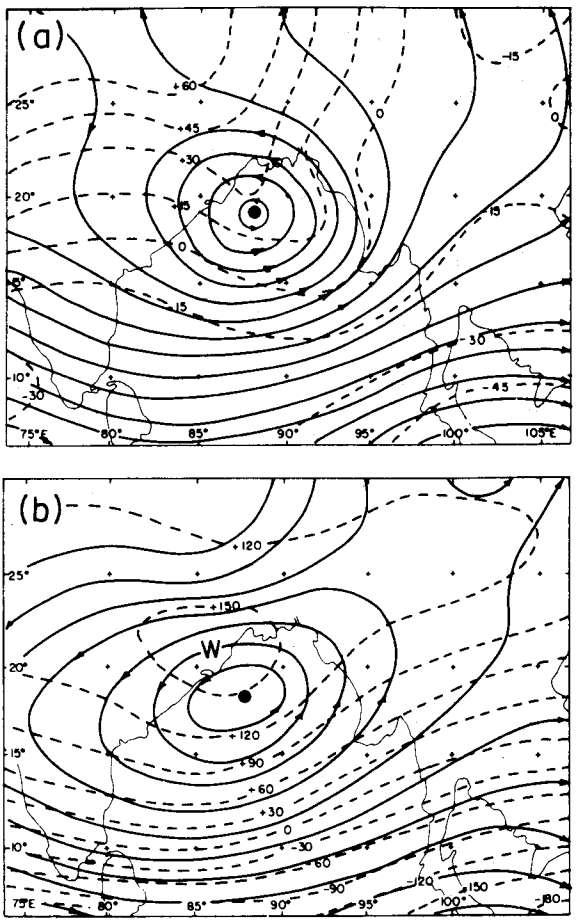

Fig. 10.35. At 1200 GMT, July 7, 1979. (*a*) Stream function in the lower troposphere and the difference of middle minus lower levels (dashed). (*b*) Stream function at middle levels and the difference of upper minus middle levels (dashed). Stream function isopleths are at intervals of 15×10^5 m^2 s^{-1}, with centers indicated by large dots. Isopleths of the stream function difference are at intervals of 15×10^5 m^2 s^{-1} in (*a*) and of 30×10^5 m^2 s^{-1} in (*b*). These represent isotherms of mean temperature between (*a*) 850 and 550 mb and between (*b*) 550 and 250 mb at intervals of approximately 0.5 and 0.6°C, respectively. Maximum is labeled W. (From Sanders 1984.)

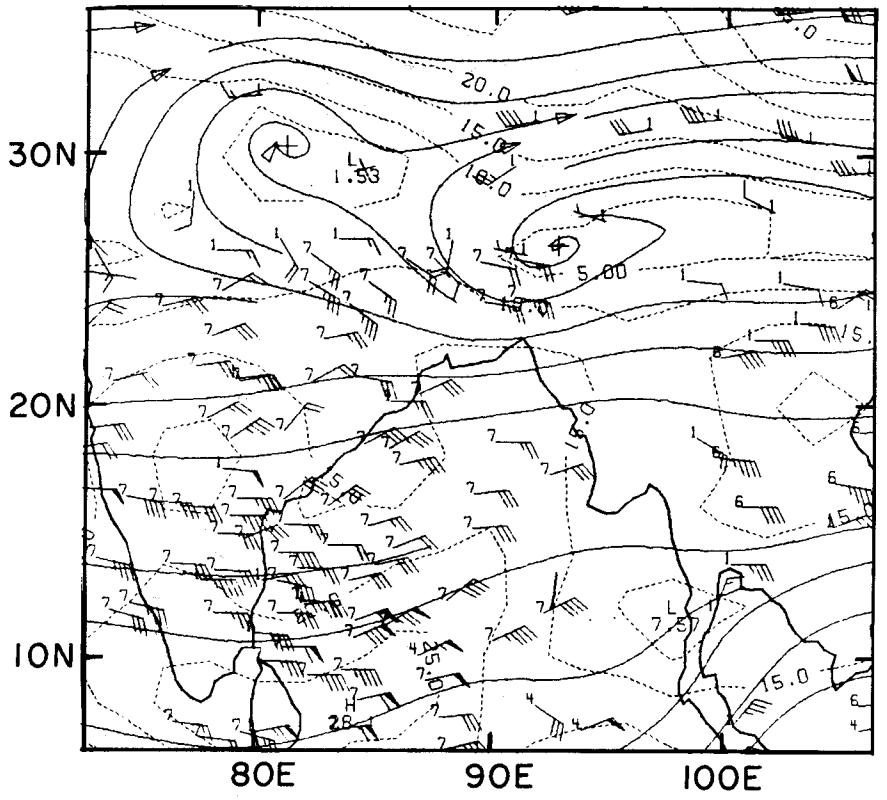

Fig. 10.36. 12 GMT, July 7, 1979, 200-mb analysis. Shown here are streamlines and isotachs (m/s). The numbers at the wind barbs indicate the type of data: 1, rawinsonde; 4, commercial aircraft; 6 and 7, satellite cloud motion vectors. (From Krishnamurti et al. 1980.)

the kinematic method) to calculate ω in this case. He separated his analyzed wind field into nondivergent (rotational) and divergent (irrotational) components. He found the latter component (represented by a velocity potential field) to be weak, variable on a small scale and bearing little relationship to observed weather patterns. The nondivergent rotational component (represented by the stream function; e.g, Fig. 10.35), on the other hand, exhibited a strong signal on a larger scale. To take advantage of this strong signal in the nondivergent wind and avoid the noisy divergence field, he computed ω from the stream function by using the quasi-geostrophic omega equation. The effects of release of latent heat were represented by using a static stability smaller than the unsaturated value in the equation.

Careful comparison of the horizontal patterns of ω computed by Nitta and Masuda (1981), Surgi (1983), and Sanders (1984) for the July 1979 Bay of Bengal depression shows little agreement. Sanders's (1984) warning about the inadequacy of kinematic calculations for this case and the strong signal in stream function suggest that ageostrophic motions were not well resolved and that his ω equation calculations, despite their limitations, give the best available estimate of the true vertical air motion pattern. Arguments advanced by Warner (1984a) (on the basis of cloud photography, thermodynamic evidence, and other information) about vertical velocities at certain points within the storm are generally consistent with Sanders's pattern. As will be shown below, Sanders's ω field is consistent with the observed cloud and precipitation fields and with the composite ω field obtained by Godbole (1977) for five Bay of Bengal depressions observed after they had made landfall.

A portion of the vertical motion pattern obtained by Sanders for 1200 GMT, July 7, at 700 mb is shown in Fig. 10.38. The pattern is superimposed on the satellite picture of 840 GMT (the satellite data time corresponding most closely to the synoptic time). The main feature of the vertical motion field is a couplet, consisting of upward motion southwest of the storm and downward motion to the northeast. This pattern agrees well with Godbole's (1977) composite. Because of the time difference between the satellite and synoptic data, and because of the large easterly shear producing blowoff to the west, all details of the two data fields cannot be easily reconciled. However,

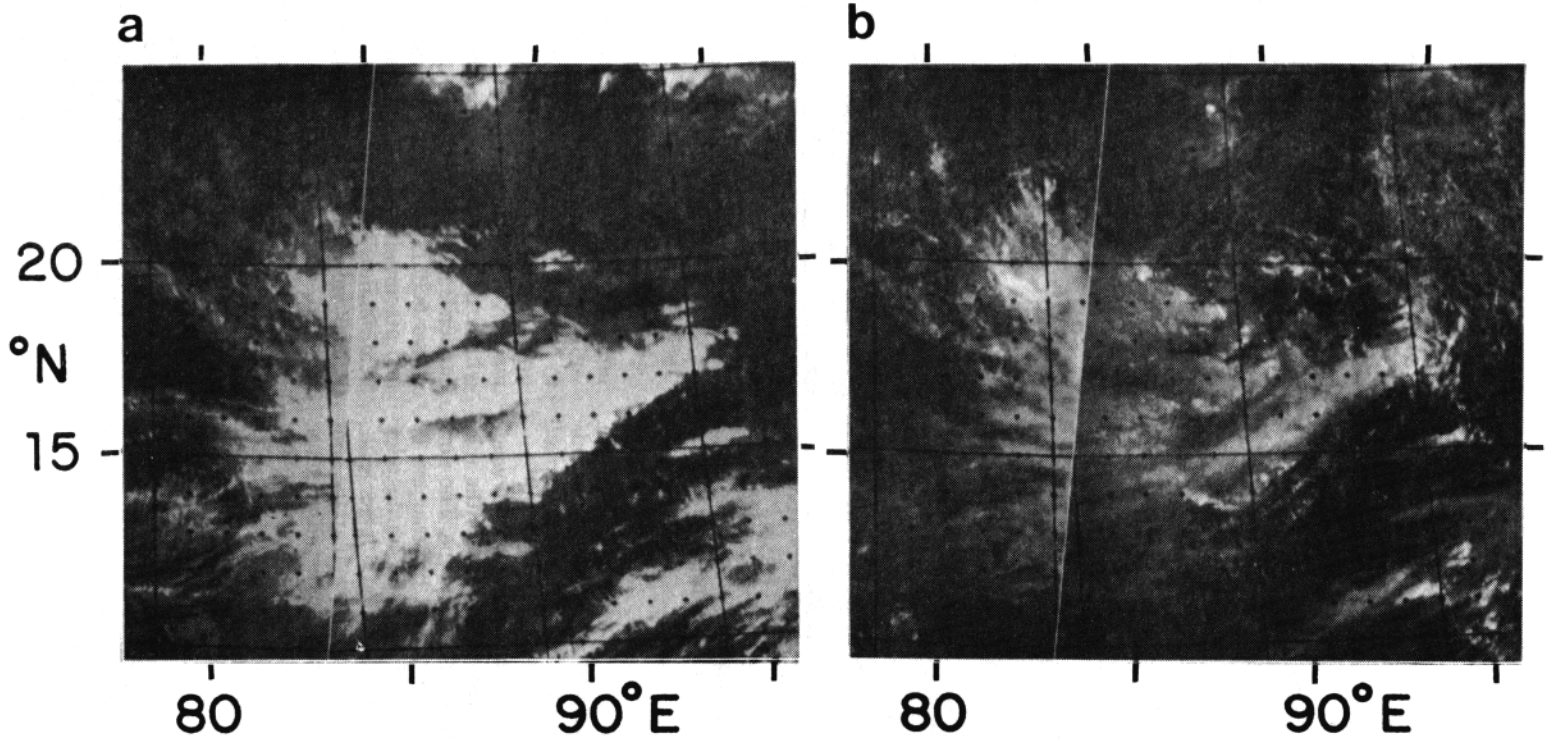

Fig. 10.37. Satellite imagery from DMSP satellite F4. (*a*) In the infrared. (*b*) In the visible. Each view is a composite from orbits 431D (right, with equator crossing at 93.8°E, 344 GMT, July 7, 1979) and 432D (left, with equator crossing at 68.5°E, 526 GMT). (From Warner 1984b.)

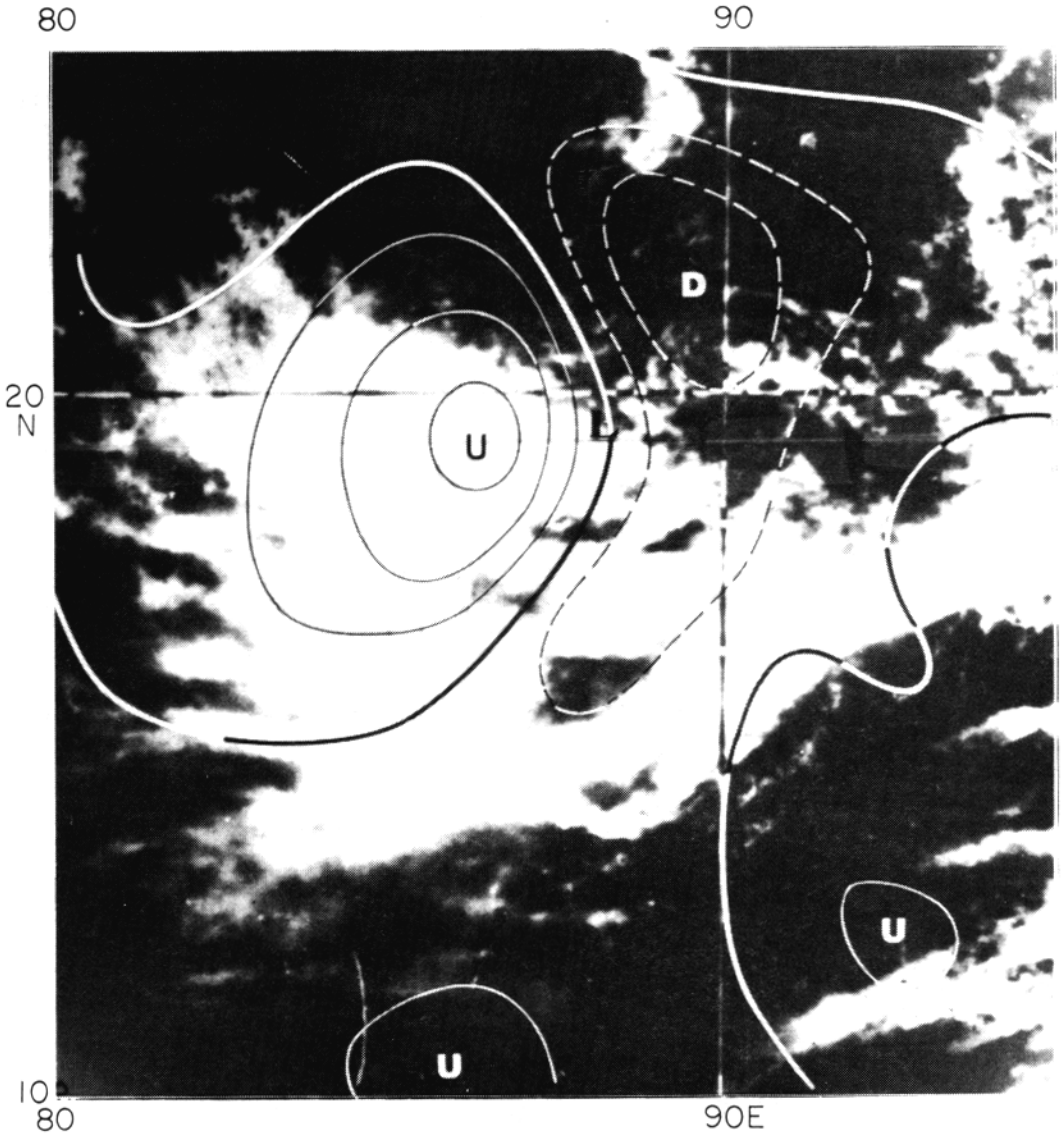

Fig. 10.38. Visible DMSP satellite photograph for 8:40 GMT, July 7, 1979, with contours of the 1200 GMT vertical air motion ω at 700 mb superimposed. The contours [from Fig. 15a of Sanders (1984)] are for $\omega = -90, -60, -30, 0, 30$, and 60×10^{-4} mb s^{-1}. Positive contours are dashed. Letter L is at depression center. Letters U and D are at centers of upward and downward motion, respectively.

the main features of the satellite imagery and vertical motion are consistent. Upper-level cloud shield was absent in the region of strongest downward motion, centered to the northeast, while extensive cloud tops are evident to the west and southwest, in the area of upward motion. The area of cloudiness seen in the satellite picture extended east-southeastward from the region of upward motion; however, the cloudiness to the east-southeast was patchy, particularly in the southward-extending tail of the region of strong downward motion. The satellite data suggest that dissipation of clouds was occurring in this southward extension of the zone of subsidence. Although at the time of the satellite data in Fig. 10.38 (840 GMT) there remained one bright east-west cloud band across this region, airborne radar data obtained about 2 h later indicated that this cloud band contained no significant precipitation and that intense rain was located in the region of upward motion to the west (see the discussion of Fig. 10.41 later).

The northeast-southwest–oriented cloud band seen lying just southeast of the tail of downward motion in Fig. 10.38 (endpoints at approximately 18°N, 92°E and 14°N, 89°E) has been studied in

detail by Warner and Grumm (1984). They found that this cloud band was tracking rapidly east-northeastward (at 24 m s^{-1}). It was characterized by a highly convective leading edge. It moved by discrete propagation and behaved somewhat like a tropical squall line. By its rapid eastward movement it was quickly becoming disconnected from the cloud pattern of the west-northwestward-moving Bay of Bengal depression.

Figure 10.39 shows the outline of the cloud shield associated with the depression, as seen in the infrared data of Fig. 10.37a. Transposed into this view are the locations of high convective cell tops illuminated in the visible photograph of Fig. 10.37(b). The deep cells occupied a small fraction of the total cloud area. They tended to be concentrated in groups (labeled X, Y, and Z in Fig. 10.39), with some apparent tendency for the small groups to be arranged in lines oriented east-northeast to west-southwest, with a bow shape convex to the southeast (e.g., Y and Z). The remainder of the cloud top pattern (outside the high cells) was apparently dominated by huge mid-to-high level stratiform (or anvil) cloud structures. From photogrammetry of the clouds, as viewed from aboard the aircraft flying through the disturbance, Warner and Grumm (1984) presented maps showing "extensive anvil cloud bases at ≈400 mb, apparently arising from cumulus."

The precipitation within the heavy boundary in Fig. 10.39 was observed by airborne radar. The echo pattern is shown in Fig. 10.40. The general shape of the precipitation area is consistent with the satellite-observed cloud pattern, and the locations of intense cores of reflectivity bear a reasonable correspondence to the cell tops observed by satellite (taking into account time differences and the fact that the satellite detects cloud while radar detects precipitation). The echoes in Fig. 10.40 were associated with the satellite-observed features X and Y. Since the flight was conducted in the vicinity of X, its radar echo pattern is well represented. Since Y was located at a considerable distance from the aircraft, only the stronger cells in that feature can be seen; any lighter precipitation surrounding them was too far away to be detected.

The most intense radar echo in X was located at the eastern end of the feature. The maximum reflectivity in a 4-km^2 grid element was 39 dBZ, corresponding to a rainfall rate of 23 mm h^{-1}, if the GATE reflectivity-rainfall rate relationship (see the discussion in Churchill and Houze 1984b) is applied. In addition to the intense convective

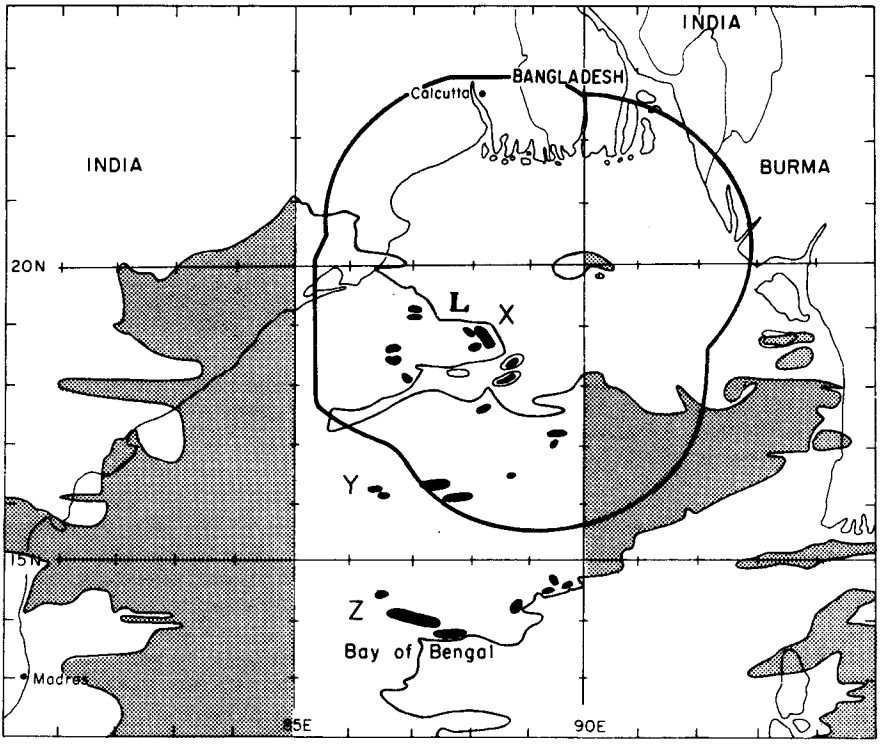

Fig. 10.39. Outline of infrared satellite cloud pattern seen in Fig. 10.37(*a*). In the unshaded region between 85 and 90°E, dark spots locate high convective cell tops illuminated in the visible photograph (Fig. 10.37*b*) as a result of a low sun angle. A heavy boundary surrounds the region in which airborne radar observations were obtained by the WP-3D aircraft. Letter L is depression center. Letters X, Y, and Z refer to features discussed in text.

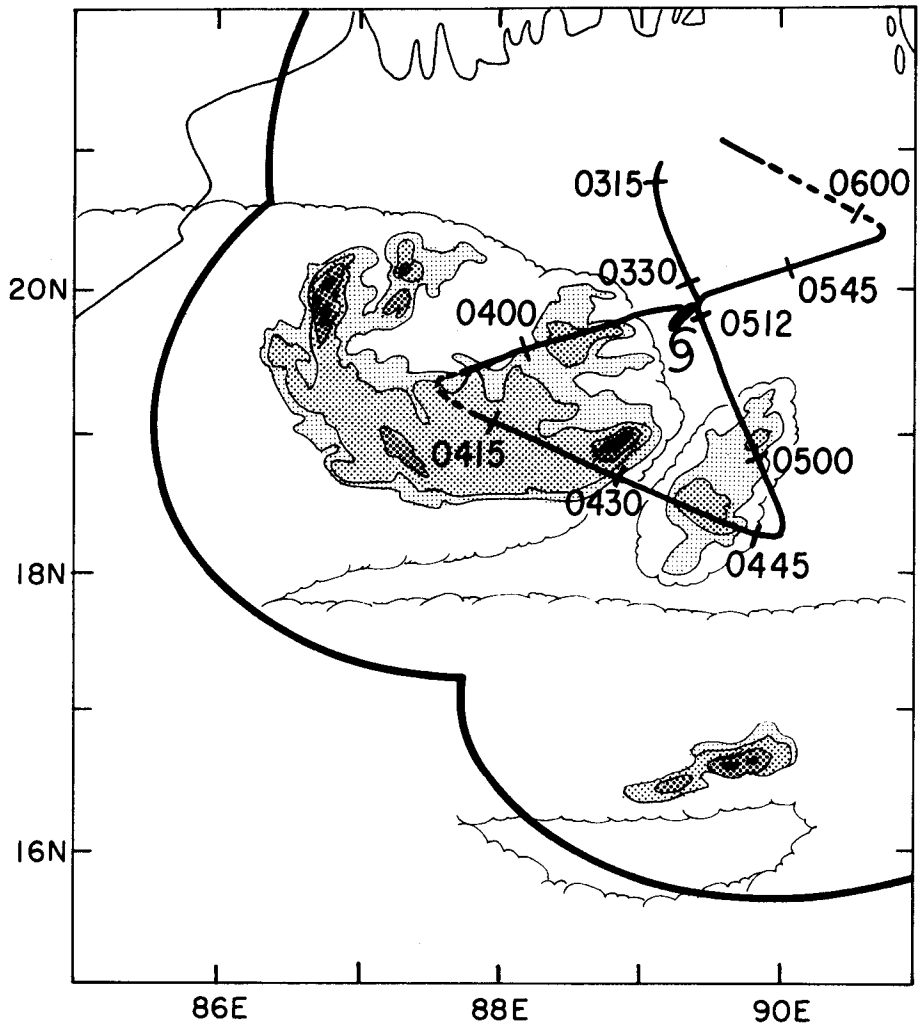

Fig. 10.40. Composite reflectivity pattern from airborne lower-fuselage radar aboard the WP-3D aircraft. Data were obtained over the Bay of Bengal on July 7, 1979. Shading thresholds are at 1, 20, 30, and 35 dBZ. Flight track of the P3 is indicated by dashed and solid lines. Solid lines denote flight path where radar data were collected and from which the composite was generated. Numbers indicate time (GMT) every 15 min. at the corresponding hash marks on the flight track. The heavy, bold curve shows outer limit of the area of radar coverage. The scalloped line indicates approximate cloud boundaries based on the 344 GMT DMSP satellite image and in-cloud microphysical observations. Hurricane symbol indicates depression center. (Adapted from Houze and Churchill 1987.)

cores, the precipitation area associated with feature X contained a large area of moderate rain (of reflectivities 25 to 30 dBZ, or rainfall rates of 1 to 4 mm h^{-1}). This more horizontally uniform moderate rain, outside the convective cores, was likely stratiform in character and falling from the extensive upper-level anvil cloud. The extent of the rain area associated with X, as defined by the 20-dBZ reflectivity contour, was some 270 km in length and 100 km in width. If the rain area moved westward approximately at the 3.5-m s^{-1} speed of the depression, then on the order of a day would be required for it to pass a point. This time scale indicates a long period of continuous, moderate-to-heavy rain at certain individual stations. However, the mesoscale spatial dimension suggests that only a few stations would receive the maximum accumulated rainfall, while others might be missed altogether. This behavior is consistent with the patchiness of 24-h rainfall patterns in Bay of Bengal depressions (Rao 1976, pp. 126–127). Hydrometeor images recorded continuously aboard the aircraft along the low-level flight path plotted in Fig. 10.40 showed that lighter rain was present outside the 25-dBZ echo contour. These observations indicate that the mesoscale rain area associated with X may have been embedded in a still larger region of very light

background precipitation. However, the primary finding of this flight is that the bulk of the rainfall in this region of the depression was located in a mesoscale precipitation area that consisted partly of convective cores and partly of a wide region of more uniform moderate rain.

The seemingly stratiform character of the more uniform rain falling outside the convective cores is indicated by a preliminary analysis of ice hydrometeor images recorded during high-level flights through the depression. The track of a flight conducted at the 7.7-km level between 9:15 and 1100 GMT on July 7 is shown in Fig. 10.41. The track is overlaid on the 834 GMT satellite cloud pattern, which was shown previously in Fig. 10.38, with Sanders's vertical motion pattern superimposed. The flight was carried out in the region of apparently dissipating cloud coinciding with the southern tail of the region of subsidence deduced by Sanders. The radar echo detected by the airborne radar showed that the more active precipitation area was to the west of the flight track (where upward motion was diagnosed). Weak precipitation was detected by radar sporadically along the flight track. The ice particle data collected along the flight path are indicated schematically. Two very pronounced occurrences of branched crystals were noted in the dissipating cloud. Columns were also seen in one area. The branched crystals were nucleated at altitudes above flight level. The occurrence of such vapor-grown crystals drifting downward to flight level also characterized the dissipating, weakly precipitating stratiform cloud shields of cloud clusters observed in winter MONEX (Section 2.3). The Bay of Bengal depression cloud shield was evidently characterized by similar stratiform precipitation mechanisms.

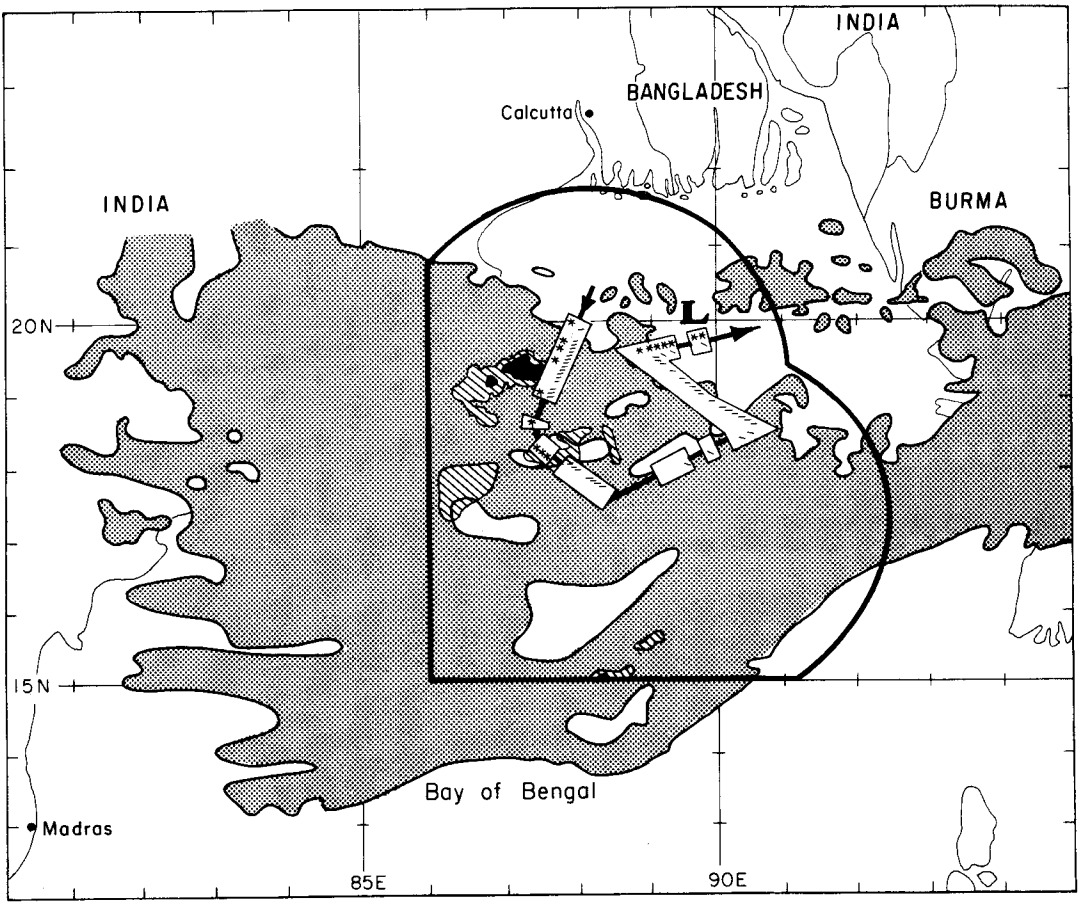

Fig. 10.41. Microphysical observations and radar-detected precipitation echoes within the cloud pattern of the July 7, 1979, Bay of Bengal depression. The shaded region is the area of visible cloud coverage at 840 GMT seen in Fig. 10.37. The heavy line encloses an area covered by the WP-3D aircraft, lower-fuselage radar observations. Echoes exceeding 1 dBZ are hatched, while those exceeding 30 dBZ are solid. The arrows show the aircraft flight track from 915 to 1100 GMT. The boxes indicate portions of the track along which ice particle images were detected. The short lines indicate each 1-min period in which columnar crystals were observed. The asterisks indicate each 1-min period in which branched crystals were observed. Letter L indicates center of depression.

Mesoscale rain areas qualitatively similar to X were likely associated with the areas of convection Y and Z seen in the satellite data of Fig. 10.39. As noted above, any light precipitation associated with these features was located too far from the aircraft to be detectable by radar. Radar observations obtained on flights into this same monsoon depression on other days (July 3, 5,* 6, and 8) confirm that the precipitation was typically concentrated in combined convective-stratiform areas of the scale and consistency of X.

Thus, aircraft data have shown that an important feature of the cloud ensemble of the summer MONEX Bay of Bengal depression was that the rain was largely concentrated in mesoscale areas (such as X), which consisted partly of intense convective precipitation and partly of relatively uniform, probably stratiform rain of moderate intensity. The data have shown the spatial arrangement of the stratiform and convective components of the precipitation areas and provided some indications of cloud microstructure. Mesoscale rain areas of the size and physical description of X also dominated precipitation patterns in the equatorial cloud regimes of winter MONEX (Section 2.3) and GATE (Houze and Betts 1981). Those mesoscale rain areas, however, were associated with cloud clusters, and the stratiform precipitation within them developed in the mature to late stages of cluster development, as an outgrowth of the convection (Fig. 10.21). The precipitation in the Bay of Bengal disturbance may have differed from the equatorial cloud regimes of winter MONEX and GATE since strong upward motion was associated with the depression itself (Fig. 10.38) and since it was characterized by a different thermodynamic stratification. The question arises whether the moderate rain adjacent to convective cells in the mesoscale precipitation areas of the depression arose as an outgrowth of the convection, as in cloud clusters, or was produced directly by the large-scale cyclonic lifting. Sanders (1984) showed, through his application of the quasi-geostrophic omega equation, that the vertical motion associated with the large-scale temperature advection within the depression was strong enough to account for the storm's total rainfall. His study, however, did not endeavor to determine whether the large-scale motions associated with the Bay of Bengal depression directly produced stratiform precipitation or whether their primary role was to provide an environment favorable for deep convection, which in turn became organized on the mesoscale and induced stratiform precipitation of the type seen in cloud clusters. It is important to make this determination in order to understand the precipitation mechanisms and the concomitant horizontal and vertical distributions of latent heat release in this type of storm.

Ongoing study of the existing airborne radar and microphysical data obtained in the depression discussed here may provide further insight into these processes. However,the existing data do not document the life cycles of the vertical structures of the Bay of Bengal disturbance's mesoscale cloud features. Therefore, future studies should document the life cycles of individual mesoscale features such as X within monsoon depressions, and vertically as well as horizontally scanning radars should be used in conjunction with airborne microphysical observations. It can then be determined whether the enhanced stratiform rain areas systematically develop in the vicinity of and subsequent to the development of convective features in a manner similar to that seen in cloud clusters.

In any case, it is evident that idealizations that envisage the latent heat release and associated processes in a Bay of Bengal depression in terms of either a simple convective population, wherein no mesoscale organization or stratiform precipitation processes exist, or a wholly large-scale cyclonic process will fall short of reality. Such idealizations, whether used prognostically or diagnostically, should be viewed with caution. It is likely that some hybrid of large-scale and convective processes are active in producing the clouds and precipitation of Bay of Bengal depressions.

3.4 Tibetan plateau

3.4.1 Heat source characteristics of the Tibetan Plateau and surrounding area. An investigation of the characteristics of the Tibetan Plateau as a heat source and a determination of its role in the summer monsoon circulation were also primary objectives of summer MONEX. Broad-scale aspects of this heat source were treated in an earlier chapter of this volume. Mesoscale aspects, to the extent that they can be determined from summer MONEX data, will be discussed in this section. Detailed observations of convective systems over the Tibetan Plateau and surrounding region were not obtained during summer MONEX due to limited resources and difficulties of measurement over complex terrain, so most of the knowledge that has been gained on mesoscale characteristics of the convection has been inferred from larger-scale observations (e.g., rawinsonde and satellite data).

Efforts to investigate diabatic heat sources over the summer monsoon area have employed FGGE/MONEX data on both global scales (Wei et al. 1983) and regional scales (Luo and Yanai 1983, 1984; Murakami 1983; Nitta 1983; Murakami et al. 1984). Japanese geostationary satellite (GMS-1) data have been used by Murakami (1983) to examine the temporal and spatial dis-

*The radar echo pattern on July 5 has been discussed by Warner (1984b).

tribution of deep convective activity during summer MONEX. His results for July 1979, presented in the form of the intensity index I_c for deep convection, are shown in Fig. 10.42. Maximum deep convection is found to be concentrated over the Assam-Bengal region and the southern portion of the Tibetan Plateau (including the Himalayas), with secondary centers at several locations over Southeast Asia and the western Pacific.

The pattern of deep convection inferred from infrared satellite data by Murakami (1983) in the summer monsoon region is in generally good agreement with distributions of vertically integrated diabatic heating published by Wei et al. (1983) and Luo and Yanai (1984). The vertically integrated apparent heat source ($\langle Q_1 \rangle$) computed by Luo and Yanai over much of the land area of the summer monsoon for a 40-day period from May 26 to July 4, 1979, is shown in Fig. 9.10. The apparent heat source Q_1 and apparent moisture sink Q_2 (Yanai et al. 1973) referred to here and in subsequent discussions are defined by

$$Q_1 \equiv c_p \left[\frac{\partial \overline{T}}{\partial t} + \overline{\mathbf{v}} \cdot \nabla \overline{T} + \left(\frac{p}{p_0} \right)^{\kappa} \overline{\omega} \frac{\partial \overline{\theta}}{\partial p} \right] \tag{10.1}$$

$$Q_2 \equiv -L \left(\frac{\partial \overline{q}}{\partial t} + \overline{\mathbf{v}} \cdot \nabla \overline{q} + \overline{\omega} \frac{\partial \overline{q}}{\partial p} \right) \tag{10.2}$$

where $\mathbf{v}$ denotes horizontal velocity, T denotes temperature, p denotes pressure, ω denotes vertical p velocity, θ denotes potential temperature, q denotes specific humidity, L denotes latent heat of condensation, $p_0 \equiv 1000$ mb, and $\kappa \equiv R/c_p$, R and c_p being the gas constant and specific heat at constant pressure of dry air. Overbars refer to an average over a horizontal area. The vertical integral of Q_1, as Luo and Yanai note, is directly related to the sum of the diabatic effects: precipitation, surface sensible heat flux, and radiative heating.

The periods of time in the two studies overlap only briefly, so a detailed comparison of Figs. 10.42 and 9.10 is not warranted; however, both do indicate abundant deep convection over the Assam-Bengal region extending eastward toward South China during the summer monsoon. The existence of heat sources over the northern and western plateau (Fig. 9.10) in regions where no deep convection is observed by satellite suggests that much of the heating of the atmosphere in these regions is a consequence of strong surface sensible heat fluxes (to be discussed further later).

3.4.2 Nature of convection and regional differences inferred from diagnostic studies. Recently, several authors (Nitta 1983; Luo and Yanai 1984) have used rawinsonde data from the Tibetan Plateau and surrounding area to diagnose the properties of convection in this mountainous region. Luo and Yanai (1984) have computed Q_1 and Q_2 in four subregions of the monsoon area in (Fig.

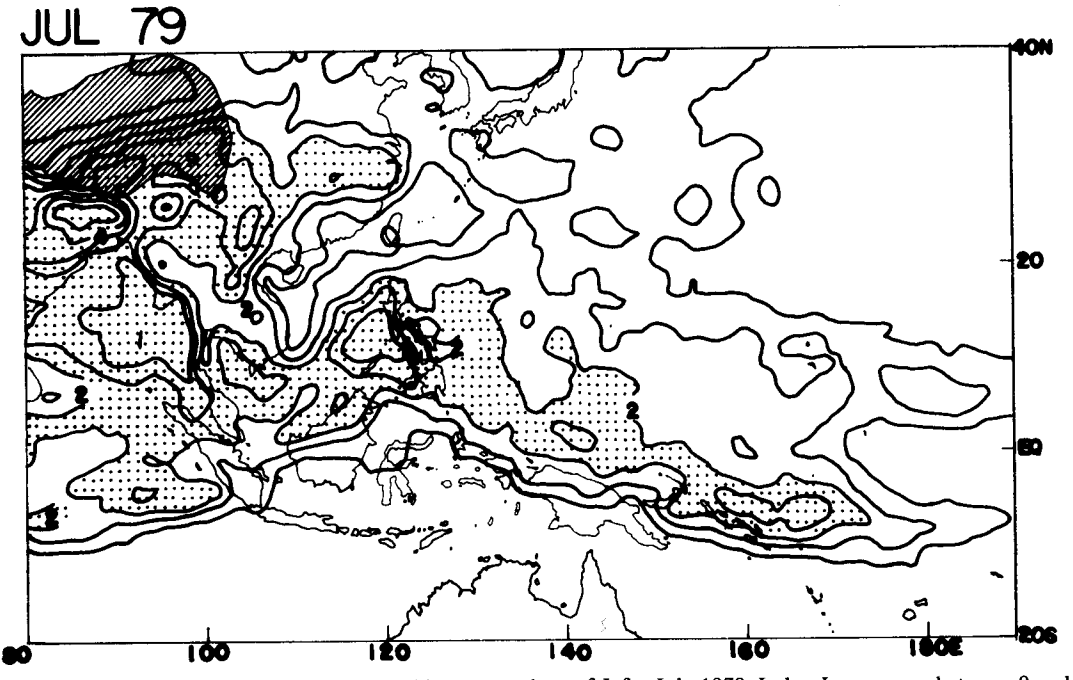

Fig. 10.42. Horizontal distribution of monthly mean values of I_c for July 1979. Index I_c can range between 0 and 10: 0 means that no cumulus tops extend above 400 mb; 10 means that all cumulus tops extend to the tropopause. The contour interval is 0.5 unit starting at 1.0. Values larger than 2.0 are shaded. The hatched area denotes elevations above 3000 m on the Tibetan Plateau. (From Murakami 1983.)

9.8): the western plateau and its vicinity (region I), the eastern plateau (region II), the Yangzi River (region III), and the Assam-Bengal region (region IV). Vertical profiles of ω, Q_1 and Q_2 averaged over the 40-day period from late May to early July for each of the four regions are presented in Fig. 9.12. These profiles indicate distinct regional differences and reflect different convective processes occurring in each region. Over the western plateau (region I) Q_1 is large in the middle to upper troposphere and has a magnitude considerably greater than Q_2. The vertical motion is weakly upward. Because Q_2 is so small in this region, the heating must be attributed to vertical convergence of eddy sensible heat flux (supplied from the dry ground surface), with the heat being mixed upward by turbulence or dry thermal convection. This conclusion is supported by the observation of little precipitation during the 40-day period over the western plateau (Luo and Yanai 1984).

The eastern plateau (region II) is characterized by stronger upward motion with large Q_1 in the upper troposphere and Q_2, while smaller than Q_1, being somewhat larger than that observed over the western plateau. Luo and Yanai point out that these 40-day average profiles reflect the combined effects of two distinctly different conditions during this period: the preonset phase of the monsoon, when the Q_1 and Q_2 profiles resembled those observed for the dry western plateau, and the postonset phase, when Q_2 increased considerably and the profiles of Q_1 and Q_2 resembled those obtained for deep cumulus convection in the tropics (Yanai et al. 1973). In this latter case there is a separation in the levels of maximum Q_1 and Q_2 and Luo and Yanai have used this feature as a signature for deep cumulus convection.

The separation may be explained by considering the alternative forms of (10.1) and (10.2) given by Yanai et al. (1973):

$$Q_1 = Q_R + L(c - e) - \frac{\partial}{\partial p}(\overline{s'\omega'}) \quad (10.3)$$

$$Q_2 = L(c - e) + L\frac{\partial}{\partial p}(\overline{q'\omega'}) \quad (10.4)$$

where Q_R denotes radiative heating rate, c denotes condensation, e denotes evaporation, s denotes dry static energy ($c_pT + gz$), and primes denote departures from horizontal averages. For deep cumulus convection the eddy heat and moisture flux ($\overline{s'\omega'}$ and $\overline{q'\omega'}$) profiles are different, with $\overline{s'\omega'}$ having a peak in the mid to upper troposphere (primarily due to the effects of many numerous, warm-core, nonentraining cumulonimbus) and $\overline{q'\omega'}$ a peak in the lower troposphere (where the strongest vertical gradients in water vapor exist). Thus, the divergence of these fluxes is different, and there is a separation of the Q_1, Q_2 peaks.

The profiles of Q_1 and Q_2 over central China (region III) are considerably different from those in other regions. Both Q_1 and Q_2 are of similar magnitudes and they are in phase. Region III is the area of Mei-Yu frontal-zone precipitation (Yeh 1981), and while considerable rainfall occurs there, it is primarily produced by stratiform cloud systems. Some deep cumulus exist, but their contribution to the total rainfall is of secondary importance. In other words, the eddy terms in (10.3) and (10.4) are relatively small, and therefore, we should expect both Q_1 and Q_2 to be closely approximated by the net condensation in the cloud systems with only a slight suggestion of deep cumulus convection in the profiles (as is observed).

The mean Q_1 and Q_2 profiles in the Assam-Bengal area to the south (region IV) show distinctly separated peaks (Q_1 above Q_2) and reflect the vigorous deep cumulus activity at the foot of the Tibetan Plateau during the summer monsoon period.

The studies by Nitta (1983) and Luo and Yanai (1984) have provided valuable insights into the nature of convection over the Tibetan Plateau and the surrounding area. Regional differences in convective structures have been deduced from rawinsonde data, but detailed subsynoptic characteristics of the convective systems still remain undetermined. This subject is a worthy goal of future measurement programs and studies.

3.4.3 Diurnal variations. As was noted earlier, the diurnal variation of deep convective systems in the near-equatorial winter monsoon region is pronounced. Similarly large diurnal oscillations in convective activity are found to occur over the Tibetan Plateau (Flohn 1968; Yeh and Gao 1979). Murakami (1983) has found, using GMS-1 infrared satellite data, that there is a minimum in deep convective cloudiness over the southern Tibetan Plateau at 900 LST and a maximum at 1600 LST Diurnal variations in the low-level circulation and vertical motion over the Tibetan Plateau have been found by Flohn (1968), Murakami (1981), Kuo and Qian (1981), Luo and Yanai (1983, 1984), and Nitta (1983). These correspond well with the cloudiness changes.

To illustrate the diurnal variations, we show the diagnostic results of Nitta for his area E (roughly corresponding to the eastern plateau, region II, of Luo and Yanai) in Fig. 10.43. Divergence and vertical motion were computed at 000 GMT ($\approx$600 LST) and 1200 GMT ($\approx$1800 LST), and averages for a 100-day period from May 30 to September 7, 1979, were prepared (Fig. 10.43a). Over the eastern plateau weak lower-tropospheric convergence and upper-tropospheric divergence are observed in the morning, but this pattern changes to strong divergence above low-level convergence in the evening. As a result, there is a large fluctuation in vertical motion, with a tri-

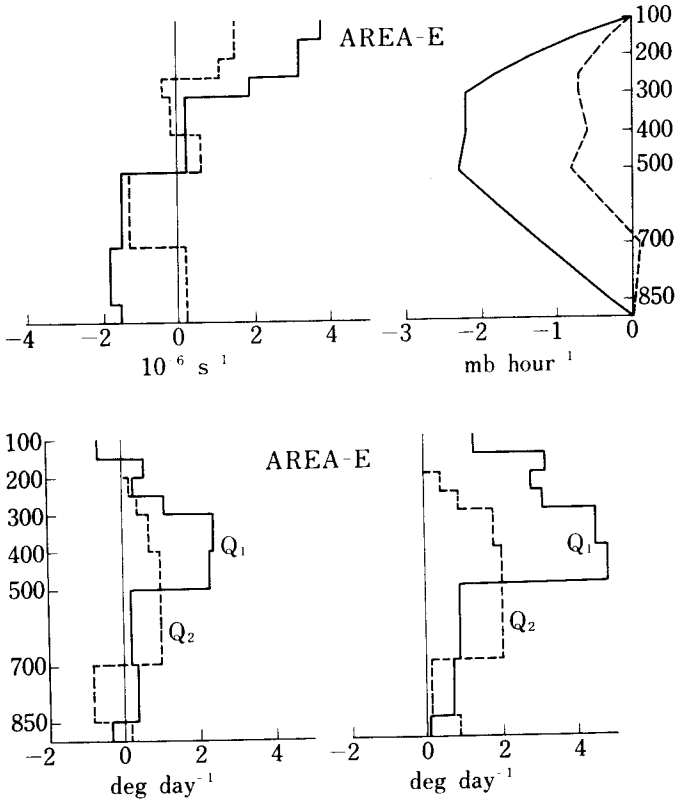

Fig. 10.43. Diurnal variations of 100-day mean quantities. (*a*) 100-day mean horizontal divergence and vertical p velocity at 000 GMT (600 LST, dashed lines) and 1200 GMT (1800 LST, solid lines) over area E (an area roughly corresponding to the eastern plateau, region II, of Luo and Yanai 1984). (*b*) 100-day mean large-scale apparent heat source and moisture sink at 000 GMT *(left)* and 1200 GMT *(right)* over area E. (From Nitta 1983.)

pling of the magnitude of upward motion in the evening. This enhanced rising motion is a result of strong surface heating during the daytime over the elevated Tibetan Plateau region. The Q_1 and Q_2 profiles (Fig. 10.43b) show corresponding changes in magnitude (not shape), with a marked increase in deep cumulus convection indicated during the evening.

4 CONCLUSIONS, QUESTIONS, AND RECOMMENDATIONS FOR FURTHER RESEARCH

4.1 Conclusions

As foreseen by Ramage (1971) (see the "Introduction," this chapter), monsoon rainfall observed during MONEX was dominated by mesoscale cloud features consisting of extensive stratiform cloud and precipitation juxtaposed with intense elements of deep convection.

The mesoscale cloud systems observed in winter MONEX were similar to GATE cloud clusters. They exhibited a life cycle consisting of an entirely convective initial stage, followed by the development of a stratiform precipitation area, which became an increasingly dominant aspect of the cloud system. About 30 to 50% of the total rainfall from these cloud systems appears to be stratiform.

In summer MONEX, the primary precipitating cloud systems in the Arabian Sea region were located upwind (with respect to the low-level flow) of the western Ghats. The precipitation areas of these cloud systems were mesoscale ($\approx$200 km wide), but the data so far analyzed from the Arabian Sea Experiment have not indicated the internal structure of these orographically triggered cloud systems. Over the Bay of Bengal region, the clouds dominating the precipitation are associated with Bay of Bengal depressions. Summer MONEX aircraft data obtained in a depression showed that the rain was concentrated in mesoscale areas, which were several hundred kilometers in dimension and consisted of convective cores coupled to large areas of moderate, apparently stratiform rain. These precipitation areas resembled winter monsoon cloud clusters in their horizontal structure and cloud microphysical characteristics. However, the data collected did not have sufficient coverage in time or in the vertical to determine whether they were entirely analogous to winter monsoon cloud systems.

Summer monsoon cloud systems in the Tibetan Plateau region were not observed directly. However, they were studied through their effects on the large-scale environment. Strong regional variations in these effects were noted. Deep convective cloud systems were indicated for the Assam-Bengal region and the post-onset period

over the eastern plateau, while stratiform cloud systems characterized the central China Plain.

The mesoscale stratiform component of precipitating monsoonal cloud systems significantly affects large-scale heating and vertical motion profiles. Within the mid-to-upper-tropospheric nimbostratus cloud layer, latent heat release provides warming, while melting of precipitation particles near cloud base and evaporation below contribute cooling in the lower troposphere. Convergence of radiative flux in the stratiform cloud layer warms and destabilizes the mid-to-upper troposphere. Radiatively and/or dynamically induced cooling at and just above the cloud layer cools the upper troposphere and lower stratosphere. Representations of monsoon cloud systems in numerical models of monsoon circulations that do not account for these effects associated with extensive precipitating cloud shields do not reflect the conditions observed in MONEX.

Strong diurnal variation of monsoon cloud systems occurred in summer MONEX over the Tibetan Plateau and in winter MONEX over the Indonesian-Malaysian maritime continent. The diurnal variation over the plateau is tied to strong daytime surface heating over elevated regions, while over the maritime continent it is the result of land-sea circulations associated with the large islands and peninsulas of the region.

4.2 Questions

Since MONEX was not designed as a mesoscale experiment, it is not surprising that significant questions remain about monsoon cloud systems. The following are among the most obvious problems.

The nature of precipitating cloud systems in the summer monsoon continues to be especially poorly known. In MONEX, no direct observations were obtained of Tibetan Plateau cloud systems. The internal structure of precipitating clouds over the Arabian Sea has not yet been analyzed. The structure of precipitation patterns in a Bay of Bengal depression has been examined but only with respect to horizontal features. These limited views of summer monsoon cloud systems make difficult their comparison with winter monsoon and GATE cloud clusters. Particular questions are: What are the life cycles and vertical structures of the precipitating components of summer monsoon cloud systems? Without this knowledge it will remain difficult to determine the similarity of these systems to other tropical precipitation systems or to determine the role of large-scale lifting in the mesoscale precipitation features of Bay of Bengal depressions.

Winter MONEX cloud clusters were observed in more detail than were cloud systems of summer MONEX. Nonetheless, important questions also remain for the winter systems. Microphysical structure was observed mainly at just one level, and questions concerning the origin and growth of the ice particles falling through the stratiform cloud cannot be answered at present. Also, the internal air motions of these cloud systems were not documented intensively and continue to be known only in a limited way through inferences from measurements of other quantities. The question remains whether these inferences are correct. Without better answers to the above questions regarding microphysics and air motions, the dynamics, precipitation growth, and radiative processes in winter monsoon cloud systems will continue to be somewhat speculative.

The prevalence of mesoscale stratiform cloud and precipitation areas that occur in conjunction with deep convection in monsoon cloud systems indicates that the diabatic heating and cooling associated with the extensive stratiform regions are significant. What are the net quantitative and qualitative effects of these stratiform processes in the energy budgets of regions such as the maritime continent in winter or India and surrounding territory in summer? This question will have to be reckoned with in the design of accurate large-scale simulations of monsoon circulations.

A question basic to understanding the winter monsoon is why the maritime continent region is selected by the large-scale circulation as a focus of general upward motion. Observations of cloud systems in winter MONEX may have a bearing on the answer to this question. A notable feature of these cloud systems was that the marked diurnal variation they exhibited did not disappear in periods of increased synoptic-scale forcing; indeed, the amplitude of the diurnal oscillation was greater in these periods. It is generally recognized that mesoscale convective systems in both midlatitudes and tropics require a triggering mechanism. The land-sea circulations in the winter MONEX area (enhanced by the mountainous terrain, warm seas, and equatorial location) produce intensified convergence alternately offshore and overland. Thus, they constitute a region of ubiquitous triggering sites for deep convection. Perhaps, then, the diurnal cycle in this region does not merely redistribute cloud systems in time and space but rather provides the triggering required to release the instability of air brought into the region by the large-scale flow. And when stronger synoptic forcing provides a supply of air more susceptible to local triggering of convection, the ever-present diurnal circulations can release more convection. This hypothesis suggests the question: What is the role of diurnal land-sea circulations in the selection of the maritime continent as a focus of large-scale lifting in the winter monsoon?

A final question from MONEX arises because the observational programs were conducted

largely over oceans. What are the differences, if any, from precipitating cloud systems over the landmasses of the monsoon regions? Obviously, our knowledge of monsoon cloud systems will remain incomplete without an answer to this basic question.

4.3 Suggestions for further research

From the foregoing questions, it is evident that there is no shortage of requirements for further research aimed at understanding monsoon cloud systems. Present gaps in this understanding can be filled if future field experiments are designed to include more thorough documentation of the cloud systems than was accomplished in MONEX.

Summer monsoon cloud systems, especially the mesoscale precipitation features in Bay of Bengal depressions, need to be observed with sufficient coverage in time and space to determine their life cycles and attendant vertical stratification of precipitation growth processes. Only then can these systems be compared adequately with other cloud systems, such as winter monsoon cloud clusters, or can the role synoptic-scale lifting in monsoon depressions plays in them be determined.

Winter monsoon cloud clusters also need to be observed with better vertical definition, and their internal air motions must be determined. Then the vertical distribution of diabatic processes associated with these cloud systems will be better established.

Much of the needed documentation of the internal structure of winter and summer monsoon cloud systems can be obtained with existing research tools. Geosynchronous satellite data, of course, will be indispensable. In addition, strategically placed ground-based research radar and sounding stations can be used in conjunction with research aircraft equipped with quantitative radar, microphysical instrumentation, and radiometers. These measurements can greatly exceed in value those obtained in MONEX if the radar (both ground-based and aircraft) are Doppler, if vertical as well as horizontal radar scanning is employed on flights, and if flights are conducted to observe the cloud systems by design rather than by serendipity. Observations should be carried out over land as well as over oceanic areas, and sounding networks should be sufficiently dense to establish budgets over regions such as the maritime continent, so that the role of the observed cloud systems within the larger-scale environment can be established.

Although the mounting of field experiments is a large undertaking, it must be considered seriously in this case. Some research can still be done with existing MONEX data. For example, airborne microphysical and radar data from summer MONEX are still being examined. And numerical modeling can be employed to a degree; however, its usefulness will be limited without confirmatory data. A major advance in understanding monsoon cloud systems cannot reasonably be expected without another field effort. As noted above, the technology exists for such an effort, and we look forward to the day when it will occur.

Acknowledgments

The authors appreciate the help and comments of C. S. Ramage, C. Warner, J. Simpson, and D. D. Churchill. We extend thanks to Gail Watson for typing the manuscript. The authors' research is supported by the National Science Foundation under Grants ATM80-17327 and ATM82-06808.

REFERENCES

Agee, E. M., and F. E. Lomax (1978). Structure of the mixed layer and inversion layer associated with patterns of mesoscale cellular convection during AMTEX '75. *J. Atmos. Sci.* **35,** 2281–3301.

Albrecht, B., and S. K. Cox (1975). The large-scale response of the tropical atmosphere to cloud modulated infrared heating. *J. Atmos. Sci.* **32,** 16–24.

Anthes, R. A. (1983). Regional models of the atmosphere in middle latitudes. *Mon. Wea. Rev.* **111,** 1306–1335.

Arakawa, A., and W. H. Schubert (1974). Interaction of a cumulus cloud ensemble with the large-scale environment. Part I. *J. Atmos. Sci.* **31,** 674–701.

Atkinson, G. D., and J. C. Sadler (1970). *Mean-cloudiness and gradient level wind charts over the tropics.* Technical Report 215, Vol. II, U.S. Air Weather Service (AD-711 832).

Atticks, M. G., and G. D. Robinson (1983). Some features of the structure of the tropical tropopause. *Q. J. R. Meteor. Soc.* **109,** 295–308.

Brown, J. M. (1979). Mesoscale unsaturated downdrafts driven by rainfall evaporation: A numerical study. *J. Atmos. Sci.* **36,** 313–338.

Chang, C. -P (1970). Westward propagating cloud patterns in the tropical Pacific as seen from time-composite satellite photographs. *J. Atmos. Sci.* **27,** 133–138.

———, and K. M. Lau (1980). Northeasterly cold surges and near-equatorial disturbances over the winter MONEX area during 1974. Part II: Planetary-scale aspects. *Mon. Wea. Rev.* **108,** 293–312.

———, J. E. Erickson, and K. -M. Lau (1979). Northeasterly cold surges and near-equatorial disturbances over the winter MONEX area during December 1974. Part I: Synoptic aspects. *Mon. Wea. Rev.* **107,** 812–829.

———, G. T. Chen, T. E Gerish, and L. C. Chou (1982). Structure of cyclonic circulations near Borneo during winter MONEX. In *Report*

of the international conference on the scientific results of the Monsoon Experiment, Denpasar, Bali, Indonesia, Section 5, 9–12. World Meteorological Organization, Geneva.

Cheang, B. K. (1977). Synoptic features and structures of some equatorial vortices over the South China Sea in the Malaysian region during the winter monsoon, December 1973. *Pure Appl. Geophys.* **115,** 1303–1333.

——— (1978). Structure of cyclonic disturbance over the South China Sea and the Malaysia region during the winter monsoon. *Indian J. Meteor. Hydrolog. Geophys.* **29** (1, 2), 16–25.

Cheng, C. -P., and R. A. Houze, Jr. (1979). The distribution of convective and mesoscale precipitation in GATE radar echo patterns. *Mon. Wea. Rev.* **107,** 1370–1381.

Chiyu, T. (1979). A preliminary study of low-level winds over peninsular Malaysia during the 1976–1977 northeast winter monsoon. *J. Meteor. Soc. Jpn.* **57,** 354–357.

——— (1984). A case study of heavy rain spell on 13th–25th December 1982 over the east coast of peninsular Malaysia and Singapore. *J. Meteor. Soc. Jpn.* **62,** 296–307.

Chong, M. (1983). Les radars météorologiques Doppler pour l'étude de la, convection orageuse: Application à l'étude d'une ligne de grains tropicale. Thèse de Doctorat d'Etat, Université de Paris, VI.

Churchill, D. D., and R. A. Houze, Jr. (1984a). Development and structure of winter monsoon cloud clusters on 10 December 1978. *J. Atmos. Sci.* **41,** 933–960.

———, and R. A. Houze, Jr. (1984b). Mesoscale updraft magnitude and cloud-ice content deduced from the ice budget of the stratiform region of a tropical cloud cluster. *J. Atmos. Sci.* **41,** 1717–1725.

Cobb, R. T. and L. J. M. Coleby (1966). *Monsoon lands. Part I: General introduction, India, Pakistan, Ceylon, Burma.* Advanced Level Geography Series. University Tutorial Press, Cambridge, England

Cox, S. K., and K. T. Griffith (1979). Estimates of radiative divergence during phase III of the GARP Atlantic Tropical Experiment. Part II. Analysis of the phase III results. *J. Atmos. Sci.* **36,** 586–601.

Danielsen, E. F. (1982). A dehydration mechanism for the stratosphere. *Geophys. Res. Lett.* **9,** 605–608.

Davidson, N. E., J. L. McBride, and B. J. McAvaney (1983). The onset of the Australian monsoon during winter MONEX: Synoptic aspects. *Mon. Wea. Rev.* **111,** 496–516.

Fein, J. S., and J. P. Kuettner (1980). Report on the summer MONEX field phase. *Bull. Am. Meteor. Soc.* **61,** 461–474.

Fitzjarrald, D. R., and M. Garstang (1981). Vertical structure of the tropical boundary layer. *Mon. Wea. Rev.* **109,** 1512–1526.

Flohn, H. (1968). *Contribution to the meteorology of the Tibetan Highlands.* Atmospheric Science Paper No. 130, Colorado State University, Fort Collins.

Frank, W. M. (1977). Convective fluxes in tropical cyclones. *J. Atmos. Sci.* **34,** 1554–1568.

——— (1983). The cumulus parameterization problem. *Mon. Wea. Rev.* **111,** 1859–1871.

Fritsch, J. M., and J. M. Brown (1982). On the generation of convectively driven mesohighs aloft. *Mon. Wea. Rev.* **110,** 1554–1563.

———, and R. A. Maddox (1981). Convectively driven mesoscale weather systems aloft. Part I: Observations. *J. Appl. Meteor.* **20,** 9–19.

Gamache, J. F., and R. A. Houze, Jr. (1982). Mesoscale air motions associated with a tropical squall line. *Mon. Wea. Rev.* **110,** 118–135.

——— and R. A. Houze, Jr. (1983). Water budget of a mesoscale convective system in the tropics. *J. Atmos. Sci.* **40,** 1835–1850.

Gan, T. L. (1970). The circulation pattern over Singapore and the east coast of West Malaya during January and February 1967 compared with that of January and February 1968. In *Forecasting of heavy rains and floods: Proceedings of the Joint Training Seminar, RAII and V, Kuala Lumpur, November 11–23, 1968,* 283–289. World Meteorological Organization, Geneva.

Godbole, R. V. (1977). The composite structure of the monsoon depression. *Tellus* **29,** 25–40.

Gray, W. M., and R. W. Jacobson, Jr. (1977). Diurnal variation of oceanic deep cumulus convection. *Mon. Wea. Rev.* **105,** 1171–1188.

Greenfield, R. S., and T. N. Krishnamurti (1979). The Winter Monsoon Experiment—Report of December 1978 field phase. *Bull. Am. Meteor. Soc.* **60,** 439–444.

Griffith, K. T., S. K. Cox, and R. G. Knollenberg (1980). Infrared radiative properties of tropical cirrus clouds inferred from aircraft measurements. *J. Atmos. Sci.* **37,** 1077–1087.

Grossman, R. L., and D. R. Durran (1984). Interaction of low-level flow with the western Ghat Mountains and offshore convection in the summer monsoon. *Mon. Wea. Rev.* **112,** 652–672.

———, and O. Garcia (1985). The distribution of deep convection over ocean and land during the summer monsoon. *Mon. Wea. Rev.* (forthcoming).

Harris, B. E., J. C. Sadler, W. R. Brett, F. P. Ho, and G. Ing (1969). *Role of the synoptic scale in convection over Southeast Asia during the summer monsoon. Hawaii Institute of Geophysics Report 69-9. University of Hawaii, Honolulu.*

Hartmann, D. L. H. H. Hendon, and R. A. Houze, Jr. (1984). Some implications of the mesoscale circulations in tropical cloud clusters for large-scale dynamics and climate. *J. Atmos. Sci.* **41,** 113–121.

Holland, G. J., and T. D. Keenan (1980). Picture of the month—Diurnal variations of convec-

tion over the "maritime continent." *Mon. Wea. Rev.* **108,** 223–225.

Holton, J. R. (1972). Waves in the equatorial stratosphere generated by tropospheric heat sources. *J. Atmos. Sci.* **29,** 368–375.

Houze, R. A., Jr. (1977). Structure and dynamics of a tropical squall-line system observed during GATE. *Mon. Wea. Rev.* **105,**1540–1567.

———, (1982). Cloud clusters and large-scale vertical motions in the tropics. *J. Meteor. Soc. J.* **60,** 396–410.

———, and A. K. Betts (1981). Convection in GATE. *Rev. Geophys. Space Phys.* **19,** 541–576.

———, and D. D. Churchill (1984). Microphysical structure of winter monsoon cloud clusters. *J. Atmos. Sci.* **41,** 3405–3411.

———, and P. V. Hobbs (1982). Organization and structure of precipitating cloud systems. In *Advances in geophysics,* Vol. 24, 225–315. Academic Press, New York.

——— and D. D. Churchill (1987). Mesoscale organization and cloud microphysics in a Bay of Bengal depression. *J. Atmos. Sci.* (In Press.)

———, and E. N. Rappaport (1984). Air motions and precipitation structure of an early summer squall line over the eastern tropical Atlantic. *J. Atmos. Sci.* **41,** 553–574.

———, S. G. Geotis, F. D. Marks, and A. K. West (1981). Winter monsoon convection in the vicinity of North Borneo. Part I: Structure and time variation of the clouds and precipitation. *Mon. Wea. Rev.* **108,** 1595–1614.

Johnson, R. H. (1980). Diagnosis of convective and mesoscale motions during phase III of GATE. *J. Atmos. Sci.* **37,** 733–753.

——— (1982). Vertical motion in near-equatorial winter monsoon convection. *J. Meteor. Soc. Jpn.* **60,** 682–690.

——— (1984). Partitioning tropical heat and moisture budgets into cumulus and mesoscale components: Implications for cumulus parameterization. *Mon. Wea. Rev.* **112,** 1590–1601.

———, and D. C. Kriete (1982). Thermodynamic and circulation characteristics of winter monsoon tropical mesoscale convection. *Mon. Wea. Rev.* **110,** 1898–1911.

———, and M. E. Nicholls (1983). A composite analysis of the boundary layer accompanying a tropical squall line. *Mon. Wea. Rev.* **111,** 308–319.

———, and D. L. Priegnitz (1981). Winter monsoon convection in the vicinity of North Borneo. Part II: Effects on large-scale fields. *Mon. Wea. Rev.* **109,** 1615–1628.

———, and G. S Young (1983). Heat and moisture budgets of tropical mesoscale anvil clouds. *J. Atmos. Sci.* **40,** 2138–2147.

Jorgensen, D. P. (1984). Mesoscale and convective-scale characteristics of mature hurricanes. Part II: Inner core structure of Hurricane Allen (1980). *J. Atmos. Sci.* **41,** 1287–1311.

Kley, D., A. L. Schmeltekopf, K. Kelly, R. H. Winkler, T. L. Thompson, and M. McFarland (1982). Transport of water vapor through the tropical tropopause. *Geophys. Res. Lett.* **9,** 617–620.

Koteswaram. P., and C. A. George (1958). On the formation of monsoon depression in the Bay of Bengal. *Indian J. Meteor. Geophys.* **9,** 9–22.

Krishnamurti, T. N., and D. Subrahmanyam (1982). The 30-50 day mode at 850 mb during MONEX. *J. Atmos. Sci.* **39,** 2088–2095.

———, P. Ardanuy, Y. Ramanathan, and R. Pasch (1979). *Quick look "Summer MONEX atlas." Part II. The onset phase.* FSU Report 79–5, Department of Meteorology, Florida State University, Tallahasee.

———, S. Cocke, R. Pasch, and S. Low-Nam (1983). *Precipitation estimates from raingauge and satellite observations, summer MONEX.* FSU Report 83–7, Department of Meteorology, Florida State University, Tallahassee.

———, M. Kanamitsu, W. J. Koss, and J. D. Lee (1973). Tropical east-west circulations during the northern winter. *J. Atmos. Sci.* **30,** 780–787.

———, Y. Ramanathan, P. Ardanuy, R. Pasch, and P. Greiman (1980). *Quick look "Summer MONEX atlas." Part III. The monsoon depression phase.* FSU Report 80–8, Department of Meteorology, Florida State University, Tallahasee.

———, M. Kanamitsu, R. Godbole, C. B. Chang, F. Carr, and J. H. Chow (1975). Study of a monsoon depression. I. Synoptic structure. *J. Meteor. Soc. J.* **53,** 227–240.

Kuo, H. L., and Y. F. Qian (1981). Influence of the Tibetan Plateau on cumulative and diurnal changes of weather and climate in summer. *Mon. Wea. Rev.* **109,** 2337–2356.

Lau, K.-M. and M.-T. Li (1984). The monsoon of East Asia and its global associations. *Bull Am. Meteor. Soc.* **65,** 114–125.

Leary, C. A. (1979). Behavior of the wind field in the vicinity of a cloud cluster in the intertropical convergence zone. *J. Atmos. Sci.* **36,** 631–639.

——— (1980). Temperature and humidity profiles in mesoscale unsaturated downdrafts. *J. Atmos. Sci.* **37,** 1005–1012.

——— (1984). Precipitation structure of the cloud clusters in a tropical easterly wave. *Mon. Wea. Rev.* **112,** 313–325.

———, and R. A. Houze, Jr. (1979a). The structure and evolution of convection in a tropical cloud cluster. *J. Atmos. Sci.* **36,** 437–457.

———, and R. A. Houze, Jr. (1979b). Melting and evaporation of hydrometeors in precipitation from the anvil clouds of deep tropical convection. *J. Atmos. Sci.* **36,** 669–679.

———, and R. A. Houze, Jr. (1980). The contribution of mesoscale motions to mass and heat fluxes of an intense tropical convective system. *J. Atmos. Sci.* **37,** 784–796.

———, and E. N. Rappaport (1983). Internal structure of a mesoscale convective complex. In *Proceedings of the 21st conference on radar meteorology, Edmonton, Alberta, Canada,* 70–77. American Meteorological Society, Boston.

LeMone, M. A., and E. J. Zipser (1980). Cumulonimbus vertical velocity events in GATE. Part I: Diameter, intensity and mass flux. *J. Atmos. Sci.* **37,** 2444–2457.

Lim, H., and C.-P. Chang (1981). A theory for midlatitude forcing of tropical motions during winter monsoons. *J. Atmos. Sci.* **38,** 2377–2392.

Love, G. (1982). The role of the general circulation in western Pacific tropical cyclone genesis. Ph.D. diss. Colorado State University, Fort Collins.

Luo, H., and M. Yanai (1983). The large-scale circulation and heat sources over the Tibetan Plateau and surrounding areas during the early summer of 1979. Part I: Precipitation and kinematic analyses. *Mon. Wea. Rev.* **111,** 922–944.

———, and M. Yanai (1984). The large-scale circulation and heat sources over the Tibetan Plateau and surrounding areas during the early summer of 1979. Part II: Heat and moisture budgets. *Mon. Wea. Rev.* **112,** 966–989.

McBride, J. L. (1983). Satellite observations of the Southern Hemisphere monsoon during winter MONEX. *Tellus* **35A,** 189–197.

Maddox, R. A. (1983). Large-scale meteorological conditions associated with midlatitude, mesoscale convective complexes. *Mon. Wea. Rev.* **111,** 1475–1493.

Malkus, J. S., and H. Riehl (1964). Cloud structure and distributions over the tropical Pacific Ocean. *Tellus* **16,** 275–287.

Manabe, S., J. L. Holloway, Jr., and H. M. Stone (1970). Tropical circulations in a time-integration of a global model of the atmosphere. *J. Atmos. Sci.* **27,** 580–613.

Mukherjee, A. K. (1980). Dimension of an "offshore vortex" in East Arabian Sea as deduced from observations during MONEX 1979. In FGGE Operations Report. Vol. 9, Part A—*Results of summer MONEX field phase research,* 176–184. World Meteorological Organization, Geneva.

Murakami, M. (1983). Analysis of the deep convective activity over the western Pacific and Southeast Asia. Part I: Diurnal variation. *J. Meteor. Soc. Jpn.* **61,** 60–76.

Murakami, T. (1978). Regional energetics of the 200 mb summer circulations. *Mon. Wea. Rev.* **106,** 614–628.

——— (1980). Temporal variations of satellite-observed outgoing longwave radiation. Part I: Long-period (15–30 day) oscillations. *Mon. Wea. Rev.* **108,** 408–426.

——— (1981). Orographic influence of the Tibetan Plateau on the Asiatic winter monsoon circulation. Part II: Diurnal variations. *J. Meteor. Soc. Jpn.* **59,** 66–84.

———, and A. Sumi (1982). Southern Hemisphere summer monsoon circulation during the 1978–79 WMONEX. Part I: Monthly mean wind fields. *J. Meteor. Soc. Jpn.* **60,** 638–648.

——— ,and M. S. Unninayar (1977). Atmospheric circulation during December 1970 through February 1971. *Mon. Wea. Rev.* **105,** 1024–1038.

———, T. Iwashima, and T. Nakazawa (1984). Heat, moisture and vorticity budget before and after the onset of the 1978–79 Southern Hemisphere summer monsoon. *J. Meteor. Soc. Jpn.* **62,** 69–87.

Newell, R. E., and S. Gould-Stewart (1981). A stratospheric fountain? *J. Atmos. Sci.* **38,** 2789–2796.

Ninomiya, K., and T. Akiyama (1976). Structure and heat energy budget of mixed layer capped by inversion during the period of polar outbreak over Kuroshio region. *J. Meteor. Soc. Jpn.* **54,** 160–174.

———, M. Ikawa, and T. Akiyama (1981). Long-lived medium scale cumulonimbus cluster in Asian subtropical humid region. *J. Meteor. Soc. Jpn.* **59,** 564–577.

Nitta, T. (1983). Observational study of heat sources over the eastern Tibetan Plateau during the summer monsoon. *J. Meteor. Soc. Jpn.* **61,** 590–605.

———, and K. Masuda (1981). Observational study of a monsoon depression developed over the Bay of Bengal during summer MONEX. *J. Meteor. Soc. Jpn.* **59,** 672–682.

———, and S. S. So (1980). Structure and heat, moisture and momentum budgets of a convective mixed layer during AMTEX '75. *J. Meteor. Soc. Jpn.* **58,** 378–393.

Ogura, Y., and M. T. Liou (1980). The structure of a mid-latitude squall line: A case study. *J. Atmos. Sci.* **37,** 553–567.

Pielke, R. A. (1984). *Mesoscale meteorological modeling.* Academic Press, Orlando, Fla.

Ramage, C. S. (1968). Role of a tropical "maritime continent" in the atmospheric circulation. *Mon. Wea. Rev.* **96,** 365–370.

——— (1971). *Monsoon meteorology.* Academic Press, New York.

Rao, Y. P. (1976). *The southwest monsoon.* Indian Meteorological Department Monograph, Synoptic Meteorology 1/1976, Indian Meteorological Department, New Delhi.

——— (1981). The climate of the Indian subcontinent. In *Climates of southern and western Asia.* Vol. 9. *World survey of climatology,* ed.

H. E. Landsberg (Volume editors K. Takahashi and H. Arakawa) Elsevier, Amsterdam.

Riehl, H. (1979). *Climate and weather in the tropics.* Academic Press, New York.

———, and J. S. Malkus (1958). On the heat balance in the equatorial trough zone. Geophysica **6,** 503–538.

Sadler, J. C. (1977). *The upper tropospheric circulation over the global tropics. Part II–Statistics.* UHMET 77–02, Department of Meteorology, University of Hawaii, Honolulu.

——— (1979). Synoptic-scale quick look for winter MONEX–December 1978. UHMET 79–02, Department of Meteorology, University of Hawaii, Honolulu.

Saha, K., F. Sanders, and J. Shukla (1981). Westward propagating predecessors of monsoon depressions. *Mon. Wea. Rev.* **109,** 330–343.

Sanders, F. (1984). Quasi-geostrophic diagnosis of the monsoon depression of 5–8 July 1979. *J. Atmos. Sci.* **41,** 538–552.

Short, D. A., and J. M. Wallace (1980). Satellite-inferred morning-to-evening cloudiness changes. *Mon. Wea. Rev.* **108,** 1160–1169.

Sikka, D. R., and S. Gadgil (1980). On the maximum cloud zone and the ITCZ over Indian longitudes during the southwest monsoon. *Mon. Wea. Rev.* **108,** 1840–1853.

———, and R. Grossman (1981). Weather summary. In FGGE Operations Report Vol. 8, *Summer MONEX Field Phase Report,* 2–1, to 2–39. World Meteorological Organization, Geneva.

Simpson, R. H., B. J. Morrison, and C. Warner (1981). Changes in the monsoon circulation of the South China Sea imposed by the surge of 10–12 December 1978. In *Report of the international conference on early results of FGGE and large-scale aspects of its Monsoon Experiment, Tallahassee, Fla.,* Section 10, 21–25. World Meteorological Organization, Geneva.

Smith, R. B., and Y. Lin (1983). Orographic rain on the western Ghats. *In Proceedings of the first Sino-American workshop on mountain meteorology,* ed. E. Reiter, Z. Baozhen, and Q. Yongfu, 71–94. Science Press, Beijing, and American Meteorological Society, Boston.

Smull, B. F., and R. A. Houze, Jr. (1984). Dual-Doppler radar analysis of an Oklahoma squall-line system. In *22nd conference on radar meteorology,* preprint volume, 43–48. American Meteorological Society, Boston.

Sumi, A., and T. Murakami (1981). Large-scale aspects of the 1978–79 winter circulation over the greater WMONEX region. Part I: Monthly and season mean fields. *J. Meteor. Soc. Jpn.* **59,** 625–645.

Surgi, N. (1983). The structure and dynamics of a monsoon depression. M. S. thesis, Florida State University, Tallahassee.

Tao, S.-Y. and Y.-H. Ding (1981). Observational evidence of the influence of the Qinhai-Xizang (Tibet) Plateau on the occurrence of heavy rain and severe storms in China. *Bull. Am. Meteor. Soc.* **62,** 23–30.

Troup, A. J. (1961). Variations in upper tropospheric flow associated with the onset of the Australian summer monsoon. *Indian J. Meteor. Geophys.* **12,** 217–230.

Wang, J. Z., and M. T. Li (1982) Cross-equatorial flow from Australian monsoon over China. *Sci. Atmos. Sin* **6,** 1–10.

Warner, C. (1981). Photogrammetry from aircraft side camera movies: Winter MONEX, *J. Appl. Meteor.* **20,** 1516–1526.

——— (1982a). *Cloud maps for 24 June 1979 over the Arabian Sea: Summer MONEX final report to NSF.* NTIS No. PB84–231018, University of Virginia, Charlottesville.

——— (1982b). Mesoscale features and cloud organization on 10–12 December 1978, over the South China Sea. *J. Atmos. Sci.* **39,** 1619–1641.

——— (1984a). Core structure of a Bay of Bengal monsoon depression. *Mon. Wea. Rev.* **112,** 137–152.

——— (1984b). *Satellite observations of a monsoon depression: Final report to NASA under Grant NAG 5–297.* NTIS No. PB84–212059, University of Virginia, Charlottesville.

——— and R. H. Grumm (1984. Cloud distributions in a Bay of Bengal monsoon depression. *Mon. Wea. Rev.* **112,** 153–172.

———, and D. P. McNamara (1984). Aircraft measurements of convective draft cores in MONEX. *J. Atmos. Sci.* **41,** 430–438.

Webster, P. J. (1972). Response of the tropical atmosphere to local, steady forcing. *Mon. Wea. Rev.* **100,** 518–541.

———, and G. L. Stephens (1980). Tropical upper-tropospheric extended clouds: Inferences from winter MONEX. *J. Atmos. Sci.* **37,** 1521–1541.

———, L. C. Chou, and K. M. Lau (1977). Mechanisms affecting the state transition and evolution of the monsoon. *Pure Appl. Geophys.* **115,** 1463–1491.

Wei, M.-Y. D. R. Johnson, and R. D. Townsend (1983). Seasonal distributions of diabatic heating during the First GARP Global Experiment. *Tellus* **35A,** 241–255.

Williams, M. (1981). Interhemispheric interactions during winter MONEX. In *Report of the international conference on early results of FGGE and large-scale aspects of its Monsoon Experiments, Tallahassee, Fla.,* Section 10, 12–16. World Meteorological Organization, Geneva.

Wirjohamidjojo. S. (1982). The main synoptic features and the relation to the distribution of rainfall over Java Sea and its surroundings during winter MONEX period. In *Report of the in-*

ternational conference on the scientific results of the Monsoon Experiment, Denpasar, Bali, Indonesia, 9–12. Section 5, World Meteorological Organization, Geneva.

WMO (World Meteorological Organization) (1976). *The Monsoon Experiment.* Global Atmospheric Research Programme (GARP), WMO–ICSU Joint Organizing Committee, GARP Publications Series No. 18, World Meteorological Organization, Geneva.

——— (1980). *Winter MONEX field phase report.* FGGE Operations Report No. 7, World Meteorological Organization, Geneva.

Yanai, M., S. Esbensen, and J. H. Chu (1973). Determination of bulk properties of tropical cloud clusters from large-scale heat and moisture budgets. *J. Atmos. Sci.* **30,** 611–627.

Yasunari, T. (1979). Cloudiness fluctuations associated with the Northern Hemisphere summer monsoon. *J. Meteor. Soc. Jpn.* **57,** 227–242.

Yeh, T. C. (1981). Some characteristics of the summer circulation over the Quinghai-Xizang (Tibet) Plateau and its neighborhood. *Bull. Am. Meteor. Soc.* **62,** 14–19.

———, and Y. -X. Gao (1979). *The meteorology of the Qinghai-Xizang Plateau. Scientific Press, Beijing (in Chinese).*

Young, J. A., H. Virji, D. P. Wylie, and C. Lo (1980). *Summer monsoon windsets from geostationary satellite data, 1 May–31 July 1979.* University of Wisconsin, Space Science and Engineering Center and Department of Meteorology, Madison.

Zhu, F.-C. (1983). Organized deep cumulus convection over the South China Sea and its interaction with cold surges. *J. Meteor. Soc. Jpn.* **61,** 839–847.

Zipser, E. J. (1969). The role of organized unsaturated convective downdrafts in the structure and decay of an equatorial disturbance. *J. Atmos. Meteor.* **8,** 799–815.

——— (1977). Mesoscale and convective-scale downdrafts as distinct components of squall line structure. *Mon. Wea. Rev.* **105,** 1568–1589.

———, and M. A. LeMone (1980). Cumulonimbus vertical velocity events in GATE. Part II: Synthesis and model core structure. *J. Atmos. Sci.* **37,** 2458.-2469.